HIGH TEMPERATURE, PERMANENT MAGNET BIASED, HOMOPOLAR MAGNETIC BEARING ACTUATOR

A Thesis

by

MOHAMMAD AHSAN HOSSAIN

Submitted to the Office of Graduate Studies of
Texas A&M University
in partial fulfillment of the requirements for the degree of

MASTER OF SCIENCE

August 2006

Major Subject: Mechanical Engineering

HIGH TEMPERATURE, PERMANENT MAGNET BIASED, HOMOPOLAR MAGNETIC BEARING ACTUATOR

A Thesis

by

MOHAMMAD AHSAN HOSSAIN

Submitted to the Office of Graduate Studies of
Texas A&M University
in partial fulfillment of the requirements for the degree of

MASTER OF SCIENCE

Approved by:

Chair of Committee,	Alan B. Palazzolo
Committee Members,	Hong Liang
	Moo-Hyun Kim
Head of Department,	Dennis O'Neal

August 2006

Major Subject: Mechanical Engineering

ABSTRACT

High Temperature, Permanent Magnet Biased, Homopolar Magnetic Bearing Actuator. (August 2006)

Mohammad Ahsan Hossain, B.S., Bangladesh University of Engineering and Technology

Chair of Advisory Committee: Dr. Alan B. Palazzolo

The EEC (Electron Energy Corporation) in conjunction with the National Aeronautics and Space Administration is researching the magnetic bearings for an alternative to conventional journal or ball bearings. The purpose of this research was to design and develop a high-temperature (1000ºF) hybrid Magnetic Bearing using High Temperature Permanent Magnets (HTPM), developed by the EEC for high performance jet engines at high speeds that supply loads of 500 lb_f. Another objective is to design and build a test rig fixture to measure the load capacity of the designed bearing.

The permanent magnet bias of the Homopolar radial magnetic bearing reduces the amount of current required for magnetic bearing operation. This reduces the power loss due to the coil current resistance and improves the system efficiency because the magnetic field of the HTPM can suspend the major portion of the static load on bearing. A high temperature radial magnetic bearing was designed via an iterative search employing 3D finite element based electromagnetic field simulations. The bearing was designed to produce 500 lb_f of force at 1000ºF and the design weight is 48 lbs. The bias flux of the Homopolar radial bearing is produced by EEC HTPM to reduce the related ohmic losses of an electromagnetic circuit significantly. An experimental procedure was developed to measure actual load capacity of the designed bearing at the test rig. All the results obtained from the experiment were compiled and analyzed to determine the relation between bearing force, applied current and temperature.

DEDICATION

To my brother (Memory remains the same).

ACKNOWLEDGMENTS

I would like to express my gratitude to all those who gave me the possibility to complete this thesis. I am deeply indebted to my supervisor, Dr. Alan B. Palazzolo, for his enthusiasm, encouragement, and untiring patience throughout the course of my study. I would also like to thank Dr. H. Liang and Dr. Moo-Hyun Kim for their knowledge and understanding. I would like to acknowledge EEC (Electron Energy Corporation) for funding the project.

I wish to express my warm and sincere thanks to Dr. Andrew Kenny for designing the Radial Bearing and Dr. Jingfang Liu of EEC for providing the funding and permanent magnets for the bearing. I would like to extend my thanks to my colleagues, Randell Tucker, Andrew Hunt and Clinton Johnson, for their constant suggestions and help. To those who shared the Vibration Control and Electromechanics Laboratory (VCEL) with me, I appreciate your patience and help.

Finally I wish to thank my family and friends in Bangladesh and my friends in College Station for their unfailing love and encouragement throughout my M.S. program.

TABLE OF CONTENTS

Page

CHAPTER

LIST OF FIGURES

Page

LIST OF TABLES

CHAPTER I

INTRODUCTION

1.1 Overview

The idea of magnetic bearing and its application in extreme environment has been conceptualized for many years. Magnetic bearing has introduced a new dimension in the application of bearings for rotary machinery for its unique properties. Magnetic bearing is one cutting edge technology that will allow engines to operate at speeds and temperature well beyond the limits of current technologies. Magnetic bearings are well suited to operate at elevated temperature, higher rotational speeds, and extreme altitudes and are a promising solution to current limitations [1]. Recent research and application has increased its application in the high temperature environment.

Among the benefits of such a bearing systems are: no contact between the rotor and stator, higher speed capabilities, and the elimination of the lubrication systems [2]. The absence of lubrication and contaminating wear make the magnetic bearing system exceptional for use in clean rooms, sterile rooms, or vacuum rooms. It has bearing losses that are less than conventional bearings resulting in lower operating costs. Magnetic bearings are being implemented into turbomachinery because of their lower maintenance costs and higher life time. It is also possible to adapt the stiffness and the damping of the bearing to absorb any vibration that might occur [3]. In addition to supporting loads, magnetic bearings directly measure bearing reaction forces. This enhances their application as engineering tools by providing a diagnostic and measurement tool for rotating machines. In order to obtain these loads the force as a function of current, air gap, operating frequency, and alignment must be known [4].

This thesis follows the style and format of *Journal of Mechanical Design*.

1.2 Objectives

The objectives of the research are as follows:

- Design and build a permanent magnet biased, radial magnetic bearing that can operate at 1000˚ F while supplying 500 lb_f load capacity.
- And also to design and build a test rig facility to measure the actual load capacity of the bearing at 1000˚ F.

1.3 Literature Review

The idea of suspending a rotating shaft using magnetic bearing has been around since 1840. In the mid-twentieth century, a successful magnetic levitation bearing was successfully demonstrated. First technical applications of levitation by magnetic field were proposed in 1937, when Kemper applied for a patent for a hovering suspension, while Beams and Holmes were working on electromagnetic suspension [5]. But permanent magnets are not able to levitate an object in all six directions. Later it is discovered that materials with diamagnetic properties would allow suitable permanent magnets to hover an object with any stability. The electromagnetic bearing comes into consideration when it is found that the magnetic forces produces by the permanent magnets are small for practical use [6].

A literature review on Homopolar electromagnetic bearing indicates that permanent magnet biased magnetic bearings has the characteristics of the coplanar geometry. Geometry of these bearings, described by Meeks [7], is usually known as Homopolar design. These Homopolar bearings could have either a permanent magnet in the back iron or an electric coil to provide the bias flux for two parallel stators. Because of this bias flux the electrical power requirement and the power lost due to coil current also reduces. Sortore et al. [8] published experimental results that indicates relatively low amount of electrical power requirement by Homopolar bearings biased with permanent magnets.

Lee, Hsiao, and Ko [9] described the detailed equations for predicting the flux paths of Homopolar bearings. They calculated the flux produced by the permanent magnet, and presented an advanced circuit model for these types of bearings and derived equations for the load capacity, current stiffness, and displacement stiffness.

A comparison between the predicted and measured force and stiffness characteristics of bearing were performed by Imlach, Blair, and Allaire[10]. Hysteresis effect is important for bearing design. A measurement including the effects of hysteresis and frequency response for the force versus coil current in a heteropolar bearing were reported by Fittro, Baun, Maslen, and Allaire [11].

This thesis is focused on a certain type of double plane bearing biased with permanent magnets in the poles. Masayuk [12], and Nagaghiko [13] have proposed bearings with magnets in the poles. However, the bearing that is presented here is different in that the poles with permanent magnets are designed for supplying 500 lb_f at 1000˚F and permanent magnets only provide the bias flux.

Palazzolo and Kenny [14] of TAMU-VCEL described the single plane magnetic bearing with permanent magnet that has lower coil resistance.

Provenza, Palazzolo, Hansen et al. [1] described the open loop, experimental force and power measurements of a radial, redundant-axis, magnetic bearing at temperatures to 1000 °F and rotor speeds to 15,000 rpm.

No paper or article was found regarding a permanent magnet bias Homopolar radial bearing of load capacity 500 lb_f that was designed to operate at high temperature.

1.4 Scope of Thesis

The need statement and function structure of the objective is addressed in chapter II. This was accomplished by using a top down engineering design procedure with technical analysis. All the significant design parameters were identified to aid the best design process for both radial bearing and test rig. All the constraints related to design are also discussed. The final design of bearing assembly and total test rig fixture are also presented.

Chapter III describes the 1-D magnetic circuit analysis of the Homopolar radial permanent bias magnetic bearing. This chapter represents the basic electromagnetic bearing circuit and equations for calculating magnetic force exerted by the stator. Finite elements simulations results of the High Temperature Radial Magnetic Bearing (HTRMB) are also presented.

Materials suitable for magnetic bearing are discussed in chapter IV. Magnetic properties of selected materials were investigated. Heat treatment and insulation of the rotor and stator laminates were performed according to ASTM standard.

Fabrication of bearing and assembly of test rig are discussed in chapter V. Special toolings were made for assembly purposes of the bearing. Calibration test for load cell with weights are also mentioned with photographs.

Test procedure and setup are addressed in chapter VI. Temperature and load measurement with varying current are plotted. Test results and failure are also discussed.

The conclusions of this research along with recommendations for future work are included in chapter VII.

1.5 Novel Contributions

The novel contributions and challenges of this project are as followings:

- Design and build a 1000˚F Magnetic Bearing Actuator (MBA) with permanent magnet bias flux.
- Measure magnetic properties of 1010 steel at 1000˚F.
- Demonstrate the performance of a radial MBA with permanent magnet bias flux, at 1000˚F.
- Design and build test fixture to measure load capacity of MBA at 1000F.
- Design and build specialized tooling to assemble MBA while subjected to very large magnet forces.
- Develop procedure to align shaft relative to the stator for load capacity tests in the presence of strong magnetic fields.

CHAPTER II

DESIGN OF MBA AND MBA TEST FIXTURE

2.1 Design Process

Design is an iterative process of translating a new idea or a need into the detailed information from which the product can be manufactured. Such design process is known as the systems engineering design process. It is used to describe the final design solution after evolution of idea in a logical and organized manner that satisfies all the objectives and requirements. Some of the main characteristics of the design process include a top down approach which views the entire system as a whole and puts an emphasis on defining functional requirements. The various stages of the design process are depicted in figure 2.1:

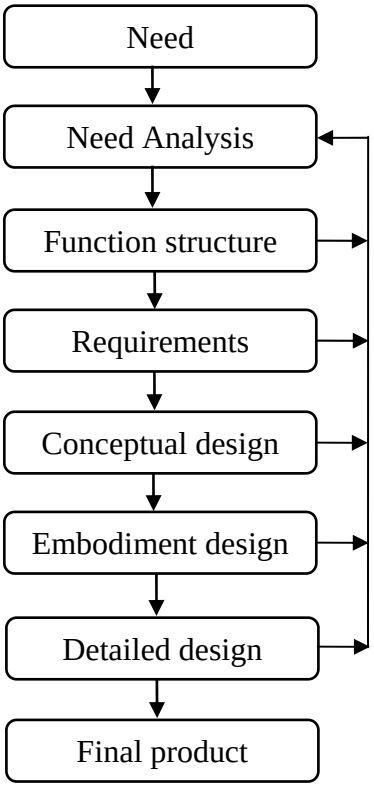

Figure 2.1 Systems Engineering Design Process

Development of the Need Statement is the most important stage of the design process. A successful identification of the real need can lead to a potentially simple but effective powerful solution. However the statement should only focus what will be satisfied by an approach regardless how many possible ways to accomplish the target.

The Need Analysis is the next stage of the design process which includes detailed interpretation of the need statement, clarification of concepts and assumptions, and identification of constraints.

The Function Structure analysis is a top down identification of functions in a hierarchical manner. It is a logical process that should be carried out without identification of a design concept. Each function in the hierarchy is considered as a single entry and exit point and implements a single independent function. One starts with the most basic functions that the design must provide and continues to decompose the functions into sub functions until specific functional requirements are achieved.

The summation of need, need analysis, and function structure analysis provide a decomposition and understanding of the design problem in such a way that one can understand basic requirements and constraints of the system. The two requirements for the design are: Functional Requirement and Performance Requirement. The functional requirements are the lowest levels of the function hierarchy structure and each function provides specific performance associated with it. Performance requirement suggests the quality that a functional requirement must be fulfilled and evaluated or related to constraints.

In Conceptual Design phase the designer completes few conceptually different solutions for addressing the need and selects the one that optimally meets the need in preliminary and detailed design stages. Throughout the design process the overall design stages are iterated which illustrates a top-down approach accompanied by a progression from the general to specific aspects of the engineering design process.

2.2 Need Statement

There is a need to design and develop a HTRMB and also a test rig that measures the actual bearing load capacity at high temperature.

2.3 Need Analysis

The above mentioned need originated from a need by EEC to develop a high-temperature (1000^{o}F) hybrid Magnetic Bearing using High Temperature Permanent Magnets (HTPM) developed by EEC. EEC also provided the funding for the test rig fixture for measuring the bearing capacity.

Several major constraints were imposed during the design process. The major constraint while designing was the physical weight of the bearing. It was required that the bearing weight would be minimum (less than 50 lbs) while using the EEC supplied rare earth magnets.

With the above background and major constraints in mind the need can be decomposed into major functions to be fulfilled. In this case, there are two top level functions derived directly from the need. First, a hybrid magnetic bearing must be designed for high temperature application. The major constraints concerning minimum weight, load capacity, ease of assembly of the bearing will be important for this function. The second major function is to design a test rig fixture to measure the actual load capacity of the bearing. Cost, easiness of rotor-stator alignment, and high temperature operating condition are the major constraints in this case.

2.4 Function Structure

The two top level functions are subdivided into sub functions until the specific requirements are achieved. Figure 2.2 depicts the function structure for the need. The function structure provides a method to organize the functional decomposition of the need.

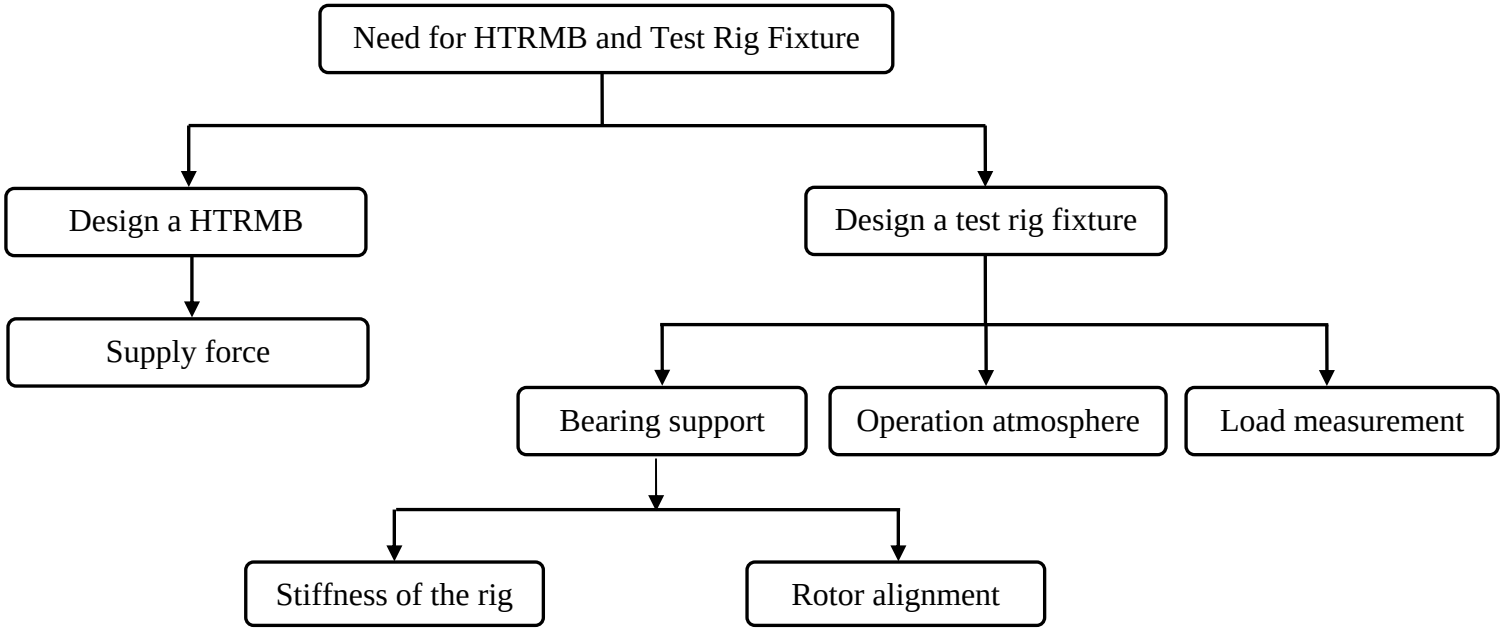

Figure 2.2 Function Structure

2.5 Performance Requirements

The functional requirements are obtained directly from the bottom of the function structure from figure 2.2. The performance requirements related with each functional requirement are briefly summarized in Table 2.1. Each of functional requirements should be satisfied by any of the design solutions.

Table 2.1 Functional and Performance Requirements for HTRMB and Test Rig

Functional Requirements	**Performance Requirements**
1. Provide force	Radial load capacity of 500 lb_f @ 14 ampere
2. Stiffness of the rig	Rig should be stiff and also allows thermal growth
3. Alignment of the rotor	A clearance of 20 mils between rotor and stator
4. Operation atmosphere	1000˚F
5. Load measurement	Ability to measure bearing load capacity

2.6 Final Design

The final design to be presented in this section was picked from few design configurations developed during the design process. The hybrid bearing is designed and analyzed with finite elements modeling software (Vector Opera) which has the advantage of including 3-D effects. The final 3-D models of the Radial Bearing are shown in figure 2.3 and 2.4. The test rig fixture is depicted in figure 2.5.

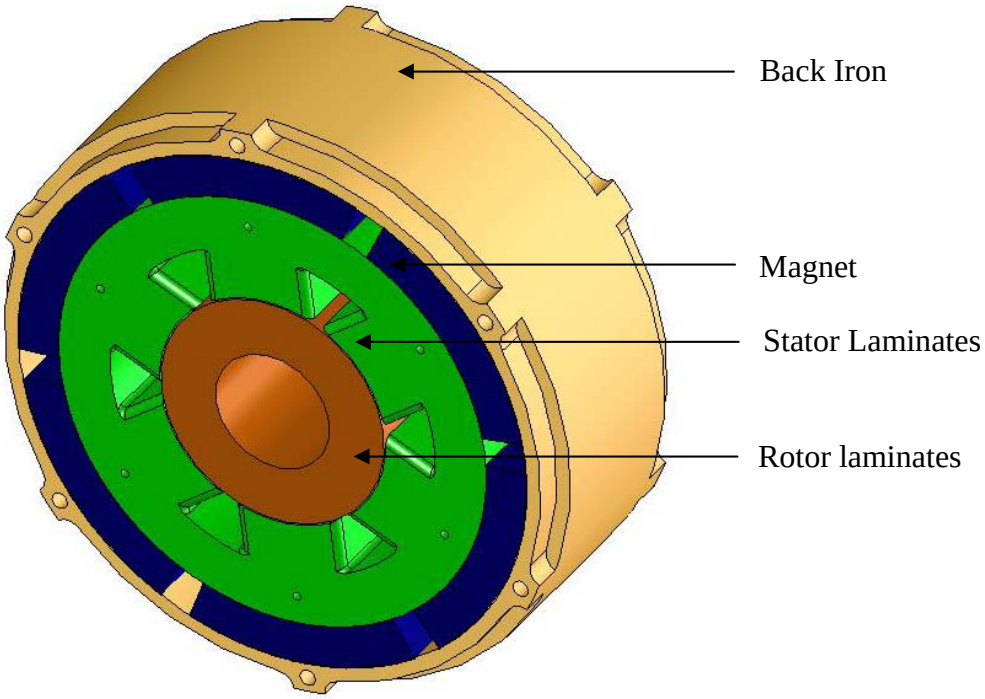

Figure 2.3 Assembly View of HTRMB

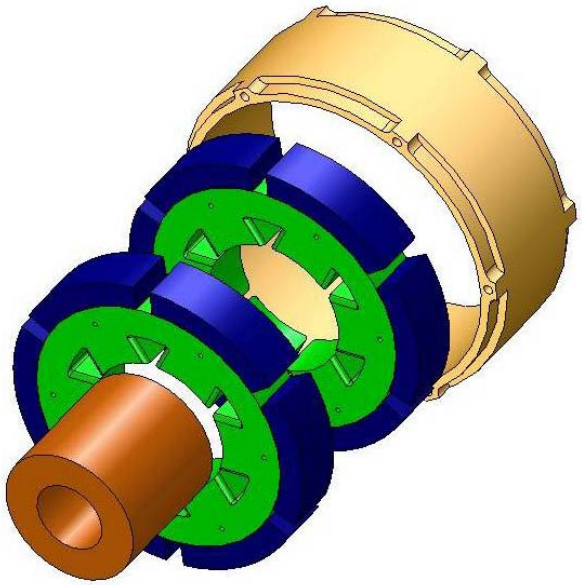

Figure 2.4 Exploded View of HTRMB Assembly

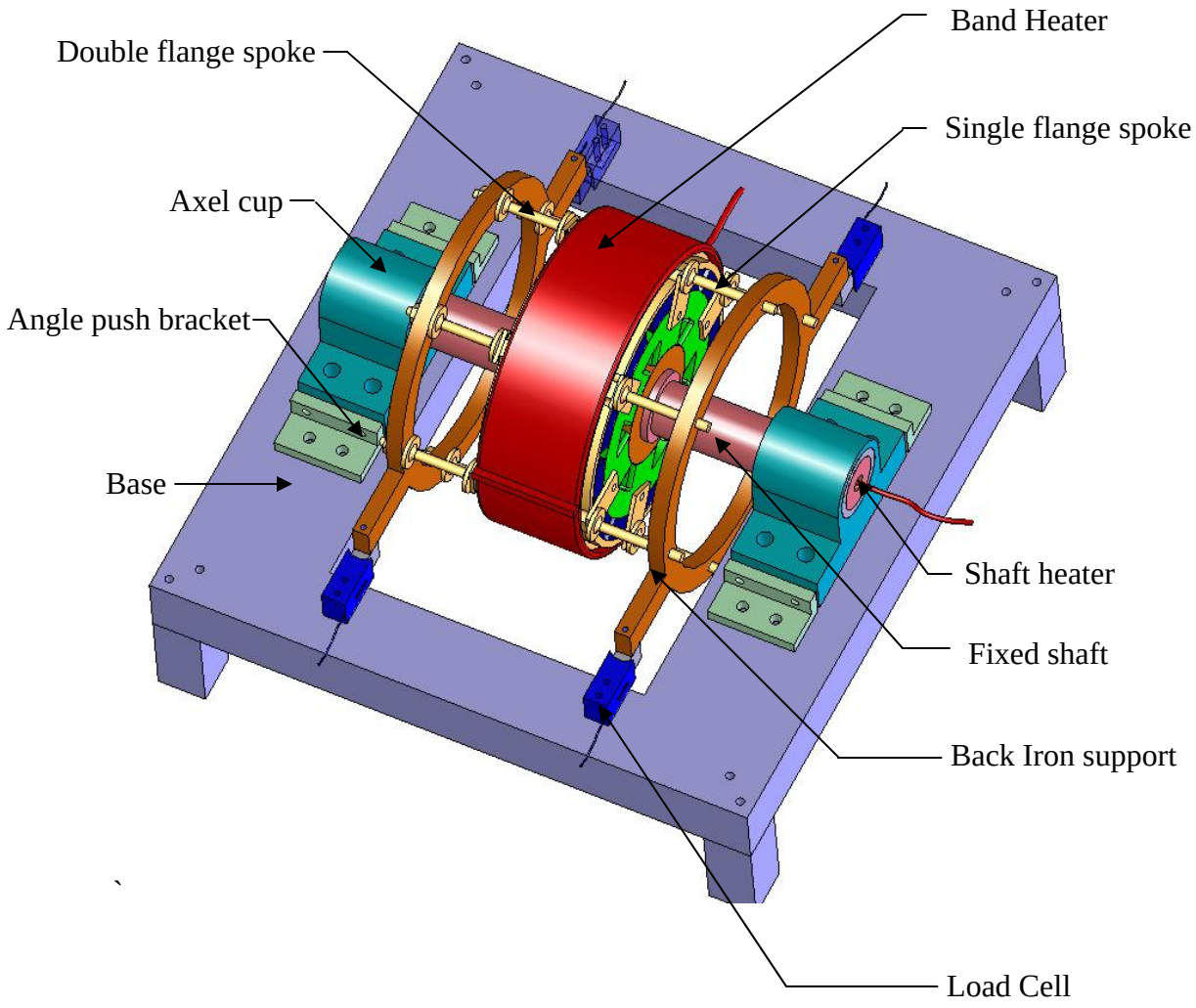

Figure 2.5 Assembly View of HTRMB Test Rig

2.7 Design of High Temperature Radial Magnetic Bearing (HTRMB)

A radial, high temperature magnetic bearing was designed via iterative search employing 3D finite element based electromagnetic field simulations (by Dr. Andrew Kenny using Vector Opera). The bearing was designed to produce 500 lb_f of force at 1000ºF and the design weight was 48 lbs. Bias flux was produced by EEC high temperature permanent magnets in order to significantly reduce the related ohmic losses of an electromagnetically biased design. The stator was designed with AISI 1002 and AISI 1010 steels to significantly reduce the cost while maintaining required saturation flux levels. The table 2.2 shows the FEA model predictions of the radial bearing.

Table 2.2 1000 ºF HTRMB FEA Model Predictions

Bearing Weight	48 lb_f
Load Capacity	573 lb_f @ 14.1 Ampere
K_i (lb_f /A)	41 lb_f/A
K_p (lb_f /inch)	30800 lb_f/inch
L (mH) for 1 coil	1.33. mH
N (turns/coil)	20
Airgap Flux (B)_bias (tesla)	0.66 T

The current stiffness (K_i) is defined here as the ratio of the total force produced by the bearing to the maximum current over all coils (which produce the force).

All the fabrication drawings for the HTRMB are shown in Appendix B.

2.8 Design of HTRMB Test Rig Fixture

The Test Rig has features to measure the load capacity, stiffness, and clearance changes for the HTRMB. The fixture employs band and rod heaters and load cells to maintain the HTRMB at 1000ºF and to measure its maximum force. A controller measures temperatures and adjusts the heating rates to maintain the target temperatures of 1000ºF.

The test bearing is mounted on flexible spokes (Ti4Al6V) in order to accommodate thermal expansions while limiting deflection for the load capacity tests. The force

generated by the energized coils is picked up by the four beam load cells. These load cells are fixed to both the table (Al alloy) and the rings (Ti4Al6V) that hold the bearing. Cool air is directed at the load cells to cool them from a vortex tube air cooler. Heat is held in the rig by using insulators and heat stops.

The fixed rotor shaft (Ti alloy) is positioned using jack bolts to move it horizontal or vertical of the table. This centered position of the rotor within the stator was determined by inserting 4 shims (nonmagnetic) along the entire length of the bearing, and spaced angularly by 90 degrees. The looseness of these shims was employed to determine an approximate centered position of the rotor within the stator.

All the fabrication drawings for the test rig are presented in Appendix C.

CHAPTER III

MAGNETIC BEARING FIELD MODELING

3.1 Introduction

Magnetic bearing is of increased importance in high speed tools and turbo machines. The operation mode of an active magnetic bearing can briefly be described through the following figure. A magnetic bearing system has three major parts: Bearing actuator, sensors, and controller with control algorithms. Active magnetic bearings are based on attractive forces. Shaft position sensors are used to provide feedback to the control system. This control signal is amplified by a power amplifier to drive the control current in the coil, causing a magnetic force to act on the rotor. The electromagnetic force has to be calculated by the controller in such a way that the rotor remains in this predefined and stable hovering position. The figure 3.1 explains electromagnetic bearings with a simple schematic.

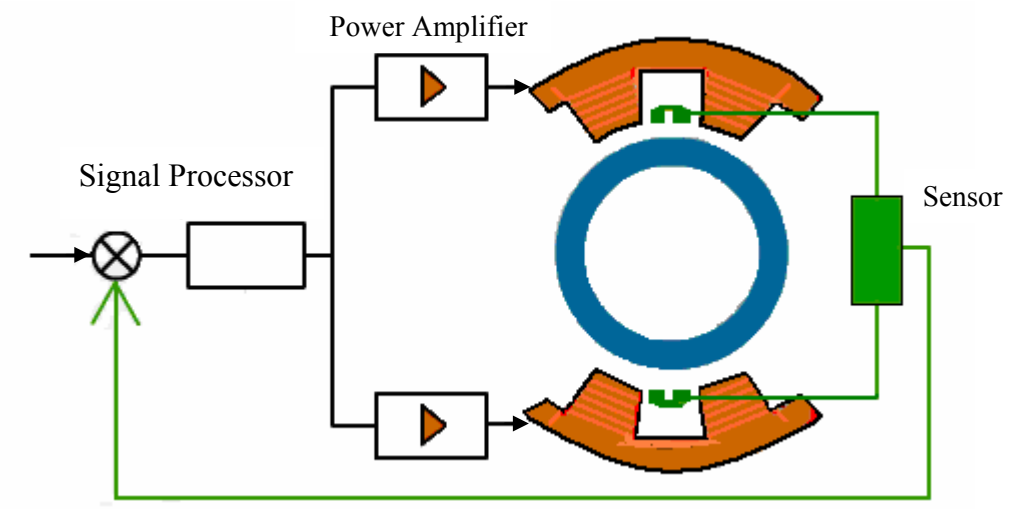

Figure 3.1 Active Magnetic Bearing System

3.2 Components of HTRMB

The Homopolar radial magnetic bearing has the following components:

- Back Iron for conducting the bias flux in axial direction
- Rotor and Stator lamination stacks for circulation of the control flux
- HTPM for permanent magnet biased operation
- Specially insulated magnet wire encapsulated in ceramic housing

3.3 Control and Bias Flux in HTRMB

In case of HTRMB, there are two planes of stator with permanent magnets. The permanent magnets in all the poles in one plane of the bearing are oriented to push the bias flux into the rotor. The flux returns out through the rotor to the other plane of stator-magnets which is reversely polarized. And the control flux circulates radially. The coils on the control poles can add or subtract a control flux to the bias flux. This way the control flux can add to the bias flux on one side of the rotor and subtract from the bias flux on the other side. Thus a controllable net force on the rotor is produced in the magnetic bearing. The figure 3.2 shows the FEA model of the radial bearing and figure 3.3 and 3.4 show the flux direction in the bearing.

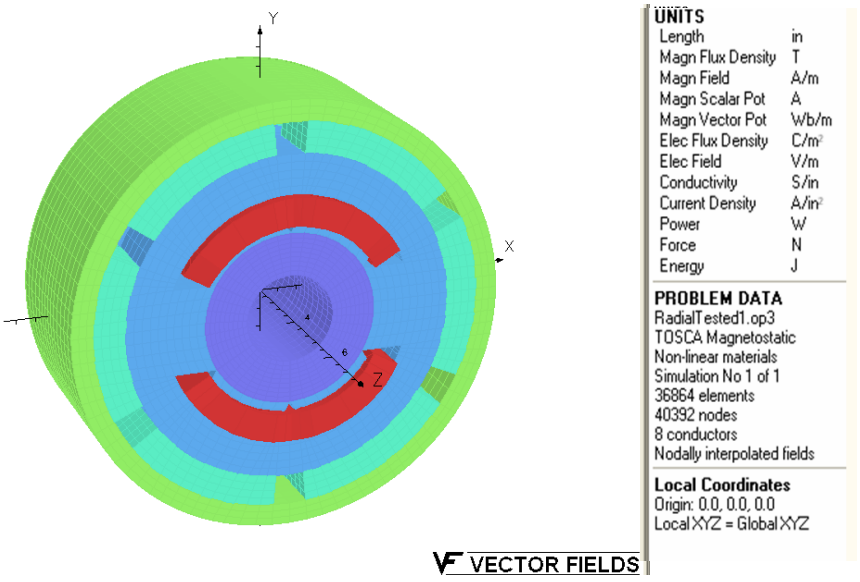

Figure 3.2 FEA Model of the HTRMB

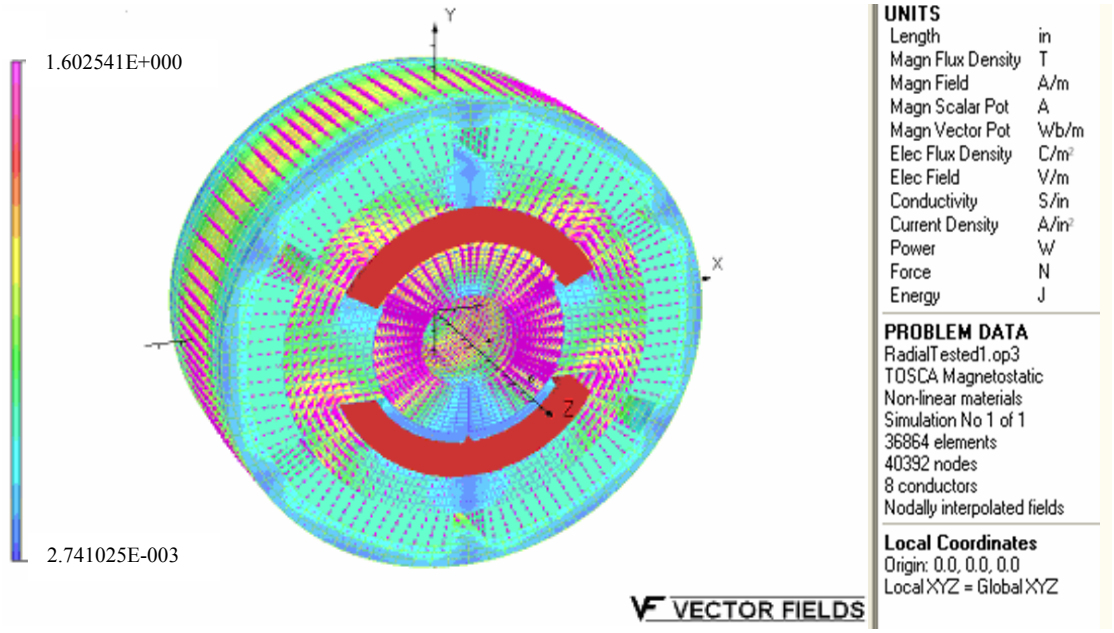

Figure 3.3 The FEA Combined Bias and Control Flux in HTRMB

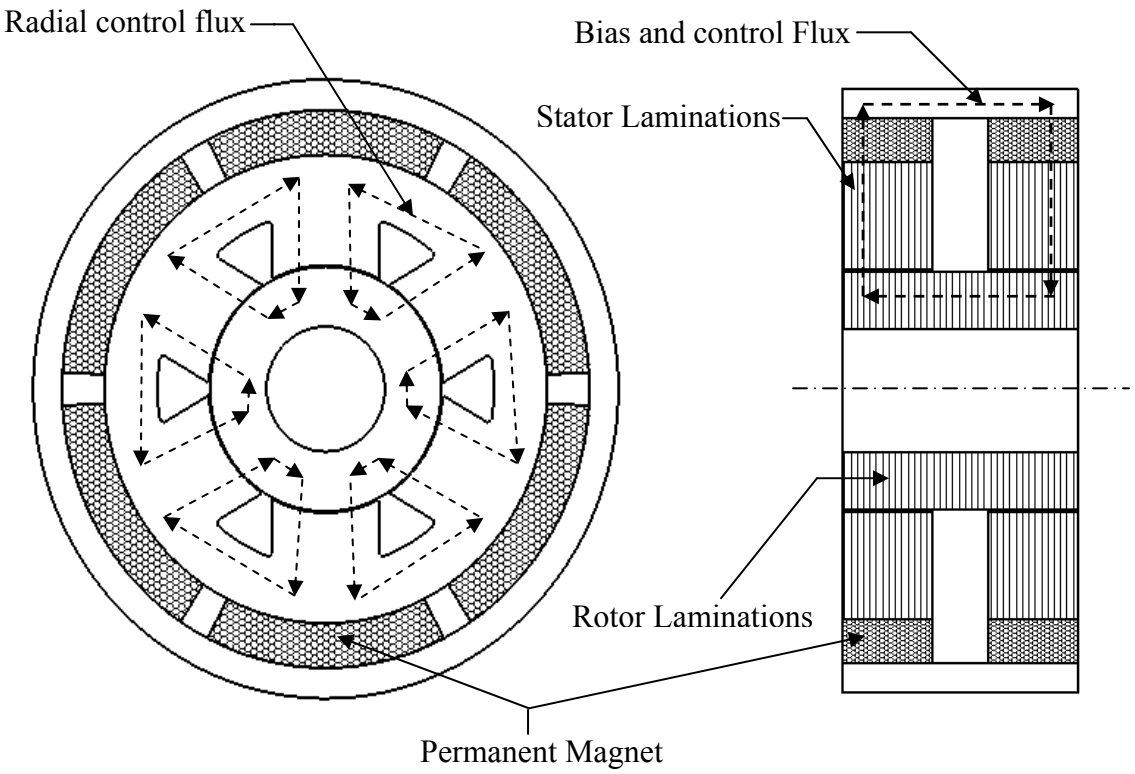

Figure 3.4 The combined Bias and Control Flux in HTRMB

3.4 Magnetic Circuit Theory

Magnetic bearing design requires the accurate prediction of the magnetic field. An exact theoretical computation of the field is rarely possible. The computations are done based on following simplified assumptions:

1. The permeability of the magnetic material for the magnetic bearing is high. It can be assumed infinity. The permeability of magnetic material is larger than that of air and the magnetic field line leave the material almost perpendicular.
2. The leakage flux is assumed negligible.
3. The flux circulates within the magnetic loop with magnetic cross-section, which is assumed to be constant along the entire loop.
4. The air gaps between the rotor and stator are assumed small to make the fringing at the gap small.

The magnetic field intensity (H) is proportional to the number of current loops the integration path encompasses. This is called Ampere's Circuital Law which defines the magnetic motive force (MMF):

$$\oint H.ds = NI \quad \text{..... (3.1)}$$

The relation between the magnetic field intensity (H) and the flux density (B) is: flowing through the magnetic circuit, (figure 2.2)

$$B = \mu_o \mu_r H \quad \text{..... (3.2)}$$

Where, μ_o is absolute permeability and μ_r is relative permeability.

The relative permeability is defined as the ratio of the permeability of the material (μ) to absolute permeability.

$$\mu_r = \frac{\mu}{\mu_o} \quad \text{..... (3.3)}$$

In isotropic homogeneous material, the magnetic flux density (B) and magnetic flux through a circuit becomes:

$$B = \mu_o \mu_r H \quad \text{..... (3.4)}$$

$$\phi = BA_s \quad \text{..... (3.5)}$$

A_s is the surface area on which B is exerted.

The magnetic reluctance (analogous to electric resistance) depends on the length (s), cross section (A), and the permeability of the path:

$$R_m = \frac{g}{\mu A} \quad \ldots\ldots\ldots\ldots\ldots\ldots\ldots\ldots\ldots\ldots \quad (3.6)$$

Figure 3.5 shows the magnetic circuit of a magnetic bearing. By comparing it with electric circuit we can find the flux density and magnetic force acting on it. \

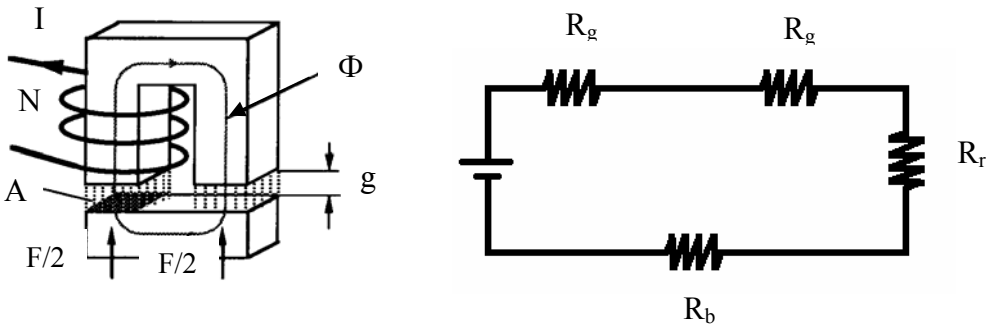

Figure 3.5 Equivalent Magnetic and Electric Circuit

Using Kirchhoff's Voltage Law the potential drop for electric equivalent circuit is:

$$\phi(2R_g + R_b + R_r) = MMF = NI \quad \ldots\ldots\ldots\ldots\ldots\ldots \quad (3.7)$$

Where Φ is the magnetic flux, R_g is the reluctance of the gap, R_b is the reluctance of back iron, R_r is the reluctance of the rotor. Since for the magnetic material, $\mu_r >> 1$, the reluctance of the material is often neglected.

$$2\phi R_g = NI \quad \ldots\ldots\ldots\ldots\ldots\ldots\ldots\ldots\ldots\ldots\ldots\ldots\ldots\ldots \quad (3.8)$$

Using the equations (3.5), (3.6) and (3.8) the flux density of circuit can be achieved:

$$B = \mu_o \frac{NI}{2.g} \quad \ldots\ldots\ldots\ldots\ldots\ldots\ldots\ldots\ldots\ldots\ldots\ldots \quad (3.9)$$

For highly permeable material the force (F) generated inside the gap under one pole can be expressed as a function of the magnetic flux density, the projected area, and the air gap size [2]. Equation (3.9) shows this developed equation based on the principle of virtual work. So the total force f the magnetic circuit is:

$$F = \frac{B^2 A}{2\mu} \quad \ldots\ldots\ldots\ldots\ldots\ldots\ldots\ldots\ldots\ldots\ldots\ldots \quad (3.10)$$

CHAPTER IV

SELECTION OF MATERIALS AND HEAT TREATMENT

4.1 Materials in Design and Process

Design is an iterative procedure to transform a new idea into a product. At every stage of design process, decision about material and process selection is required to make. Normally the preference of suitable materials is decided by the design requirements. Initially a vast number of materials are available for a certain design. But with the iteration of the design, the objective becomes more focused and the selection criterions are specified. So the lists of suitable materials which can satisfy the requirements become limited.

4.2 Materials for Electromagnetic Bearings

Selection of proper material for bearing's rotor and stator has a great influence on magnetic bearing load capacity and power requirement. Because of their magnetic properties soft magnetic materials (mainly iron-silicon alloys) are considered as the best for magnetic bearing design. Iron and low carbon iron have high magnetic saturation density and it is also cheaper. Silicon-Iron crystalline alloy has better electric resistivity and mechanical strength. Iron-Cobalt alloy has highest saturation magnetization among all soft magnetic materials. The following properties of the soft magnetic alloys play important role in the selection process:

- Saturation flux density
- Magnetic Permeability
- Electrical Resistivity
- Mechanical strength
- Machinability and cost

There is a gap between bearing rotor and stator. So the resultant permeability and flux density in operation condition are less than the ideal theoretical non-gapped magnetic circuit. This causes the using of alloys with high permeability for magnetic bearings. So Iron-Cobalt alloys are generally used for bearing rotor and stator.

Among all the properties the saturation of magnetization of the material is the most important property for magnetic bearing design. As the total magnetic force is proportional to the square of the flux density, the higher the magnetization saturation limit the higher the force it can provide. The Iron-Cobalt alloys have the maximum saturation point of magnetization among all material in soft magnetic materials. The presence of Cobalt in the alloy increases the saturation of magnetization.

The Eddy Current energy loss (loss = I^2R, loss is proportional to R and square of I) can be minimized by increasing the resistivity of the material. So alloys with higher electrical resistance should be used. But alloys with higher electrical resistivity have lower saturation magnetization. To reduce the eddy current effect laminates are used for both stator and rotor instead of solid.

Mechanical strength of the magnetic alloy is another consideration for selection of materials for magnetic bearing. The bearing is operated in high temperature and high speed. Better mechanical properties for the bearing materials are desired. Iron-Cobalt alloys have greater mechanical strength. Heat treatment of the alloys improves the strength of bearing materials. Coefficient of thermal expansion of materials is also considered for high temperature application.

Machinability of the materials is also an important criterion for selection of bearing materials. Some of the alloys are brittle and difficult to machining. Special type of CNC milling operation or EDM (electron discharge machining) is required for them, which increases the cost.

Considering all the facts and reasons the magnetic bearing is designed with Hiperco 50 HS (an iron-cobalt-vanadium soft magnetic alloy) for rotor laminates and AISI 1010 for stator laminates.

The properties of Hiperco 50 HS and AISI 1010 are shown in the table 4.1:

Table 4.1 Material Properties of Hiperco 50 and AISI 1010

Properties	Hiperco 50	AISI 1010
Density	0.2930 lb/in^3	0.284 lb/in^3
Poison's ratio	0.33	0.29
Modulus of Elasticity	30.0x10^3 ksi	29.7x10^3 ksi
Thermal conductivity	206.8 BTU-in/hr/ft^2/˚F	346 BTU-in/hr/ft^2/˚F
Curie Temperature	1720 ˚F	1500˚F
Tensile strength	185 ksi	52.9 ksi
Coeff. of thermal expansion	5.9 µin/in/˚F @ 1000˚F	7.89 µin/in/˚F @ 868˚F
Flux Density (tesla)	2.1 tesla	1.3 tesla

4.3 Standard Procedure for Testing Magnetic Properties of AISI 1010

This section describes the layout and procedure used in testing the magnetic properties of AISI 1010. This includes schematic drawings and descriptions of the actual setup, procedure and results.

Standard ASTM A 773M-91 specification and method was followed for testing magnetic properties of AISI 1010. This method provides basic magnetic properties of the material in the form of link or ring and other shapes that may be cut, stamped, machined or ground from cast, compacted, sintered, forged or rolled materials.

As in making most magnetic measurement, a ring specimen is wound with an exciting winding (the primary) and a search coil (the secondary) for measuring the change in flux. When an exciting current, I, is applied to the primary winding, a magnetic field, H, is produced in the coil, and this in turn produces magnetic flux ϕ in the specimen. As the ring has no air gap, all of the exciting current is used to magnetize the specimen, and H is proportional to I in accordance with the following equation (Ampere's law),

$$\oint Hdl = NI \quad \ldots\ldots\ldots\ldots\ldots\ldots\ldots\ldots\ldots\ldots\ldots\ldots\ldots\ldots \quad (4.1)$$

Where,

H magnetic field strength, Oe (A/m)

I current in the exciting coil

N constant determined by the number of primary turns the magnetic path length of the specimen

Magnetic flux can be determined by integration of the instantaneous electromotive force that is induced in the secondary coil when the flux is increased or decreased by a varying H. The instantaneous voltage, V, is equal to:

$$V = N\frac{d\phi}{dt} = NA\frac{dB}{dt} \quad \ldots\ldots\ldots\ldots\ldots\ldots\ldots\ldots\ldots \quad (4.2)$$

And $$\phi = \frac{1}{N}\int V dt \quad \ldots\ldots\ldots\ldots\ldots\ldots\ldots\ldots\ldots\ldots\ldots \quad (4.3)$$

In general, magnetic material tends to have non-uniform properties throughout the body of the test specimens. Therefore uniformly distributed test winding and uniform specimen cross-section are highly desirable to average non-uniform behavior to a tolerable degree.

Dimension of the Test Specimen

A ring type specimen of AISI 1010 was chosen for the test according to ASTM standard dimensions. A mean diameter of 3.5 inch ring had 100 primary and 50 secondary turns. When an exciting current is applied in the primary winding, a magnetic flux is generated. This flux is proportional to the number of turns in the primary winding. The flux passes thorough the material and induces a voltage in the secondary winding.

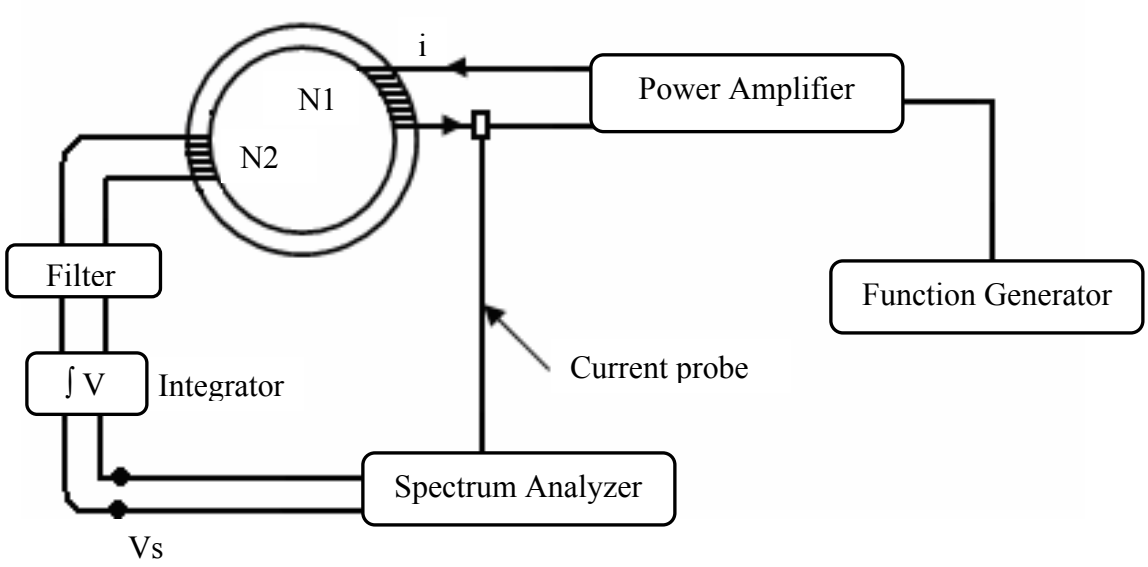

Figure 4.1 Block Diagram of Material PropertiesTesting Setup

Experimental Configuration

The experimental set-up consisted of several components. The block diagram of the experiment is shown in figure 4.1. The circuit starts with a Function Generator set for a sinusoidal wave between 0 Hertz and 400 hertz. The sine signal went from the function generator to the Power Amplifier. This was set in current mode in order to deliver a constant output current to the primary coils regardless of load. The current was measured through a current probe. The power amplifier was used to produce sufficient current for maximum magnetization. Filter and Integrator were used to reduce the noise in the reading. The input and output values were recorded and plotted with Spectrum Analyzer. The test specimen was also kept in a heater for testing magnetization properties of AISI 1010 at different temperature.

The induced voltage was also checked by the voltmeter. All these outputs and input reference voltage to the power amplifier was put into the spectrum analyzer to plot all waveforms. The actual setup for the experiment is shown in figure 4.2.

Figure 4.2 Actual Setup for testing magnetic properties of AISI 1010

Test Results

The testing for material properties for AISI 1010 was performed at various temperatures. In the experiment the input current and frequency were varied by power amplifier and function generator and induced flux density and voltage at the secondary were measured in the analyzer. The summary of the test is presented in the table 4.2.

Table 4.2 Material Testing Data for AISI 1010

Bias current (Ampere)	Temp. (F)	Frequency (Hz)	Current RMS (Ampere)	Flux (Tesla)
0	75 (room)	5	-	1.7
0	75 (room)	20	4.67	1.5
0	75 (room)	400	4.67	1.2
0	594	20	5.00	1.6
0	594	400	4.32	1.1
0	985	20	5.00	1.3

Figures 4.3 – 4.5 show B (in Tesla) vs. current in amperes for a room temperature test. The respective impressed current frequency values for these figures are 5, 20 and 400 Hz, and the respective peak B values were 1.7, 1.5 and 1.2 Tesla, respectively. Figure 4.6 shows B vs. time at room temperature and an excitation frequency of 400 Hz. With increasing frequency the flux density reduces.

Figures 4.7 and 4.8 show B (in Tesla) vs. current in amperes for a 594 F temperature test. The respective impressed current frequency values for these figures are 20 and 400 Hz, and the respective peak B values were 1.6 and 1.1 Tesla, respectively. Figure 4.9 shows B vs. time at a 594 F temperature and an excitation frequency of 400 Hz.

Figure 4.10 shows B (in Tesla) vs. current in amperes for a 985 F temperature test. The respective impressed current frequency values for this figure is 20 Hz, and the respective peak B value is 1.3 Tesla.

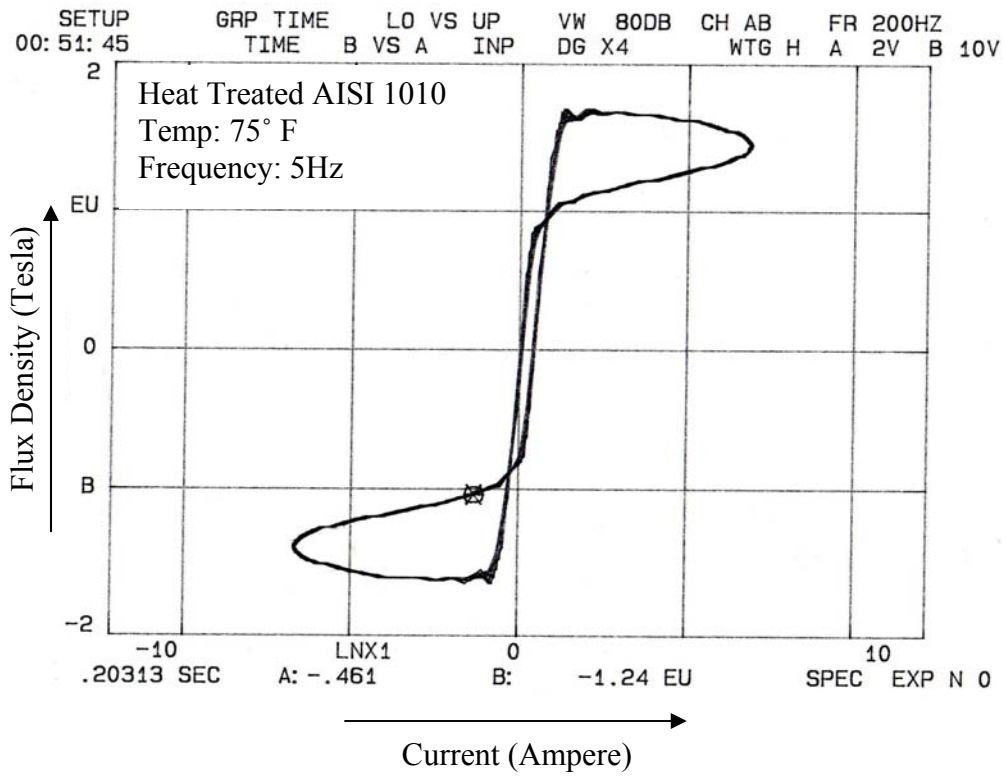

Figure 4.3 Flux Density versus Current Curve @ 75˚F & 5 Hz

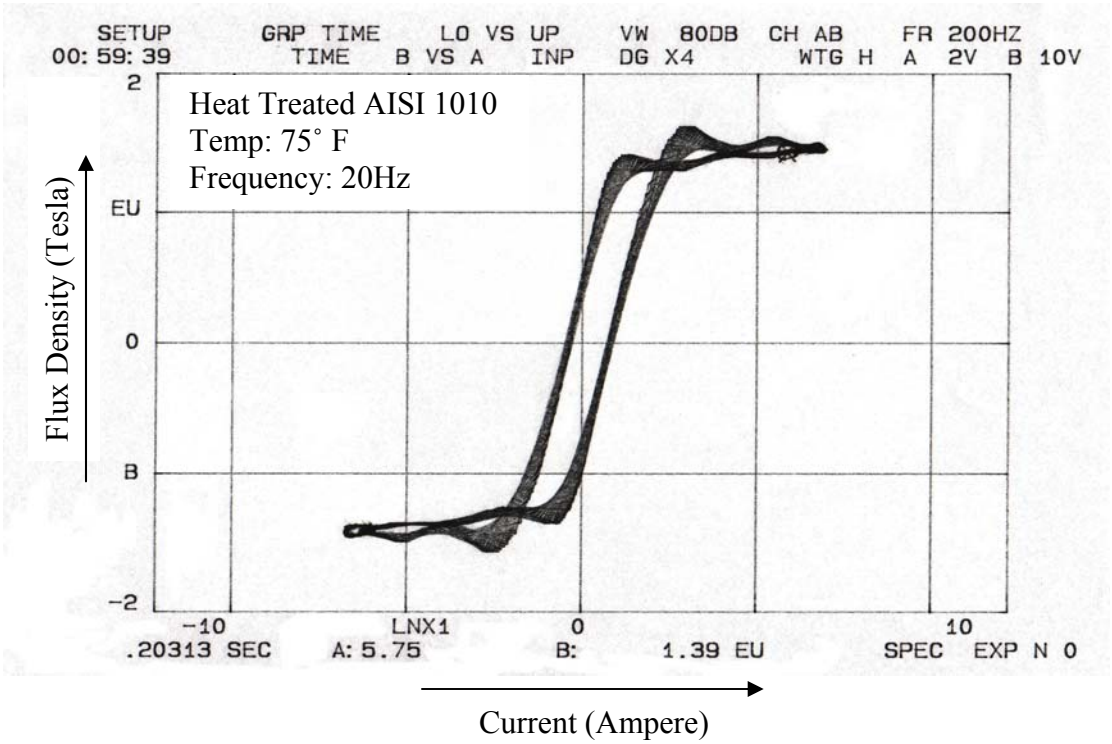

Figure 4.4 Flux Density versus Current Curve @ 75˚F & 20 Hz

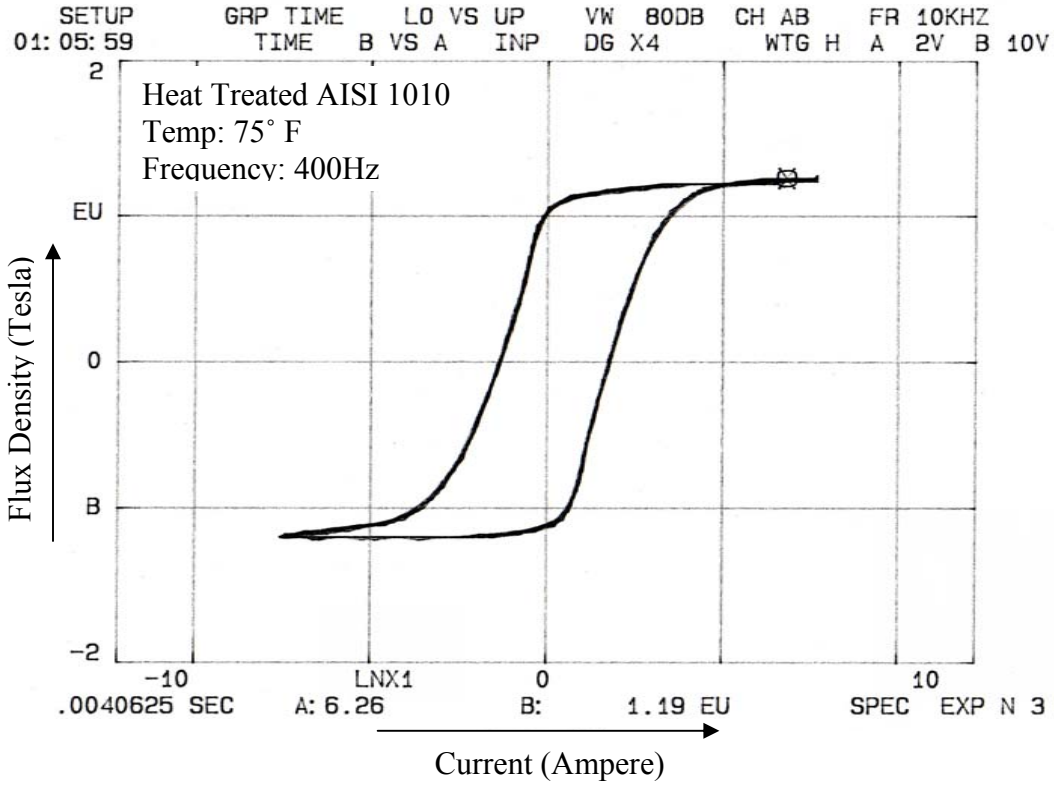

Figure 4.5 Flux Density versus Current Curve @ 75˚F & 400 Hz

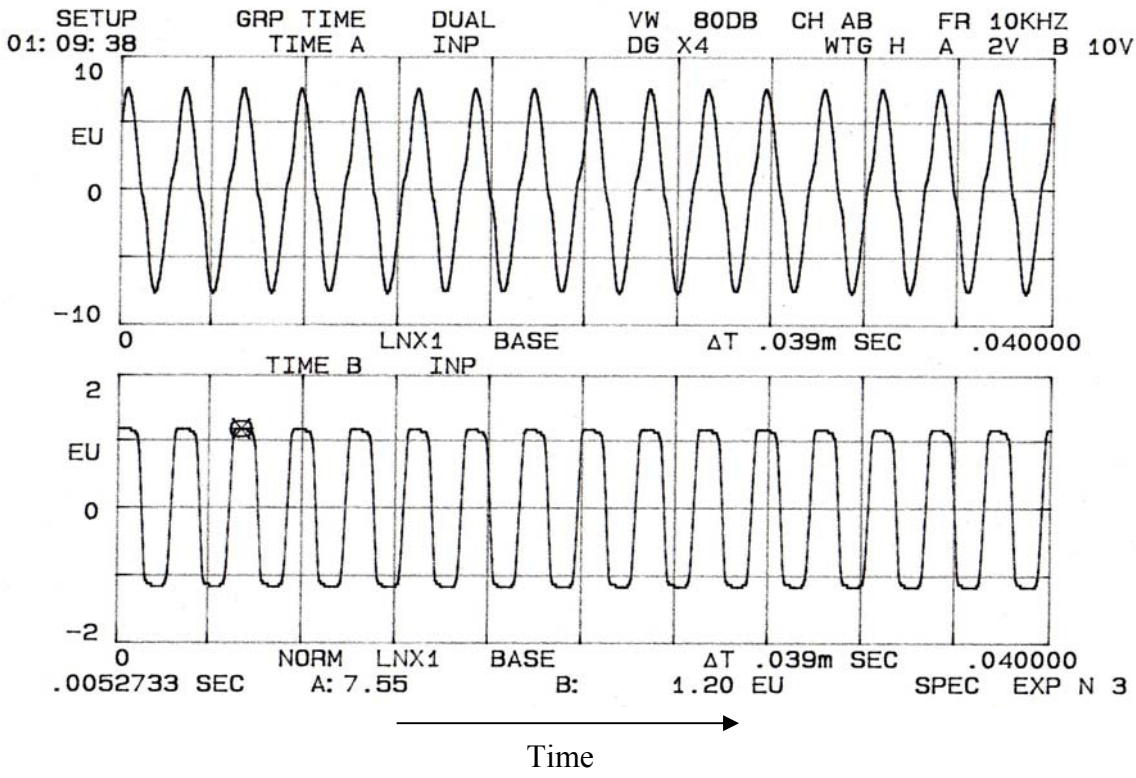

Figure 4.6 Flux Density versus Time Curve @ 75˚F & 400 Hz

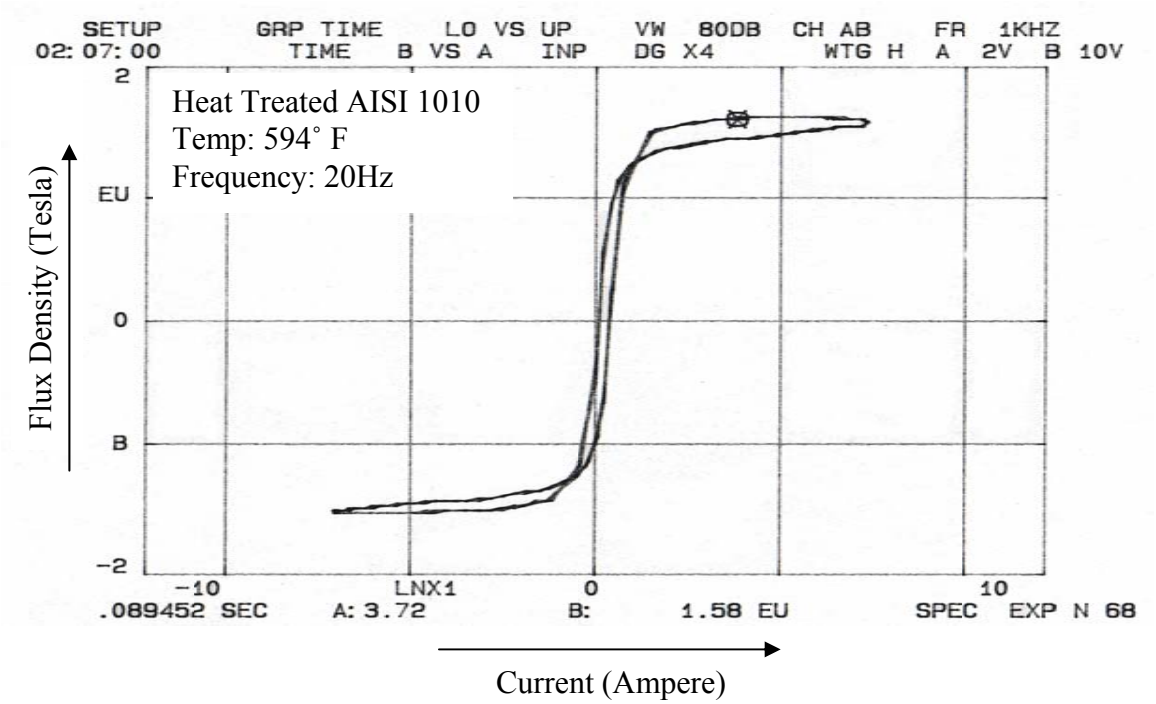

Figure 4.7 Flux Density versus Current Curve @ 594˚F & 20 Hz

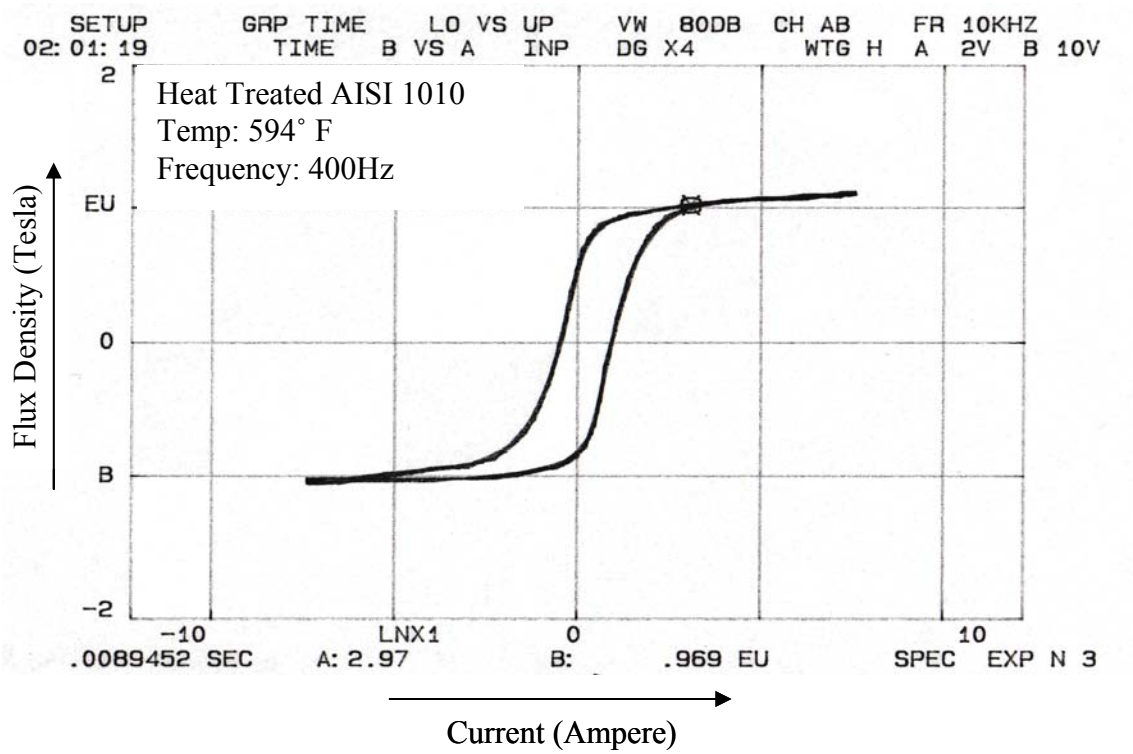

Figure 4.8 Flux Density versus Current Curve @ 594˚F & 400 Hz

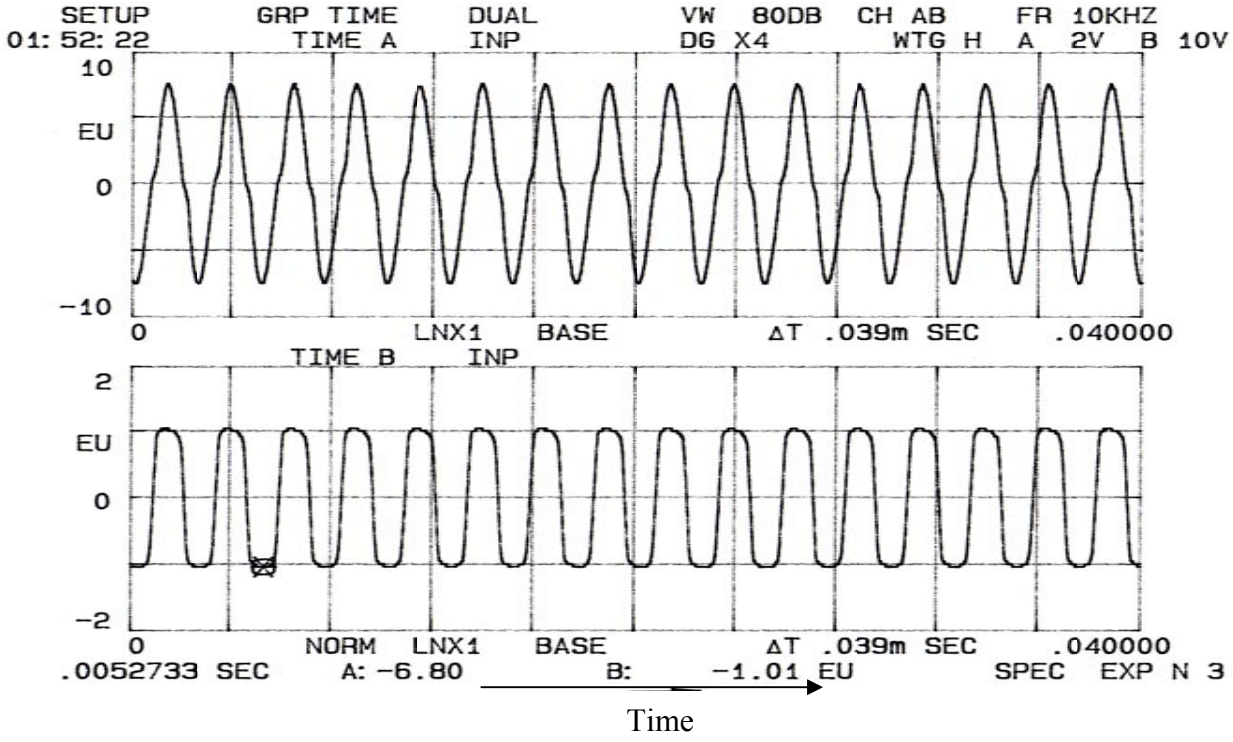

Figure 4.9 Flux Density versus Time Curve @ 594˚F & 400 Hz

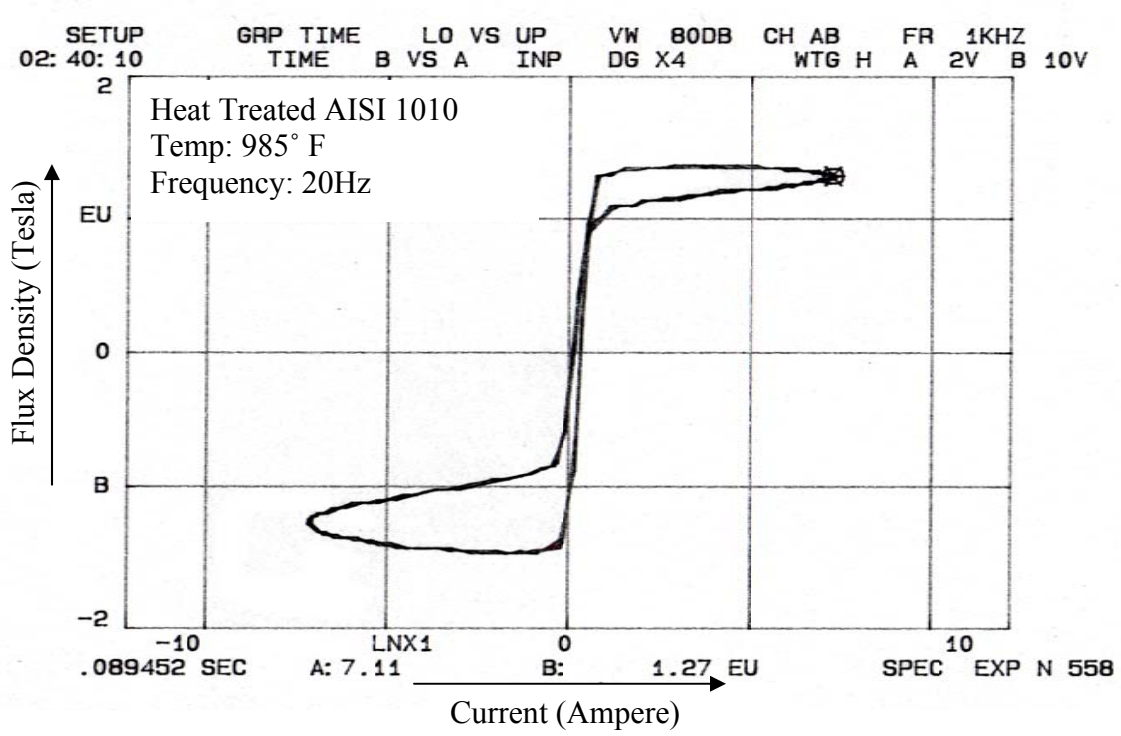

Figure 4.10 Flux Density versus Current Curve @ 985˚F & 20 Hz

4.4 Heat Treatment Schedule for Hiperco 50 and AISI 1010

The eddy current and hysteresis losses measure the performance of ferromagnetic alloys in an electro-magnetic circuit. During the course of magnetic bearing's fabrication, the heat treatment of the steel can affect these parameters. The presence of oxygen, carbon and sulphur in the steel increase the eddy current and hysteresis losses and reduce the magnetic permeability in the circuit. Carbon has the most detrimental effect. So heat treatment is required to reduce the carbon levels in the materials.

The heat treatment schedule for AISI 1010 laminations was:

- Hold for 2 hour at 750˚C in dry hydrogen or vacuum
- Slow cool down at 60˚C per hour

The heat treatment schedule for Hiperco50 HS laminations was:

- Hold for 2 hour at 740˚C in dry hydrogen or vacuum
- Slow cool down at 85˚C per hour

4.5 Insulation of Laminations by Oxidation

In order to reduce the eddy current losses between the laminations of the rotor and stator, the inter-laminar resistance needs to be increased. Coatings of organic, in-organic or a coating of magnetite (Fe_3O_4) can increase the resistance between laminates.

Both Hiperco 50 HS and AISI 1010 laminates were heated to 200˚C for 2 hours. As a result a coating of oxidation formed in laminates. This coating greatly increases resistance between laminations and reduces the eddy current loss.

CHAPTER V

FABRICATION AND ASSEMBLY OF HTRMB AND TEST RIG

5.1 Overview

This chapter describes the design and fabrication issues related to HTRMB that include mold design and coil potting procedure for bearing and, the special tooling that was made for the assembly process. The assembly of the test rig includes installation of the test rig components, mounting bearing on the rig, and calibration process of the load cell to measure to bearing force.

5.2 Stator and Rotor Laminations and Coil Winding

The materials used for stator and rotor lamination were AISI 1010 and Hiperco 50 respectively. The individual laminates were heat treated to maximize flux saturation and oxidation for electrical isolation. The AISI 1010 and Hiperco 50 were 10 mils and 6 mils thick respectively. The stator laminates were riveted to get a design thickness of 1.36 inch. The rotor thickness was 3.57 inch and the rotor laminates were mounted on a fixed shaft compressed by locknuts.

The permanent magnets (SmCo217-16T550C) were provided by EEC. These rare earth magnets have high performance at elevated temperature (550˚C). The 55˚ arc magnets (segmented in to five 11˚ arc magnets) were attached into outer side of the stator in the position of the poles.

For high temperature bearing, special wire was required for coil to satisfy both conductor and insulation challenges. The wire conductor challenges included low resistance change as a function of applied temperature and resistance to oxidation. Bare copper was not selected for high temperature application as it oxidized at high temperature. Commercially available 99.9% pure, 18 gage silver wire was chosen as silver is a good electrical conductor and does not oxidize easily.

The insulation of the wire had to satisfy many requirements for high temperature application. It should be pliable to allow for small radius turns during coil winding process. The insulation must maintain the dielectric integrity during many thermal cycles

at high temperature. It should also have good adhesive quality, toughness and tensile strength for winding.

The silver wire was “Triple - Glass Wrapping” insulated which provided the desired requirements. The process of coating is repeated three times, leaving a wire ceramic triple coated.

Each pole of the stator had 20 turns of wire. The poles were covered with bobbin material to protect the wire from sharp edge of the laminates. The stator with the coils is shown in figure 5.1.

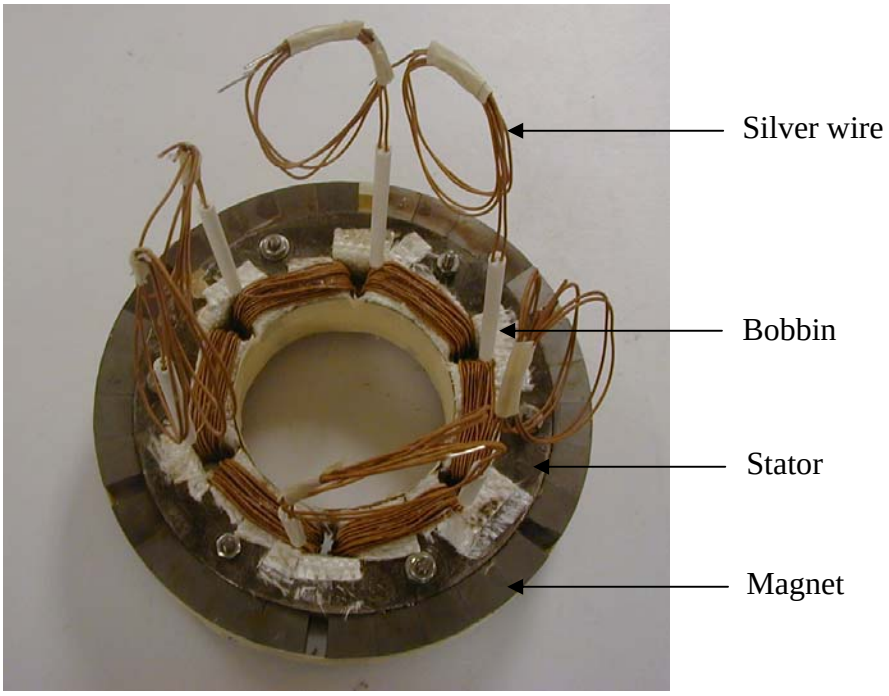

Figure 5.1 Stator Lamination with Magnets and Winding

5.3 Mold Design for Bearing Stator

The bearing consists of two planes of stator stacks with a gap of 0.85 inch between them. The magnetic winding wire needed to be encapsulated in ceramic housing. So there was a need to design and fabricate a mold for stator stacks for that requirement.

A potting mold was designed for this purpose with a requirement of safely removal of ceramic bonded stator stacks from the mold, outlet for winding wires, and easier dismantling of the mold parts. The figure 5.2 and 5.3 show the mold for stator potting.

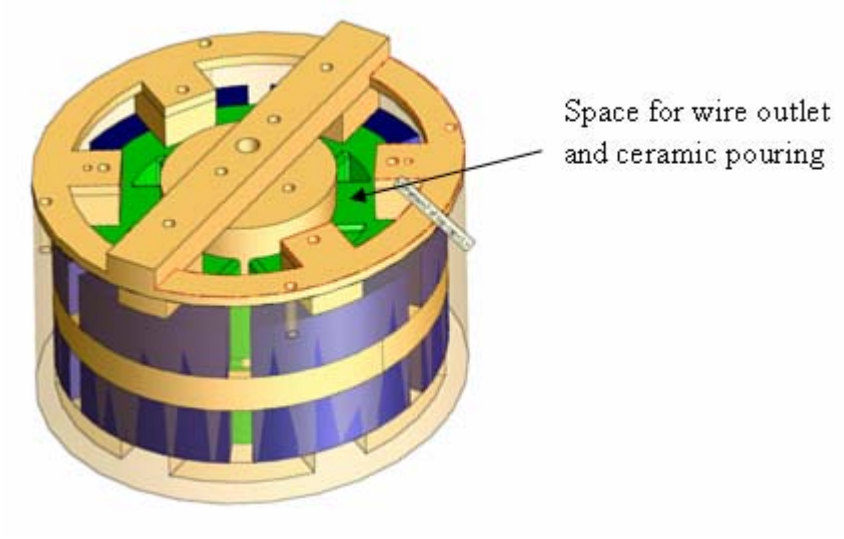

Figure 5.2 The Mold Assembly with Stators

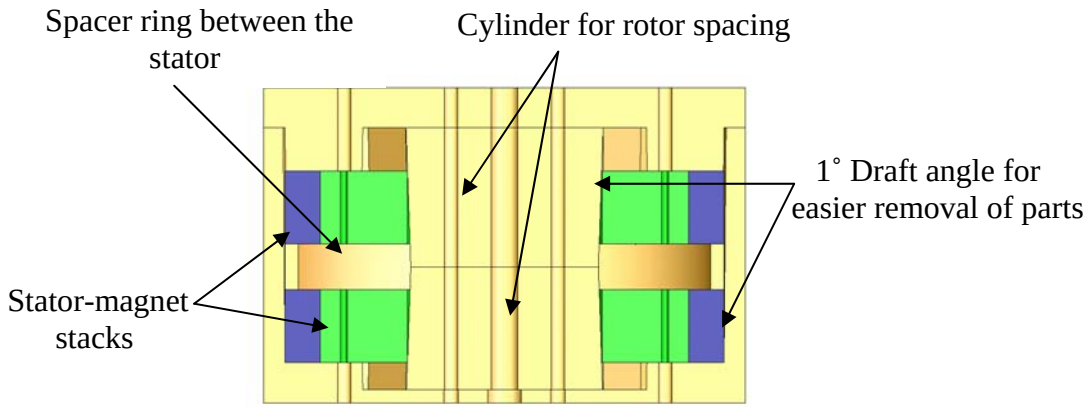

Figure 5.3 The Cross Section of Mold Assembly

5.4 Molding Process

The stator stacks was inserted in the mold and a two piece of cylinders was kept inside of the stator to provide the space for the rotor. The ceramic material was poured and it covered all the free space of between the poles. Then the mold was put in a vacuum chamber to remove the bubbles. The figure 5.4 shows the molding process.

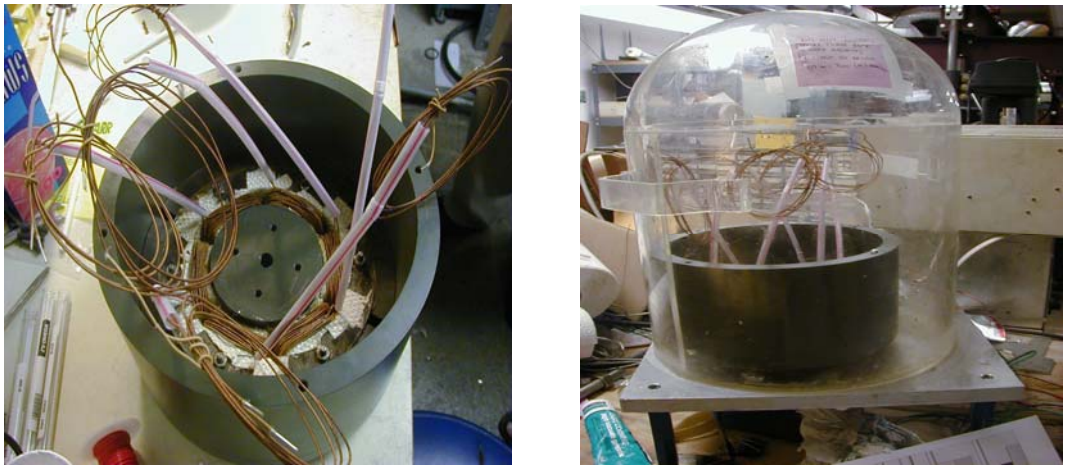

Figure 5.4 The Molding Process of the Bearing

Two spacer rings were inserted in the top of the bottom stator to keep the distance between the stators. And ceramic material was poured and degasified in the vacuum chamber. All the winding wires were out through the top of the mold. The completed molding process is shown is figure 5.5.

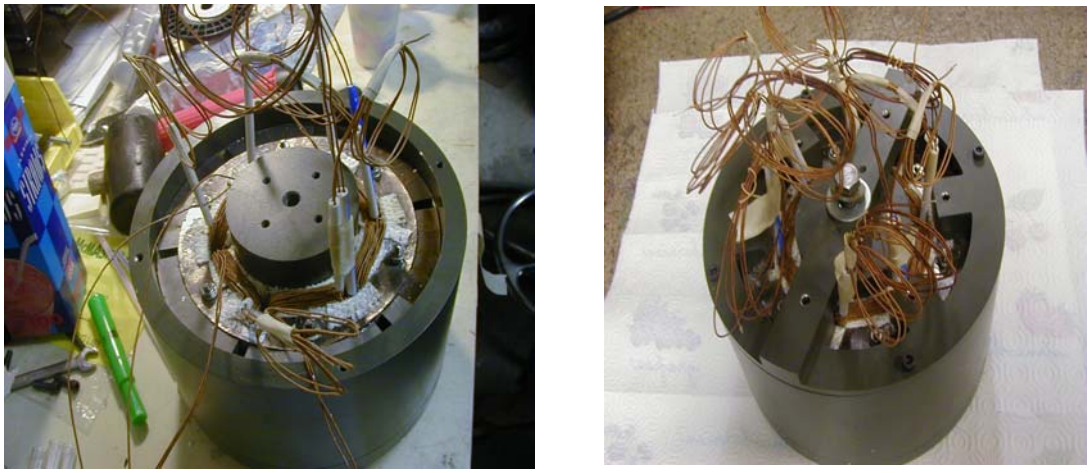

Figure 5.5 The Completed Molding Process

The mold was cured at room temperature for 24 hours and then it was cured for 3 hours at 200˚F and 2 hours for 250˚F.

The stator assembly was removed from the mold after heat curing. The coatings and draft angle of the mold helped removal of the stator assembly from the mold. The continuity test of the coils was performed. And it was found that all the coils were continuous.

The fabrication drawings for the mold are in Appendix D.

5.5 Assembly of Bearing

The stator-magnet assembly was then inserted into the back iron. Because of huge magnetic field it was very difficult to put the stator to back iron. Magnetic shield materials in the form of little bar around the back iron to negate the magnetic field were used but that was not enough. So a tripod clamp was designed and made that could perform the job. One base of the clamp was attached with the stator and other base containing the back iron was gradually moved towards the stator. Along with the clamp magnetic shields and ‘Anti-seeze’ were used during the process. The assembly of stator in back iron with the help of tripod clamp is shown in figure 5.6.

Figure 5.6 The Assembly Process of Stator in Back Iron with Special Tool

5.6 Assembly of Test Rig

The rotor with fixed shaft was inserted in to the bearing. The assembled bearing was then attached with heater band and side insulations and with the help of spokes and holder the whole bearing was mounted on the load cells of the test rig. The force generated by the energized coils is picked up by the four beam load cells. These load cells are fixed to both the table and the rings that hold the bearing. The test rig is shown in figure 5.7.

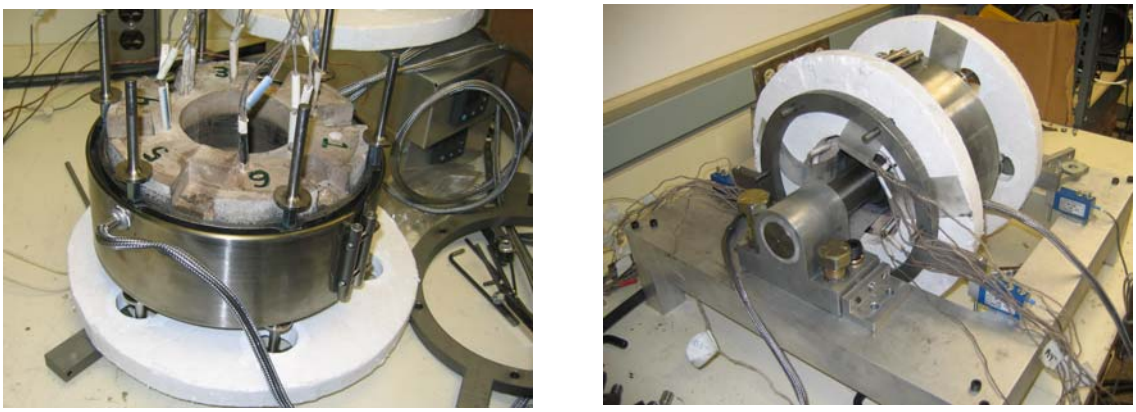

Figure 5.7 The Assembly Process of Test Rig

The two edge of the fixed shaft of rotor was inserted into the axel cups which were bolted to the base table. The axel cup was allowed horizontal and vertical movement with the help of jack bolts.

The load cells were connected in parallel and energized by a power source with 10 Volt. The readings of the load cells were taken by a voltmeter through a switchbox.

The insulation covered the bearing to provide the desired atmosphere of 1000˚F. A controller controls the temperature of the heater. To remove the fume away vent hood was installed above the bearing rig. To keep the load cell at normal temperature a cooling arrangement was provided. The load cells were cooled to below 110˚F via air jets that circulated through an ice water bath. The whole test rig at operation condition is shown in figure 5.8.

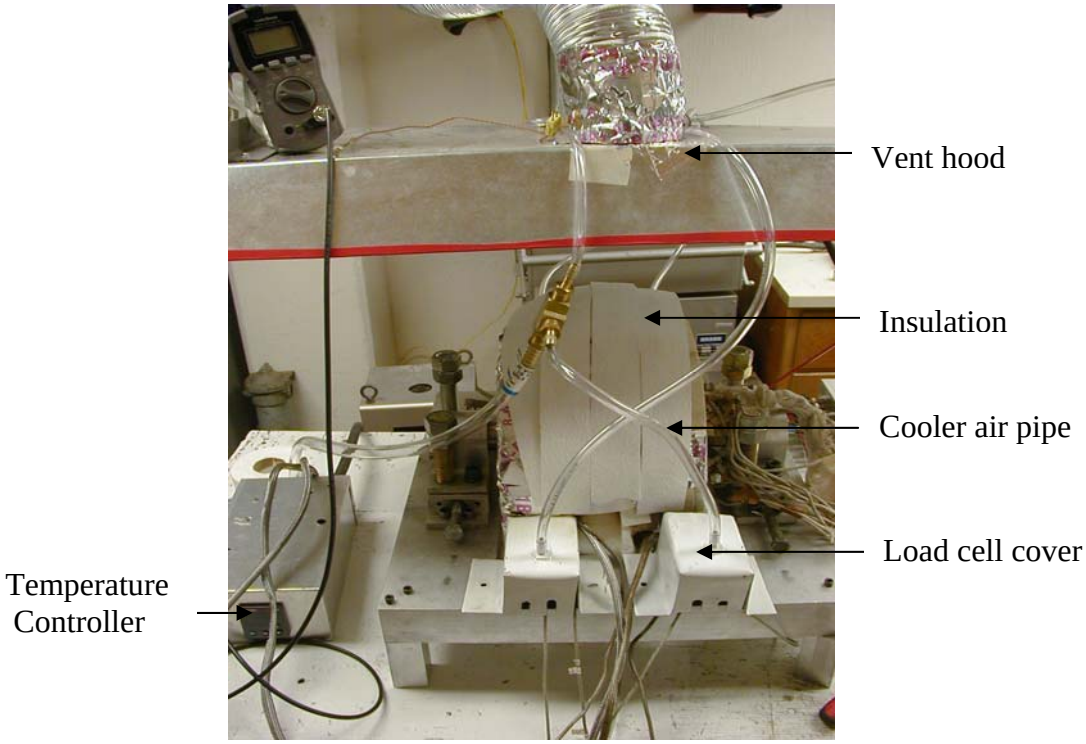

Figure 5.8 The Test Rig at Operating Condition

CHAPTER VI

TESTING OF HTRMB

6.1 Overview

The objective of this test was to measure the force due to application of control current and to compare the results to our predictions obtained via 3D finite element based electromagnetic modeling. This chapter describes the layout and test procedure used in this study. This includes the explanation of test setup and the measurement of temperature and load of the bearing in the designed test rig fixture. The test results are explained and the test history is evaluated.

6.2 Explanation of Test Setup

The requirement of high temperature for the bearing load tests mandates flexibility in the support (spokes) of the stator to accommodate thermal expansions. An unwanted side effect of the flexible support for the stator is that it allows the stator to change position with the application of current during the tests. This position change produces a force change due to the approximate 35 lb_f/mil position stiffness contributed by the permanent magnet induced flux. Thus, the measured forces result not only from the currents, but also from the changes in relative position of the rotor and stator during the test.

The position change induced force was minimized during the tests by re-centering the rotor within the stator whenever either temperature or current was changed. This centered position was determined by inserting 4 non magnetic shims along the entire length of the bearing, and spaced angularly by 90 degrees. The looseness of these shims was employed to determine an approximate centered position of the rotor within the stator. Each shim was approximately 5 mils thick and was made of stainless steel. The shims remained inserted in the gaps throughout all tests.

6.3 Test Procedure

Current was passed through the four energized coils causing the control magnetic flux to circulate across the rotor-stator gaps. The resulting downward force on the stator was measured by 8 air-cooled load cells that also support the weight of the stator. The schematic diagram of the load measurement is shown in figure 6.1.

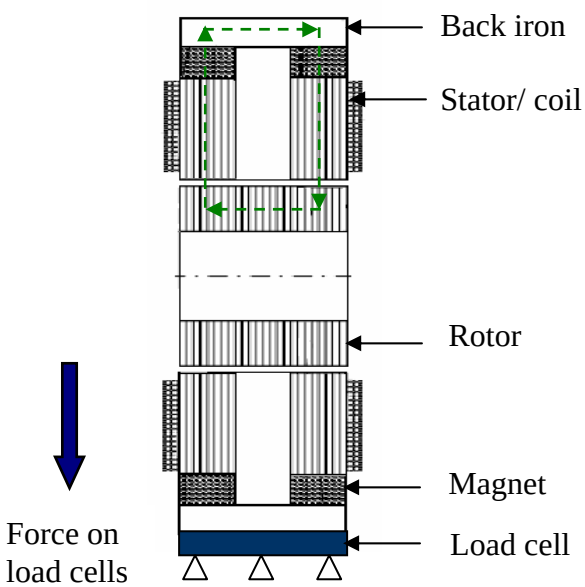

Figure 6.1 Schematic Diagram of Load on Load Cells

Each load cell has an average sensitivity of 3.2mV/V and a capacity of 250 lb_f load. The excitation voltage for each load cell is 10V. The load calculation formula is:

$$load = \frac{250 * reading}{32} \quad \ldots\ldots\ldots\ldots\ldots\ldots\ldots\ldots\ldots\ldots \quad (6.1)$$

Zero-force output voltages of the load cells were recorded by making all four shims loose within the rotor-stator gap, at zero current and at the certain test temperature. These voltages were subtracted from the “with current applied” voltages to obtain an estimate of the voltages due solely to the applied current induced forces. Then the control current of I amps was passed through the coil at that same temperature. This caused a slight change in the relative positions between the rotor and stator due to the magnetic force acting between them. The rotor position was changed manually via horizontal and vertical jack

bolts to return the system to the desired gaps between the rotor and stator, which caused all the shims inserted in the gaps to become loose. The readings from all of the load cells are then recorded via a switchbox and voltmeter. The load of each load cell for I amp current case is calculated using the above equation 6.1. The total load is the sum of all eight load cell forces.

The figure 6.2 shows the four poles that are energized with current and their positions relative to the net force direction.

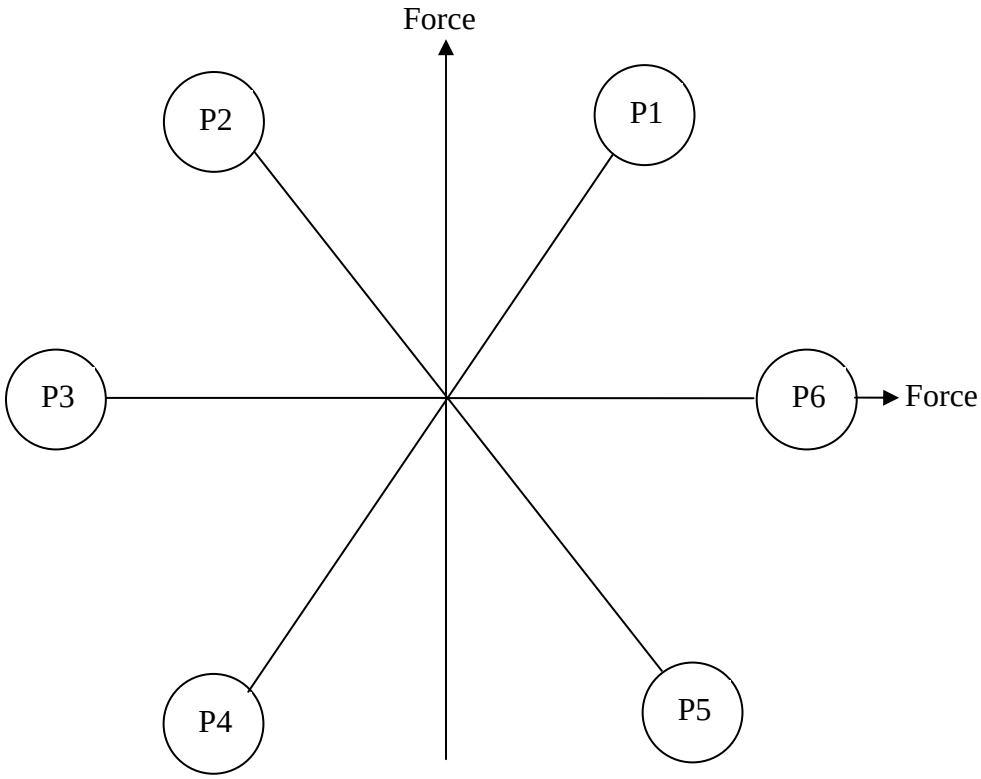

Figure 6.2 The Energized Four Poles (1, 2, 4, 5) of the Bearing

6.4 Calibration of Load Cells

A test was conducted utilizing static weights to check the calibration of the load cells. Weights were put in the bearing and the same test procedure was performed at room temperature. The calibration experiment shows that the load cells provide 90% of the actual value of the load (weight). The calibration process is shown in figure 6.3.

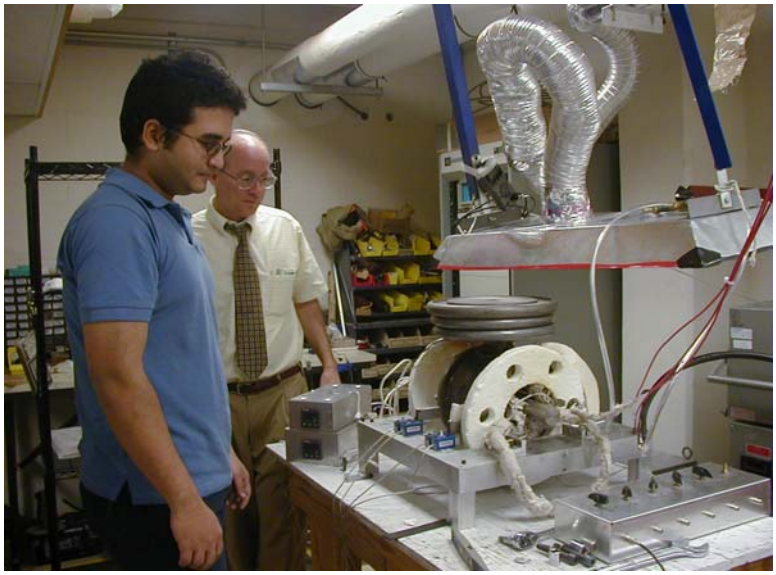

Figure 6.3 Calibration Test of the Load Cells and Test Procedure

6.5 Test Measurement

Temperature and current were the test variables. The same test procedure was performed for different currents at different temperatures. Current was varied by the linear switch amplifier and the desired temperature level was maintained by the temperature controller. The temperature was measured at various points of the bearing and rig by thermocouples. At a certain temperature the same test procedure was conducted for different amount of current. This was done to find out the relation of load and current and also for load and temperature.

The figure 6.4 shows the red hot color of stator and heater at 1000˚F which is the desired operating condition of the HTRMB. The temperature map over different parts of the bearing and rig are shown in figure 6.5 and 6.6. The temperatures at different points of the bearing systems are shown in table 6.1.

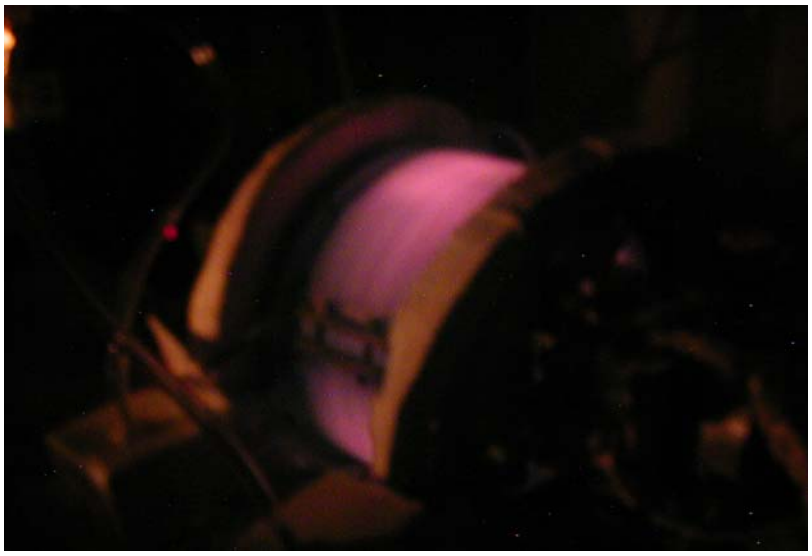

Figure 6.4 The Red Hot Color of the Stator at 1000˚F

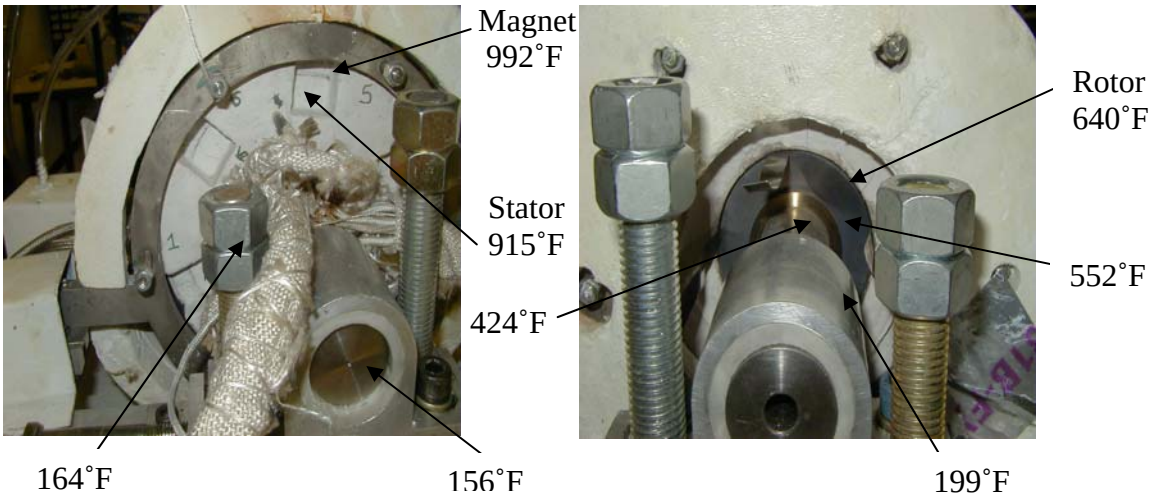

Figure 6.5 Temperature Map at Different Points of the Bearing

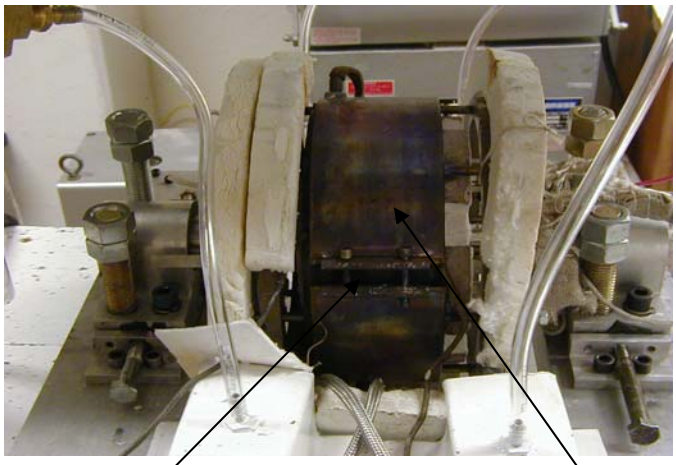

Figure 6.6 Temperature at Back Iron and Heater

Table 6.1 Temperature Distribution of Bearing

Band heater	1116˚F
Back Iron	1035˚F
Magnet	992˚F
Stator	915˚F
Rotor	640˚F

6.6 Results and Discussion

The Force versus Current graph (31st January 2006) shows that the load is nearly linear with current. A 550 watt linear amplifier was employed with a maximum voltage (36V) and a maximum current (15 amps). The resistance of the coils increases with temperature which eventually requires a voltage greater than 36V to drive 15 amps at 1000F. At the time of this test because of the unavailability of a higher voltage supply measurement was not taken at 15 amps and 1000˚F. A measurement at 14 ampere and 1000˚F was made. The plot of force versus. current is almost linear allowing the load at 15 ampere and 1000˚F to be estimated by extrapolation to be approximately 375 lb_f.

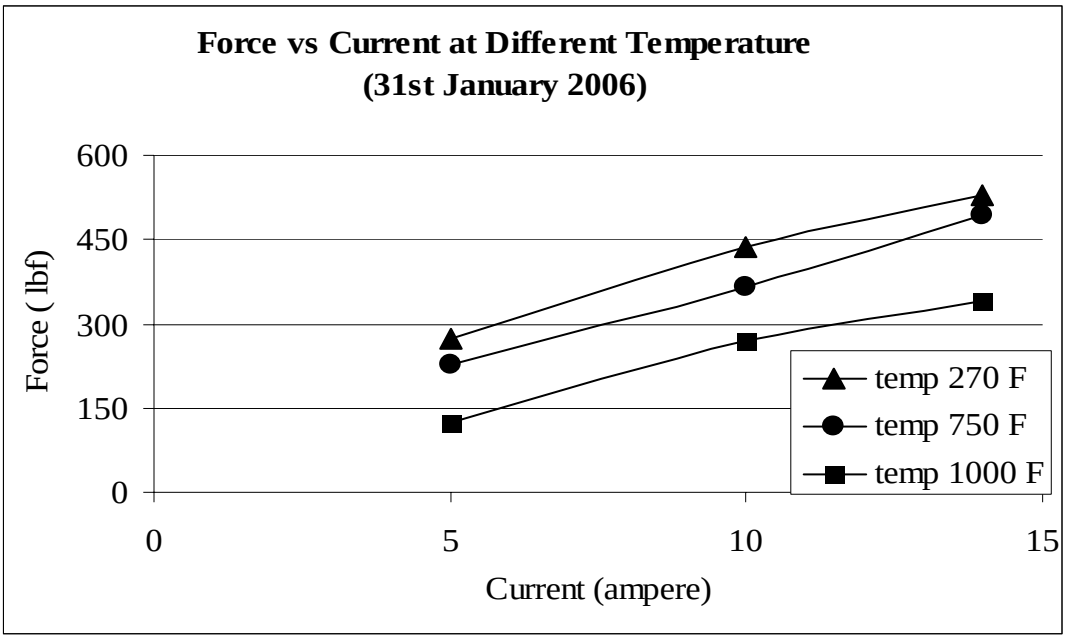

Figure 6.7 Force versus Current at Different Temperature (31st January 2006)

The drop in force with increasing temperature is most likely due to two causes:

- Increase in gaps between rotor and stator with temperature as flux density is inversely proportional to gap and force is quadratic to flux density.
- The demagnetization of the magnet starts with increasing temperature. The Curie temperature (T_c) is the temperature at which the magnet will be completely demagnetized. Even though it may still be a magnetic material (a material that has the ability to retain a magnetic field when magnetized), it would have completely demagnetized.

The Force vs. Current graph (3rd February 2006) shows the same pattern of behavior as previous one. And the extrapolated prediction for load at 1000˚F temperature and 15 amps is 438.09 lbs. The extrapolated prediction for load (for 6 February 2006) is 402.42 lbs.

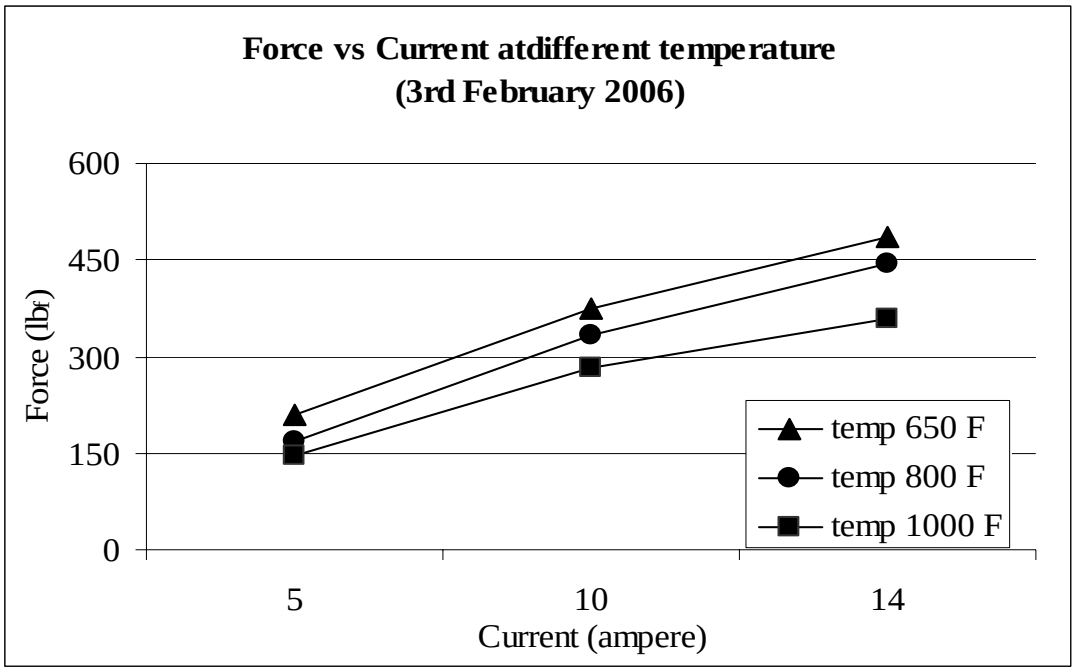

Figure 6.8 Force versus Current at Different Temperature (3rd February 2006)

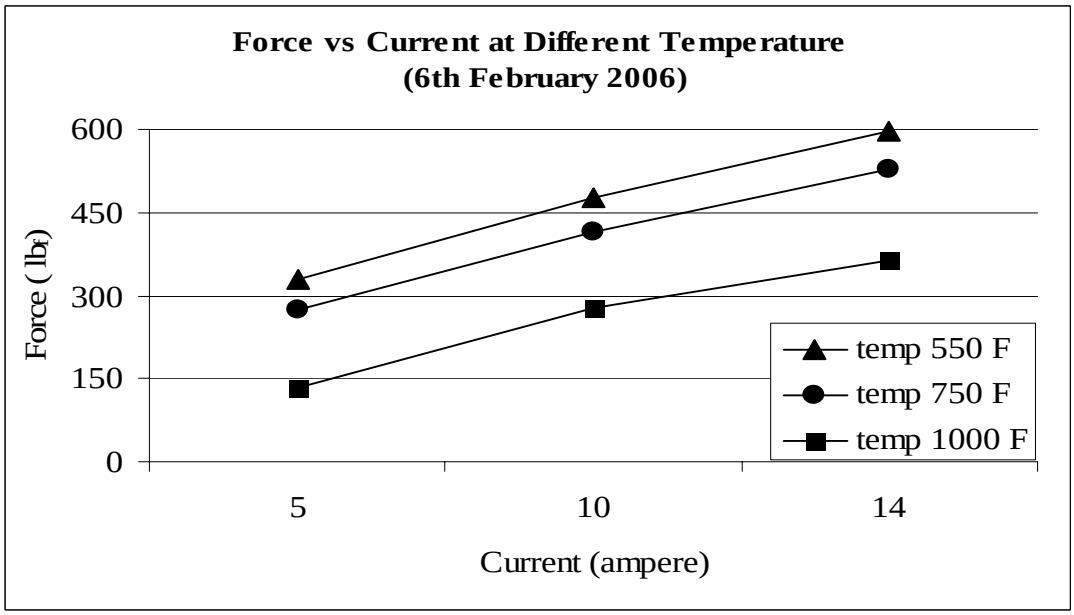

Figure 6.9 Force versus Current at Different Temperature (6th February 2006)

The relationship of force and temperature with current are shown in figures 6.10, 6.11, 6.12.

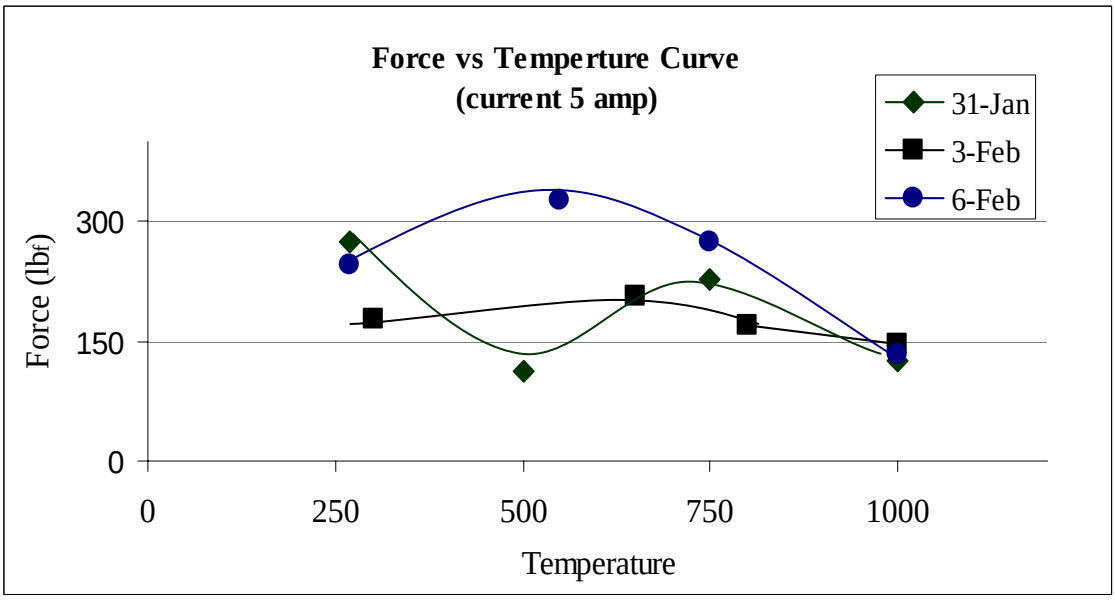

Figure 6.10 Force versus Temperature (Current 5 amps)

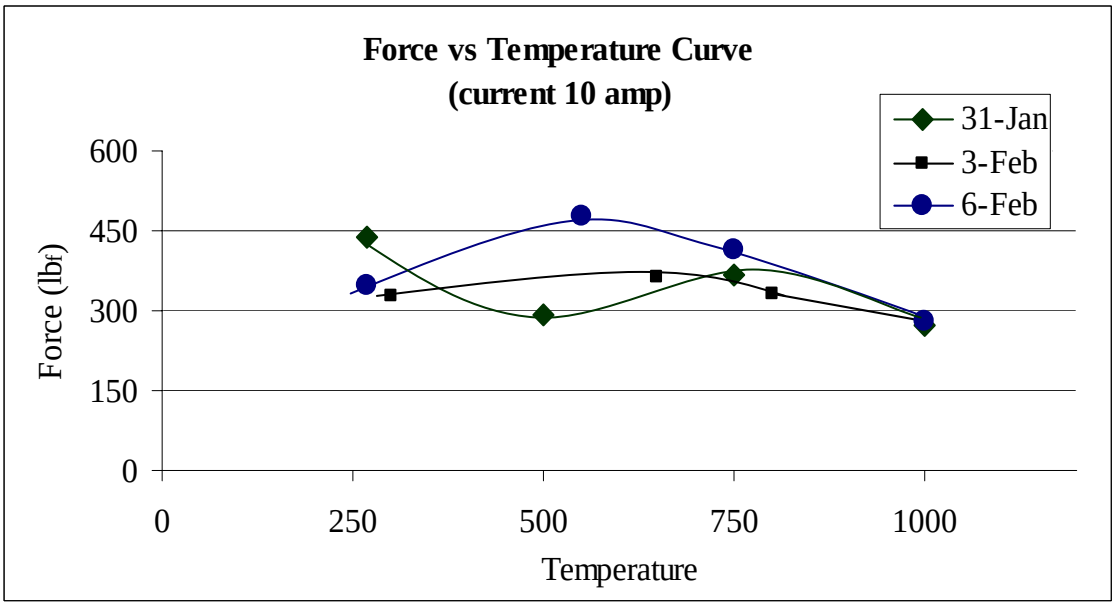

Figure 6.11 Force versus Temperature (Current 10 amps)

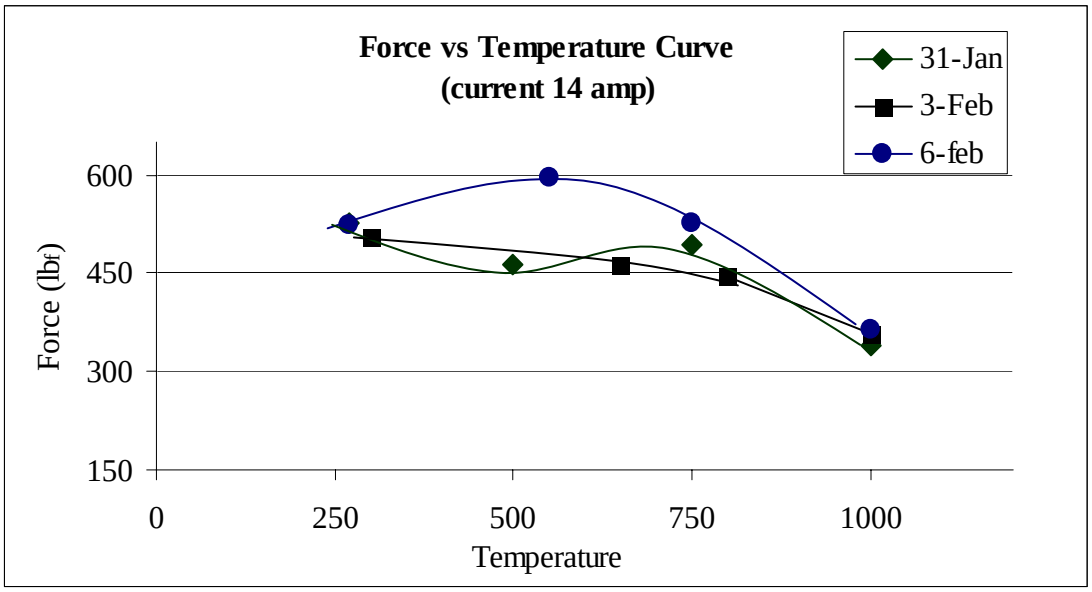

Figure 6.12 Force versus Temperature (Current 14 amps)

From the above three figures it is shown that force decreases with increasing temperature. It was estimated that the minimum rotor-stator gap is between 7 – 10 mils at room temperature and increases to approximately 20 mils at 1000˚F. Thus the uncertainty of centering increases with temperature. This was minimized by inserting larger shims into the gaps at certain points to assist in centering. Probably this explains the scatter in the data, and that when viewed as a whole the data provides a clear picture of force versus current relationship and it is close to the design value of 500 lb_f at 1000˚F.

6.7 Uncertainty Analysis

Uncertainty analysis is the relation between given variability and probability on input parameters and the variability and probability of output parameters. With this information, the engineer assesses the robustness of a design.

A probable bound on the error of an experiment can be estimated. This bound is called uncertainty. Each measurement includes some uncertainty, and these uncertainties will create an uncertainty in the calculated result. Finding the uncertainty in a result due to uncertainties in the independent variables is called the propagation of uncertainty. Under the approximation that y is a linear function of the independent variables (x_1, x_2, …

…, x_n) and each measured value has some uncertainty (u_1, u_2, … …, u_n) then the uncertainties will behave like standard deviations:

$$u_y = \sqrt{\left(\frac{\partial y}{\partial x_1}u_1\right)^2 + \left(\frac{\partial y}{\partial x_2}u_2\right)^2 + \ldots\ldots\ldots + \left(\frac{\partial y}{\partial x_n}u_n\right)^2} \quad \ldots\ldots\ldots\ldots\ldots\ldots (6.2)$$

The uncertainties, u_i may be either bias or precision uncertainties.

For the experiment:

$$F_m = K_p x + K_i i$$

$$Fi = K_i i = F_m - K_p x \quad \ldots\ldots\ldots\ldots\ldots\ldots\ldots\ldots\ldots.\ldots\ldots\ldots\ldots\ldots .. (6.3)$$

F_m = Measured force value (lb_f)

K_p = Stiffness (lb_f/inch)

Ki = Current stiffness (lb_f/ampere)

x = Displacement (inch)

And the values are:

F_m = 0.6 lb_f

K_p = 30800 lb_f/inch ± 1000 lb_f/inch

x = 0.02 inch ± 0.03 inch

$$\Delta Fi = \sqrt{\left(\frac{\partial Fi}{\partial F}\Delta F\right)^2 + \left(\frac{\partial Fi}{\partial K_p}\Delta K_p\right)^2 + \left(\frac{\partial Fi}{\partial x_n}\Delta x_n\right)^2}$$

$$\Delta Fi = \sqrt{(\Delta F)^2 + (-x\Delta K_p)^2 + (-K_p \Delta x_n)^2}$$

$$\Delta Fi = \sqrt{(0.6)^2 + (0.02 * 1000)^2 + (30800 * 0.003)^2}$$

$$\Delta Fi = 94.54 lb_f$$

The uncertainty in the measurement is mainly due to the position stiffness. Each time the stator changed its position and the rotor was tried to recenter manually. The uncertainty arises because of the fact that the rotor was not centered precisely all the time.

6.8 Bearing Failure

The whole procedure for design, assembly and measurement of load for high temperature radial magnetic bearing was time consuming and constantly required innovation and modification to achieve the goal at every steps.

Initially the rig was not stiff enough to conduct the test. To investigate this gooseneck and dial indicators were installed in the base to measure the movements of the rotor and stator on both vertical and horizontal direction. To stiffen the rig a lot of changes in the test rig were done. First the position of the load cells was changed to make the bearing stiffer. But it was proven not enough. So changed the shape of the spokes that hold the stator with back iron and the stator support was changed**.** After changing the shape of spokes and positions of the load cells the rig became stiffer.

At higher temperature (500˚F) because of the changes of dimension of the bearing all the shims were not loose and also four load cells were not enough to support the whole bearing. So four extra load cells with the existing load cells were installed and lifted the whole bearing to cover the thermal growth and put piece of iron over the load cells to adjust the distance.

The operating temperature for the bearing was 1000˚F. It took 5/6 hours for achieving 1000˚F temperatures. With linear power amplifier the reading at 1000˚F with 15 ampere current was not conducted. At higher temperature the resistance of the wire increased so it required a more powerful power supply to push a current of 15 ampere. So the Linear Amplifier was replaced by Switching Amplifier. At that time one of the coils shorted to the ground was found. So the whole bearing was reassembled in the test rig to change the position of the coils. After repositioning of the coils, the experiment was conducted with the switching amplifier. But at that time an Open Voltage was found in the circuit. This could happen because of the fact that at high temperature the coil wire might melt (because of higher resistance of coil at high temperature) and showed an open voltage. And after that the whole bearing was tearing down to investigate the problems for improvement of the bearing fabrication in future.

CHAPTER VII

CONCLUSION AND FUTURE WORKS

This thesis was an investigation to fulfill the objective whether it was possible to design a permanent bias Homopolar radial magnetic bearing that will operate reliably under the conditions set by the EEC sponsors, namely:

- Operating temperature of 1000^{o}F
- 500 lb_f capacity of radial load

The simulations, design and tests that had been employed to answer this question included the following:

- 3-D magnetic field analysis
- Saturation flux density test of AISI 1010
- A test rig design and fabrication
- An experimental procedure development to test the load capacity of the bearing

The results of the research showed that all of the design objectives set forth by EEC sponsor are satisfied. The test rig is capable to measure the actual load capacity of the bearing to near design values. Though the rotor is not levitated and the shaft is stationary, the test demonstrates the baseline industry performance characteristics of magnetic bearing for actual hardware.

The performance of the EEC permanent magnets for providing significant bias flux for the HTRMB at a temperature of 1000^{o}F is truly remarkable and will significantly enhance the prospects for commercialization of high temperature magnetic bearings and motors.

7.1 Future Works

The future works is to design and develop a universal test rig with radial and thrust bearing. The following changes will be implemented to increase the reliability of the HTRMB at 1000˚F with 15 amps operating state, and to facilitate its assembly.

- Rebuild HTRMB with 16 gage wire and thicker bobbin material so that the heat generation will be less at higher temperature.
- Dummy stator and mold parts are to be made for an experiment to verify the effectiveness of the lower gage wire and thicker bobbin.
- Improved Test rig design for HTRMB for easier alignment of stator and rotor
- Axially splitting the Back Iron so that the stator could be installed easily within it.
- Reducing the thickness of the potting material in the bearing.
- Improved mold design.

7.2 Dummy Stator Pole Tests for Improving Coil Integrity

The Radial Bearing experienced a short between a coil and a pole, and an open circuit, when the current was raised to 15 amps at 1000F. In order to remedy this weakness for future radial bearing a dummy pole was machined and wrapped with an improved bobbin along with employing 16 gage wires in place of the 19 gage wire. In addition the edges of the dummy pole were intentionally left in a sharpened state to expose the coils to the worst scenario conditions. The figure 7.1 and 7.2 show the dummy pole and experimental setup respectively.

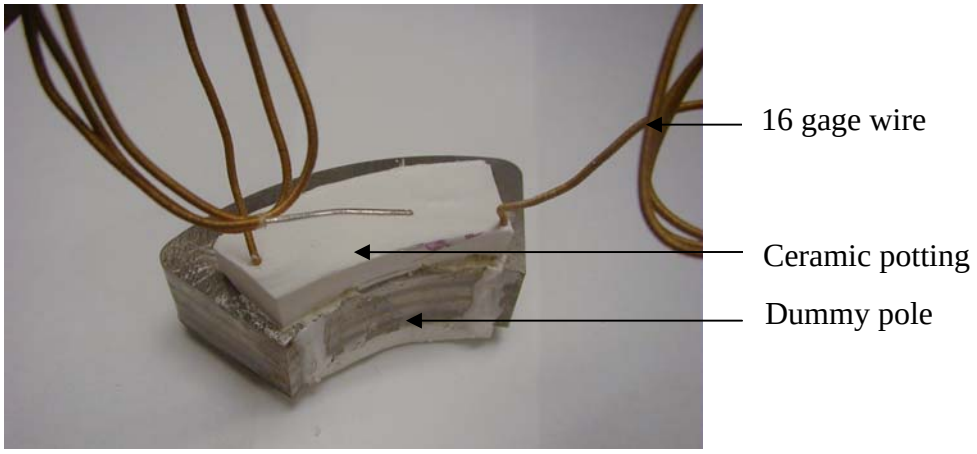

Figure 7.1 Dummy Pole Prior to Testing

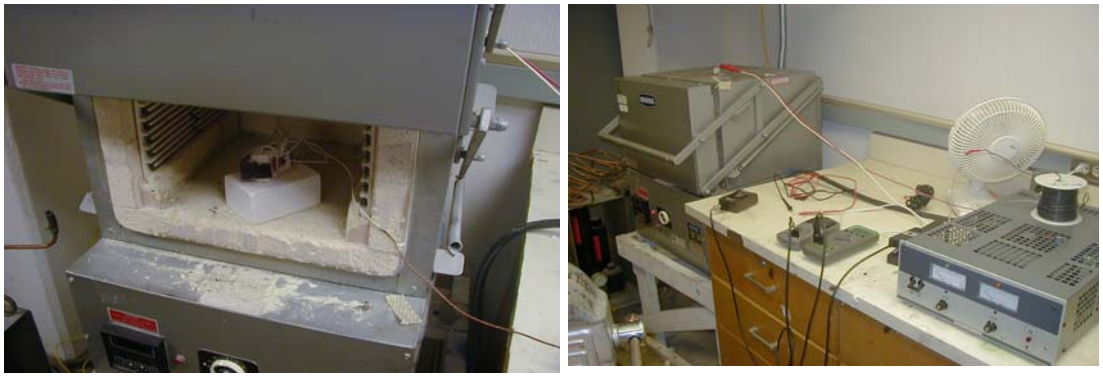

Figure 7.2 Experimental Setup for Dummy Pole Testing

Fifteen cycles of current at 16 and 20 amps were applied at every test temperature (1000˚F, 1250˚F, 1400˚F, 1500˚F). Each cycle lasted for approximately 3 minutes and the temperatures were measured directly on the ceramic surface of the coil. These conditions were considered to provide a very conservative test for the new radial bearing which is planned to operate with a maximum temperature of only 1000˚F and maximum current of only 15 amps. The ceramic coil cover on one side of the dummy pole showed a hairline crack and the cover on the other side did not have any cracks. The discoloration shown in figure 7.3 on the ceramic cover resulted from the attachment of the thermocouple.

Figure 7.3 Condition of Dummy Pole after the Experiment

7.3 Improved Test Rig Design for HTRMB

An improved HTRMB test fixture concept for measuring the bearing force vs. current and temperature is also developed. This fixture will be much stiffer so that the problems due to the attraction force between the rotor and stator will be eliminated. Finite element analysis is performed to design the bearing support. The fixture utilizes two dimensional positioning tables at each bearing to facilitate rotor-stator alignment precisely. Finally the new fixture design will employ high temperature position sensors which will accurately indicate the rotor-stator alignment. The figure 7.4 shows the new test rig design concept.

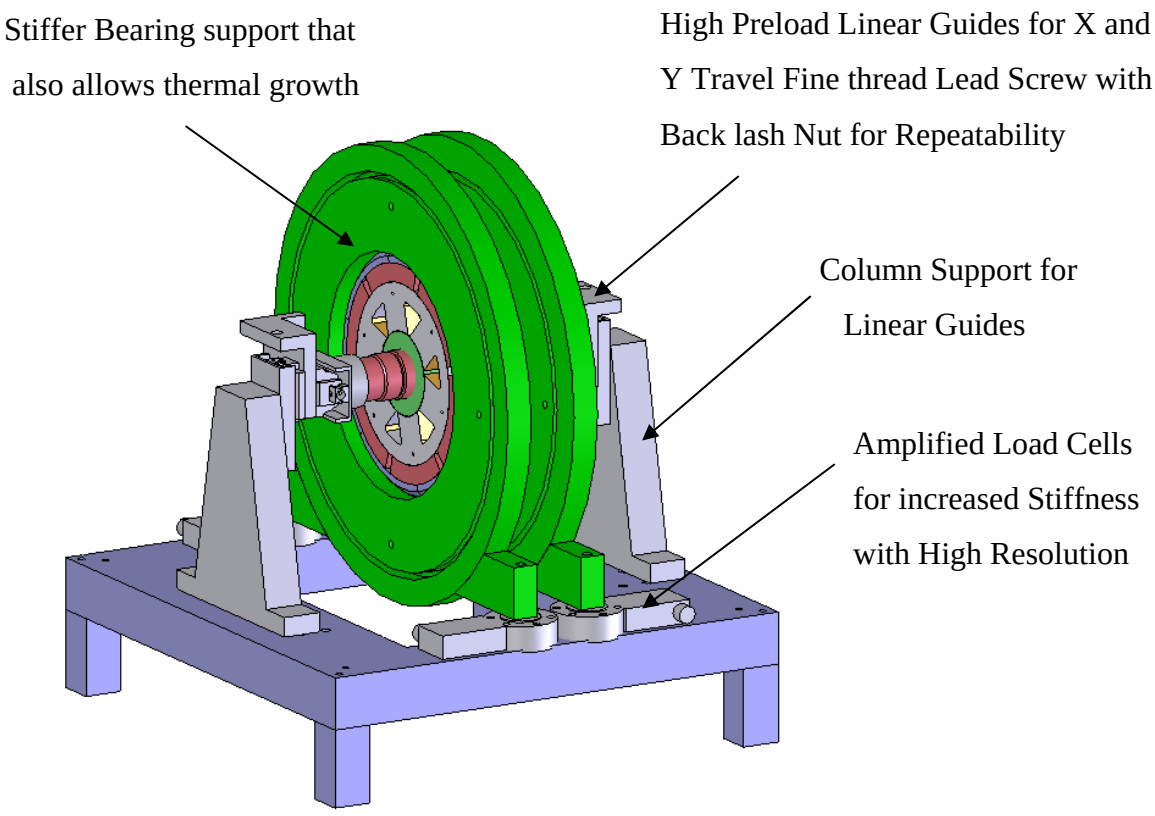

Figure 7.4 Solid Model of New Test Rig Design Concept

7.4 Benefit of Research

The efficiency of magnetic bearings operating at ultra high temperatures will be significantly enhanced by the proposed Homopolar, high temperature magnetic bearings. This results from the bias flux being supplied entirely by permanent magnets with the Homopolar design instead of by electromagnet coils, as employed with heteropolar magnetic bearings. This reduces ohmic losses significantly. This concept will be of a great aid to the next generation Magnetic bearing design.

REFERENCES

[1] Provenza, A., Montague, G., Jansen, M., Palazzolo, A., Jansen, R., 2005, “High Temperature Characterization of a Radial Magnetic Nearing for Turbomachinery,” Journal of Engineering for Gas Turbines and Power, **127,** pp.437-444.

[2] Bornstein, K. R., 1990, “Dynamic Load Capabilities of Active Electromagnetic Bearings,” Journal of Tribology, **90**-Trib-50, pp. 1-6.

[3] Schweitzer, G., Bleuler, H., Traxler, A., 1994, “Basics, Properties and Applications of Active Magnetic Bearings,” Active Magnetic Bearings, **210**, pp. 1-112.

[4] DeWeese, R.T., 1996, “A Comparison of Eddy Current Effects in a Single Sided Magnetic Thrust Bearing,” M.S. Thesis, Department of Mechanical Engineering, Texas A&M University, College Station.

[5] Polajzer, B, 2003, “Design and Analysis of an Active Magnetic Bearing Experimental System”, Ph. D. Dissertation, Department of Electrical Engineering and Computer Science, University of Maribor, Slovenia

[6] Schweitzer, G., Bleuler, H., Traxler, A., 1994, “Basics, Properties and Applications of Active Magnetic Bearings,” Active Magnetic Bearings, **210**, pp. 1-112.

[7] Meeks, C. R., DiRusso, E., and Brown, G. V., 1990, "Development of a Compact, Light Weight Magnetic Bearing," *Proceedings of the 26th Joint Propulsion Conference* AIAA/SAE/ASME/ASEE, Orlando.

[8] Sortore, C. K., Allaire, P. E., Maslen, E. H., Humphris, R. R., and Studer, P. A., 1990, "Permanent Magnetic Biased Bearings—Design, Construction, and Testing," *Proceedings of the Second International Symposium on Magnetic Bearings*, Tokyo, pp. 175–182.

[9] Lee, A., Hsio, F., and Ko, D., 1994, “Analysis and Testing of Magnetic Bearing With Permanent Magnets for Bias,” JSME Int. J., Ser. C, **37**, pp. 774-782.

[10] Imlach, J., Blair, B. J., and Allaire, P. E., 1990, "Measured and Predicted Force and Stiffness Characteristics of Industrial Magnetic Bearings," *Joint ASME/STLE Tribology Conference*, Toronto, **90**-Trib-70.

[11] Fittro, R. L., Baun, D. O., Maslen, E. H., and Allaire, P. E., 1997, "Calibration of an 8-Pole Planar Radial Magnetic Actuator," *Proceedings of the 1997 International Gas Turbine & Aeroengine Congress & Exposition*, Orlando, **97**-GT-18.

[12] Kenny, A., Palazzolo, A., 2003, "Single Plane Radial, Magnetic Bearings Biased With Poles Containing Permanent Magents," Transactions of the ASME, **125**, pp. 178-185.

[13] Masayuk, Y., "Magnetic Bearing Device," Japanese patent 11101234A, 1999.

[14] Nagahiko, N., "Magnetic Bearing," Japanese patent 61180019A, 1986.

Supplementary Sources Consulted

Ashby, M. F., 1999, *Materials Selection in Mechanical Design*, 2nd Edition, Butterworth Heiemann.

ASTM Designation A 773/ A 773M-96, "Standard Test Method for DC Magnetic Properties of Materials Using Ring and Permeameter Procedures with DC Electronic Hystersigraph," American Society of Testing and Materials, Philadelphia, pp. 155-163.

Minihan, T. and Palazzolo, A.B., et al, 2002, "Fail Safe, High Temperature Magnetic Bearings", *ASME Turbo Expo 2002*, June 3-6, 2002, Amsterdam, Paper no. GT-2002-30595, pp. 1-10.

Mohiuddin, M., 2002, "Design of high Temperature high Speed Electromagnetic Axial Thrust Bearing," M.S. Thesis, Department of Mechanical Engineering, Texas A&M University, College Station.

Palazzolo, A., Kim, Y., Tucker, R., Na, U.J., Lei, S., Montague, G.T., Provenza, A., Kascak, A. and Lingefelter, N., 2001, "Fail-Safe, High Temperature Magnetic Bearing for High Efficiency Gas Turbine Engine Applications," IGTI Turbo Expo. Conference, Paper 2001-GT-0295.

Preuss, J., 2004 "Design and Analysis of a Composite Flywheel Preload Loss Test Rig," M.S. Thesis, Department of Mechanical Engineering, Texas A&M University, College Station.

Provenza, A., Montague, G., Jansen, M., Palazzolo, A., 2003 “High Temperature Characterization of a Radial Magnetic Bearing for Turbomachinery,” *IGTI Conference 2003,* (2003-GT-38870).

Shigley, J., E., Mischke, C., R., 2001, *Mechanical Engineering Design*, 6th Edition, McGraw Hill, Inc.

Sue, S., 2004, *Class note for MEEN 632*, Deparment of Mechancial Engineering, Texas A & M University, College Station.

APPENDIX A

LENGTH AND RADIUS CALCULATION FOR SPOKES

LENGTH AND RADIUS CALCULATION FOR SPOKES

The function of the spokes of test rig was to hold the bearing and also to allow the thermal expansion due to heating. The length and diameter of the spokes need to be calculated.

The thermal deflection of the spoke due to heat is δ_T.

$\delta_T = r\alpha T = 4.25 * 5.10^{-6} * 1000 = 21.25.10^{-3} inch$

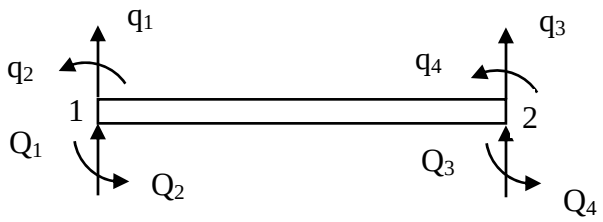

Figure A.1 Simple Beam Nodal Notation

The force and moment for the simple beam can be shown by:

$$\begin{Bmatrix} Q_1 \\ Q_2 \\ Q_3 \\ Q_4 \end{Bmatrix} = \left[K_{ij} \right] \begin{Bmatrix} q_1 \\ q_2 \\ q_3 \\ q_4 \end{Bmatrix}$$

$$[K_{ij}] = \frac{2EI}{l^3} \begin{bmatrix} 6 & -3l & -6 & -3l \\ -3l & 2l^2 & 3l & l^2 \\ -6 & 3l & 6 & 3l \\ -3l & l^2 & 3l & 2l^2 \end{bmatrix}$$

$q_1 = 0$

$q_2 = 0$

$Q_3 = \frac{12EI}{l^3} \delta_T$

$Q_4 = \frac{6EI}{l^2} \delta_T$

Force, $V_{\max} = \frac{12EI}{l^3}\delta_T$

Moment, $M_{\max} = \frac{6EI}{l^2}\delta_T$

Total Stress, $\sigma_T = \frac{M_{\max}\frac{d}{2}}{I} + \frac{V_{\max}}{A}$

Or, $\sigma_T = \delta_T(\frac{\frac{d}{2}}{I}\frac{6EI}{l^2} + \frac{12EI}{l^3}\frac{1}{\frac{\pi d^2}{4}})$

Or, $\sigma_T = \delta_T E(\frac{3d}{l^2} + \frac{3d^2}{4l^3})$

and $\sigma_T = \delta_T E(\frac{3d}{l^2} + \frac{3d^2}{4l^3}) < \sigma_{\max}$ … … … … … … … … … … (i)

$\sigma_y = 140000\,psi$ (For Titanium)

$\sigma_{\max} = 100000\,psi$ (For Titanium)

K_s = Stiffness of individual spoke

K_t = Total stiffness of 12 spokes

F = Force exerted by the bearing

$K_t = 12 * \frac{12EI}{l^3}$

And $\delta_F = \frac{F}{K_t x}$

Or, $\delta_F = \frac{F}{144\frac{E}{l^3}\frac{\pi d^4}{64}}$

Or, $\delta_F = \frac{64Fl^3}{144\pi Ed^4}$ … (ii)

$E = 12.10^6\ psi$ (For Titanium)

$\delta_F = 0.003 inch$

$F = 500 lb_f$

$\sigma_{\max} = 100000\ psi$

$\delta_T = 22.10^{-3} inch$

By Solving the Equation (i) and Equation (ii) the radius and length of the spoke is obtained:

Length, l = 1.56 inch

Diameter, d = 0.29 inch

APPENDIX B

FABRICATOIN DRAWINGS FOR HTRMB

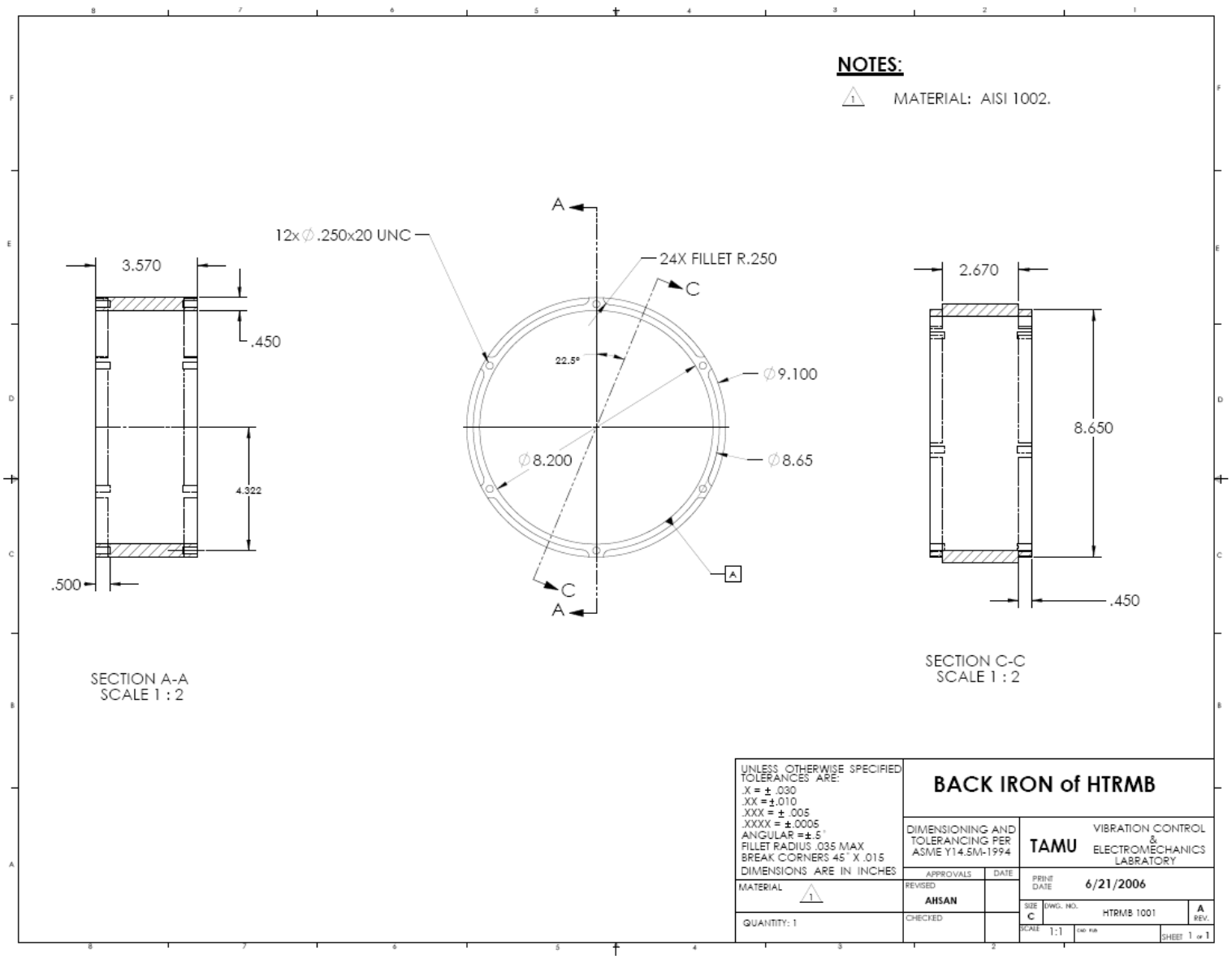
NOTES:
1 MATERIAL: AISI 1002.
12x ∅.250x20 UNC
24X FILLET R.250
22.5°
∅9.100
∅8.200
∅8.65
3.570
.450
4.322
.500
2.670
8.650
.450
SECTION A-A
SCALE 1 : 2
SECTION C-C
SCALE 1 : 2
UNLESS OTHERWISE SPECIFIED TOLERANCES ARE:
.X = ± .030
.XX = ± .010
.XXX = ± .005
.XXXX = ± .0005
ANGULAR = ± .5 °
FILLET RADIUS .035 MAX
BREAK CORNERS 45 ° X .015
DIMENSIONS ARE IN INCHES
MATERIAL
QUANTITY: 1
BACK IRON of HTRMB
DIMENSIONING AND TOLERANCING PER ASME Y14.5M-1994
APPROVALS
DATE
REVISED
AHSAN
CHECKED
TAMU
VIBRATION CONTROL & ELECTROMECHANICS LABRATORY
PRINT DATE
6/21/2006
SIZE C
DWG. NO.
HTRMB 1001
REV. A
SCALE 1:1
SHEET 1 of 1

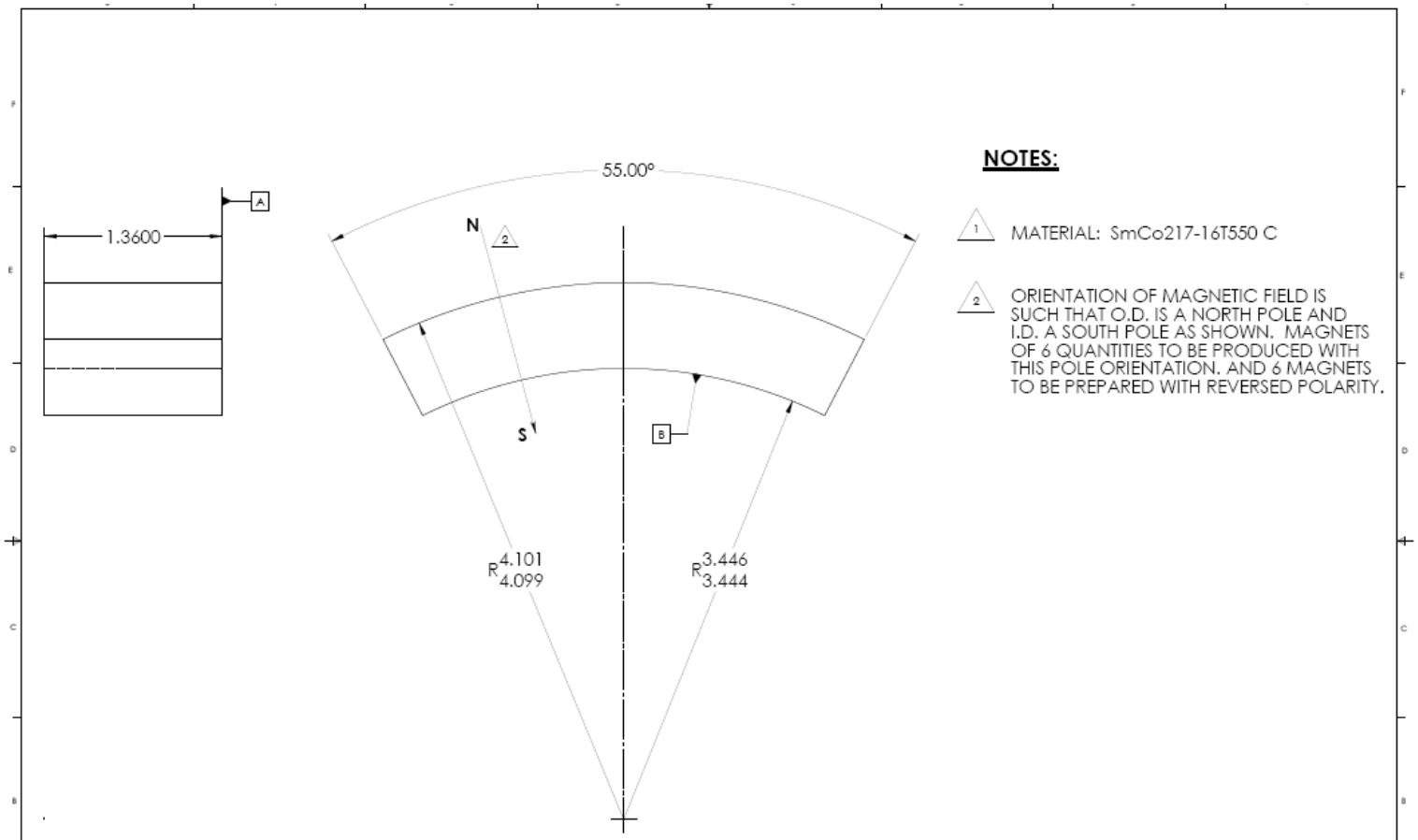
55.00°
1.3600
A
N
2
S
1
B
R 4.101 4.099
R 3.446 3.444
NOTES:
1 MATERIAL: SmCo217-16T550 C
2 ORIENTATION OF MAGNETIC FIELD IS SUCH THAT O.D. IS A NORTH POLE AND I.D. A SOUTH POLE AS SHOWN. MAGNETS OF 6 QUANTITIES TO BE PRODUCED WITH THIS POLE ORIENTATION. AND 6 MAGNETS TO BE PREPARED WITH REVERSED POLARITY.
UNLESS OTHERWISE SPECIFIED TOLERANCES ARE:
.X = ± .030
.XX = ± .010
.XXX = ± .005
.XXXX = ± .0005
ANGULAR = ± .5°
FILLET RADIUS .035 MAX
BREAK CORNERS .005 - .015
DIMENSIONS ARE IN INCHES
MATERIAL 1
FINISH
DO NOT SCALE DRAWING
MAGNET of HTRMB
DIMENSIONING AND TOLERANCING PER ASME Y14.5M-1994
APPROVALS DATE
REVISED AHSAN
quantity: 12
TAMU VIBRATION CONTROL & ELECTROMECHANICS LABRATORY
PRINT DATE 6/21/2006
SIZE C DWG. NO. HTRMB1oo2 A REV.
SCALE 1:1 SHEET 1 OF 1

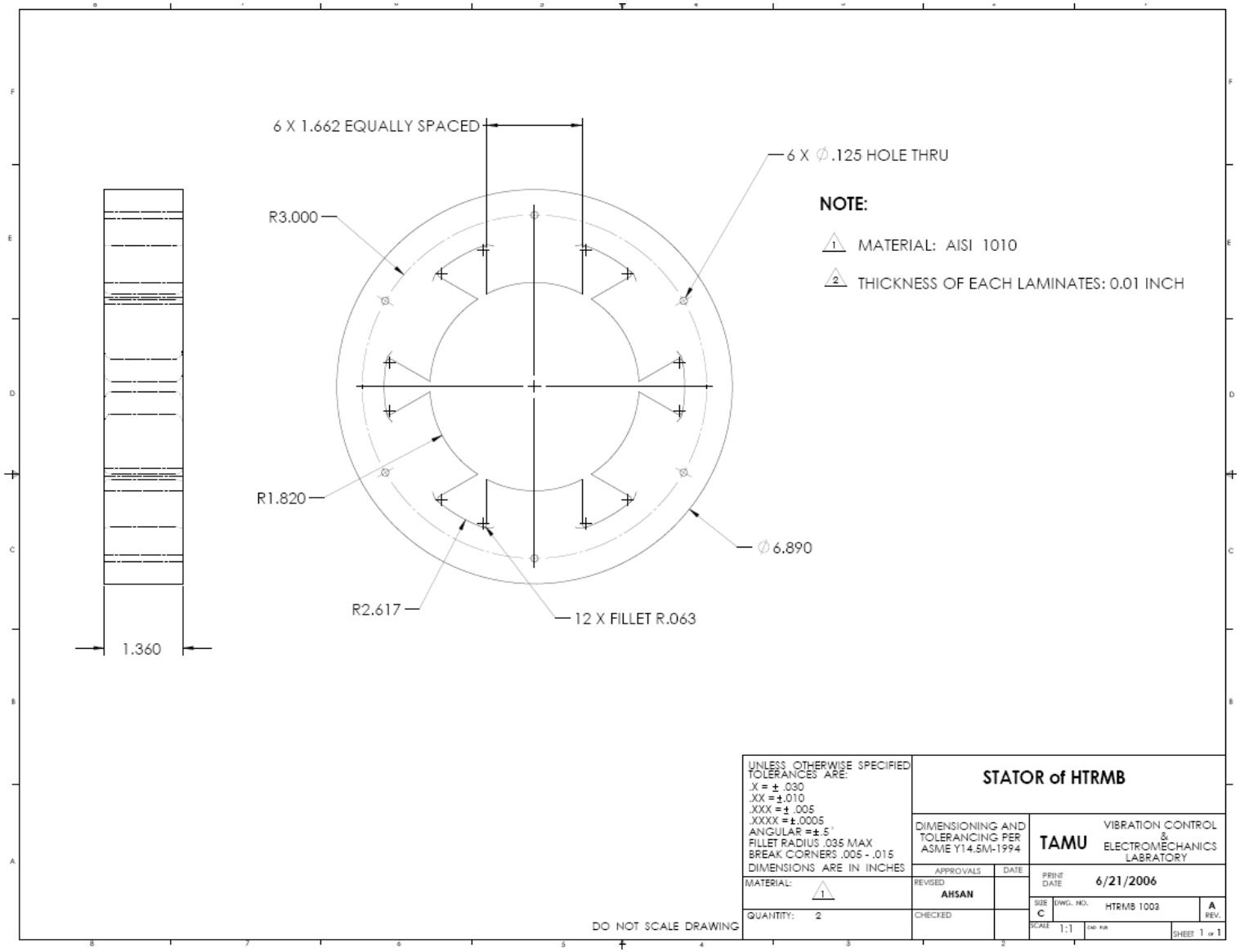
6 X 1.662 EQUALLY SPACED
6 X ∅.125 HOLE THRU
R3.000
R1.820
R2.617
12 X FILLET R.063
∅6.890
1.360
NOTE:
1 MATERIAL: AISI 1010
2 THICKNESS OF EACH LAMINATES: 0.01 INCH
UNLESS OTHERWISE SPECIFIED TOLERANCES ARE:
.X = ± .030
.XX = ±.010
.XXX = ± .005
.XXXX = ±.0005
ANGULAR = ± .5°
FILLET RADIUS .035 MAX
BREAK CORNERS .005 - .015
DIMENSIONS ARE IN INCHES
MATERIAL: 1
QUANTITY: 2
DO NOT SCALE DRAWING
STATOR of HTRMB
DIMENSIONING AND TOLERANCING PER ASME Y14.5M-1994
APPROVALS
DATE
REVISED
AHSAN
CHECKED
TAMU
VIBRATION CONTROL & ELECTROMECHANICS LABRATORY
PRINT DATE 6/21/2006
SIZE C
DWG. NO. HTRMB 1003
REV. A
SCALE 1:1
SHEET 1 OF 1

NOTES:

1. MATERIAL: HIPERCO 50HS
2. THIKCNESS OF EACH LAMINTES: 0.006 INCH

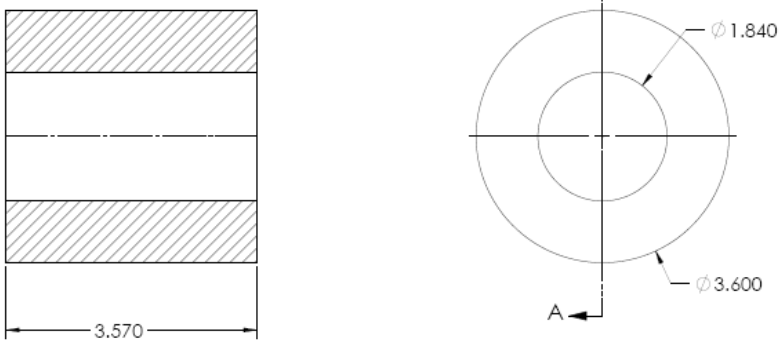

SECTION A-A

DO NOT SCALE DRAWING

UNLESS OTHERWISE SPECIFIED TOLERANCES ARE: .X = ± .030 .XX = ±.010 .XXX = ± .005 .XXXX = ±.0005 ANGULAR =±.5° FILLET RADIUS .035 MAX BREAK CORNERS 45° X .015 DIMENSIONS ARE IN INCHES	**ROTOR of HTRMB**	
	DIMENSIONING AND TOLERANCING PER ASME Y14.5M-1994	**TAMU** VIBRATION CONTROL & ELECTROMECHANICS LABRATORY
	APPROVALS / DATE	PRINT DATE 6/21/2006
MATERIAL	REVISED AHSAN	SIZE C / DWG. NO. HTRMB 1004 / REV. A
QUANTITY: 1	CHECKED	SCALE 1:1 / SHEET 1 OF 1

APPENDIX C

FABRICATOIN DRAWINGS FOR HTRMB TEST RIG

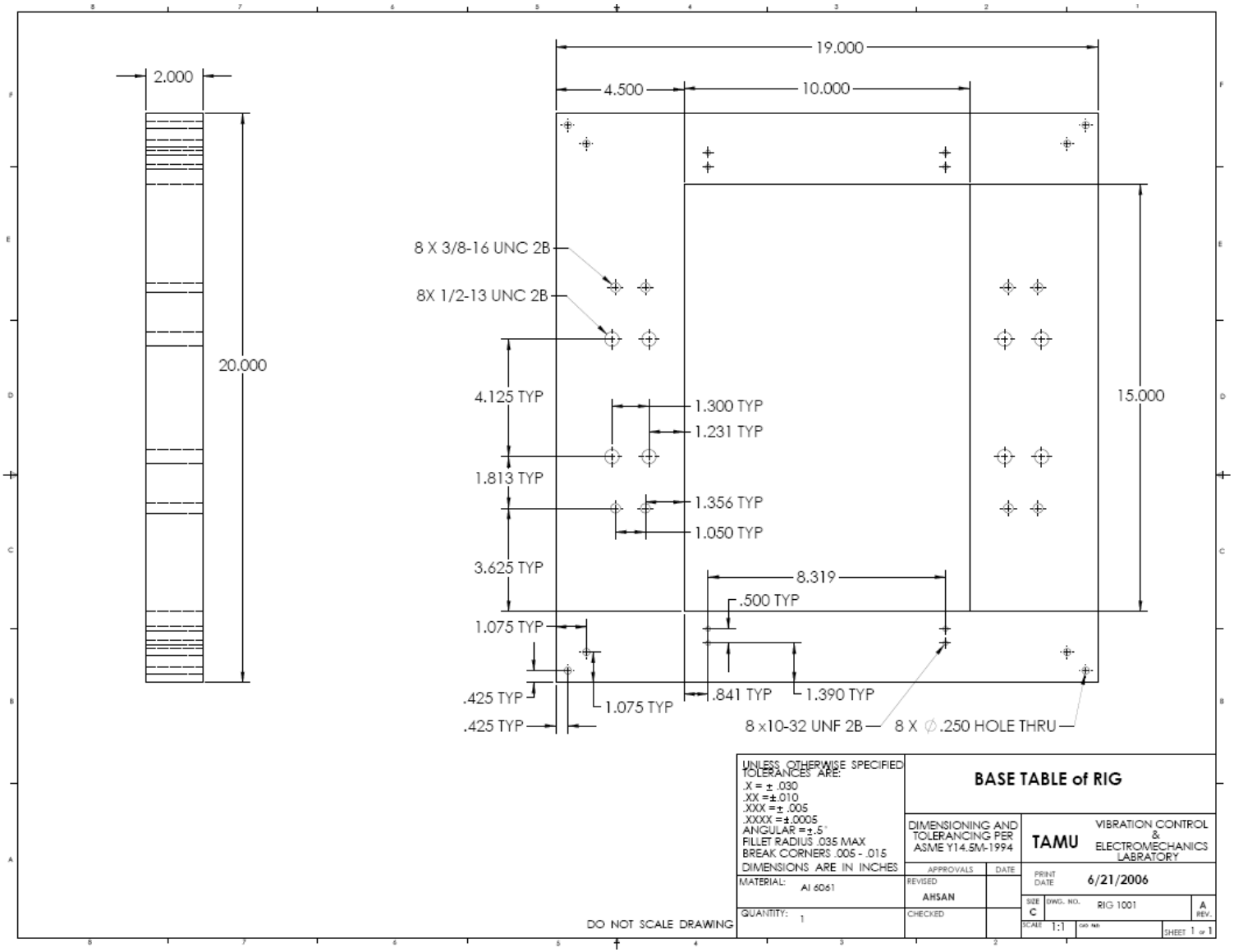
2.000
20.000
19.000
4.500
10.000
15.000
8 X 3/8-16 UNC 2B
8X 1/2-13 UNC 2B
4.125 TYP
1.813 TYP
3.625 TYP
1.075 TYP
.425 TYP
.425 TYP
1.300 TYP
1.231 TYP
1.356 TYP
1.050 TYP
8.319
.500 TYP
.841 TYP
1.390 TYP
1.075 TYP
8 x10-32 UNF 2B
8 X ∅.250 HOLE THRU
DO NOT SCALE DRAWING
UNLESS OTHERWISE SPECIFIED TOLERANCES ARE:
.X = ± .030
.XX =±.010
.XXX =± .005
.XXXX =±.0005
ANGULAR =±.5°
FILLET RADIUS .035 MAX
BREAK CORNERS .005 - .015
DIMENSIONS ARE IN INCHES
MATERIAL: Al 6061
QUANTITY: 1
BASE TABLE of RIG
DIMENSIONING AND TOLERANCING PER ASME Y14.5M-1994
APPROVALS
DATE
REVISED
AHSAN
CHECKED
TAMU
VIBRATION CONTROL & ELECTROMECHANICS LABRATORY
PRINT DATE 6/21/2006
SIZE C
DWG. NO. RIG 1001
REV. A
SCALE 1:1
SHEET 1 of 1

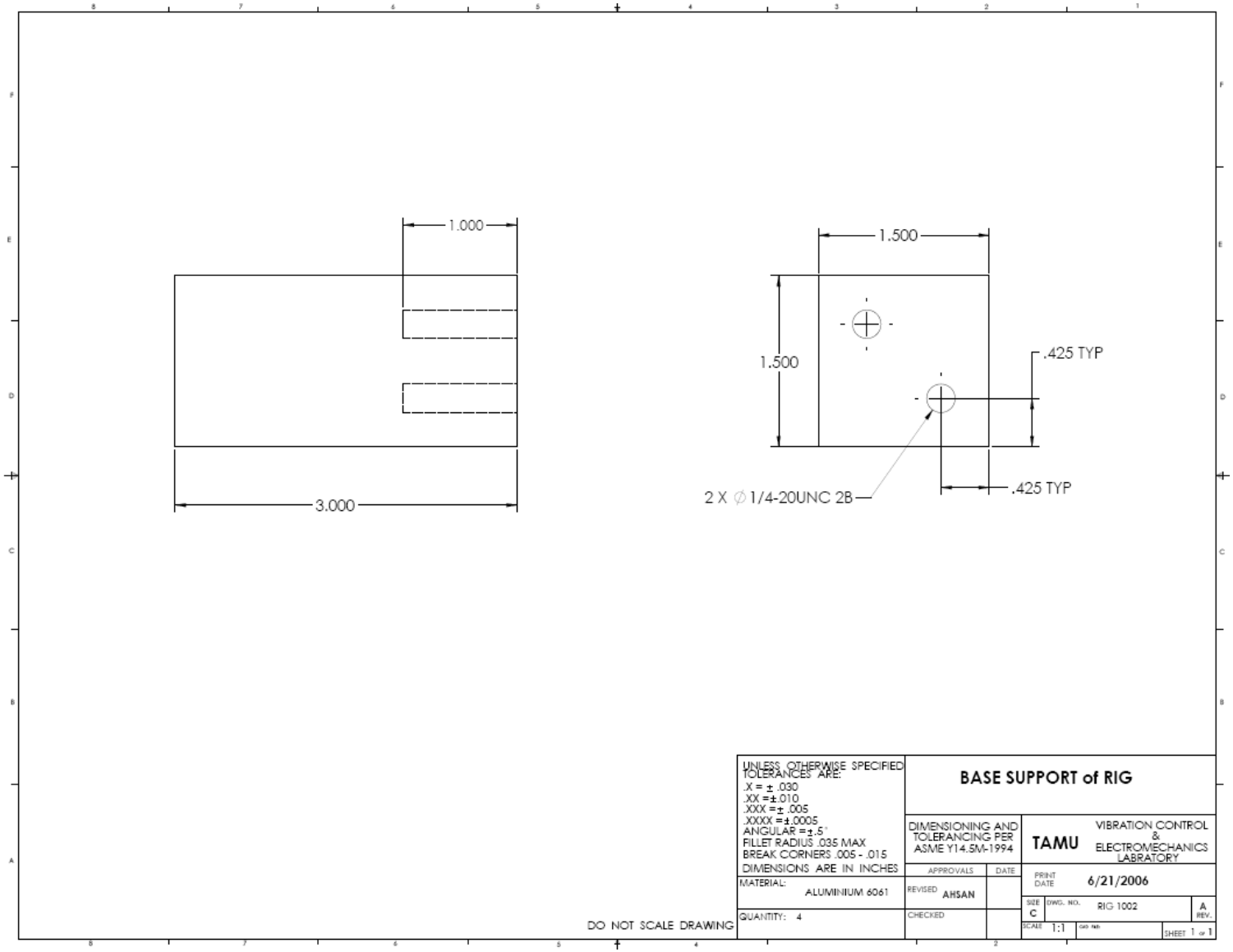
1.000
3.000
1.500
1.500
.425 TYP
.425 TYP
2 X ∅1/4-20UNC 2B
UNLESS OTHERWISE SPECIFIED TOLERANCES ARE:
.X = ± .030
.XX =±.010
.XXX =± .005
.XXXX =±.0005
ANGULAR =±.5°
FILLET RADIUS .035 MAX
BREAK CORNERS .005 - .015
DIMENSIONS ARE IN INCHES
MATERIAL: ALUMINIUM 6061
QUANTITY: 4
DO NOT SCALE DRAWING
BASE SUPPORT of RIG
DIMENSIONING AND TOLERANCING PER ASME Y14.5M-1994
APPROVALS
DATE
REVISED AHSAN
CHECKED
TAMU
VIBRATION CONTROL & ELECTROMECHANICS LABRATORY
PRINT DATE 6/21/2006
SIZE C
DWG. NO. RIG 1002
A
REV.
SCALE 1:1
SHEET 1 of 1

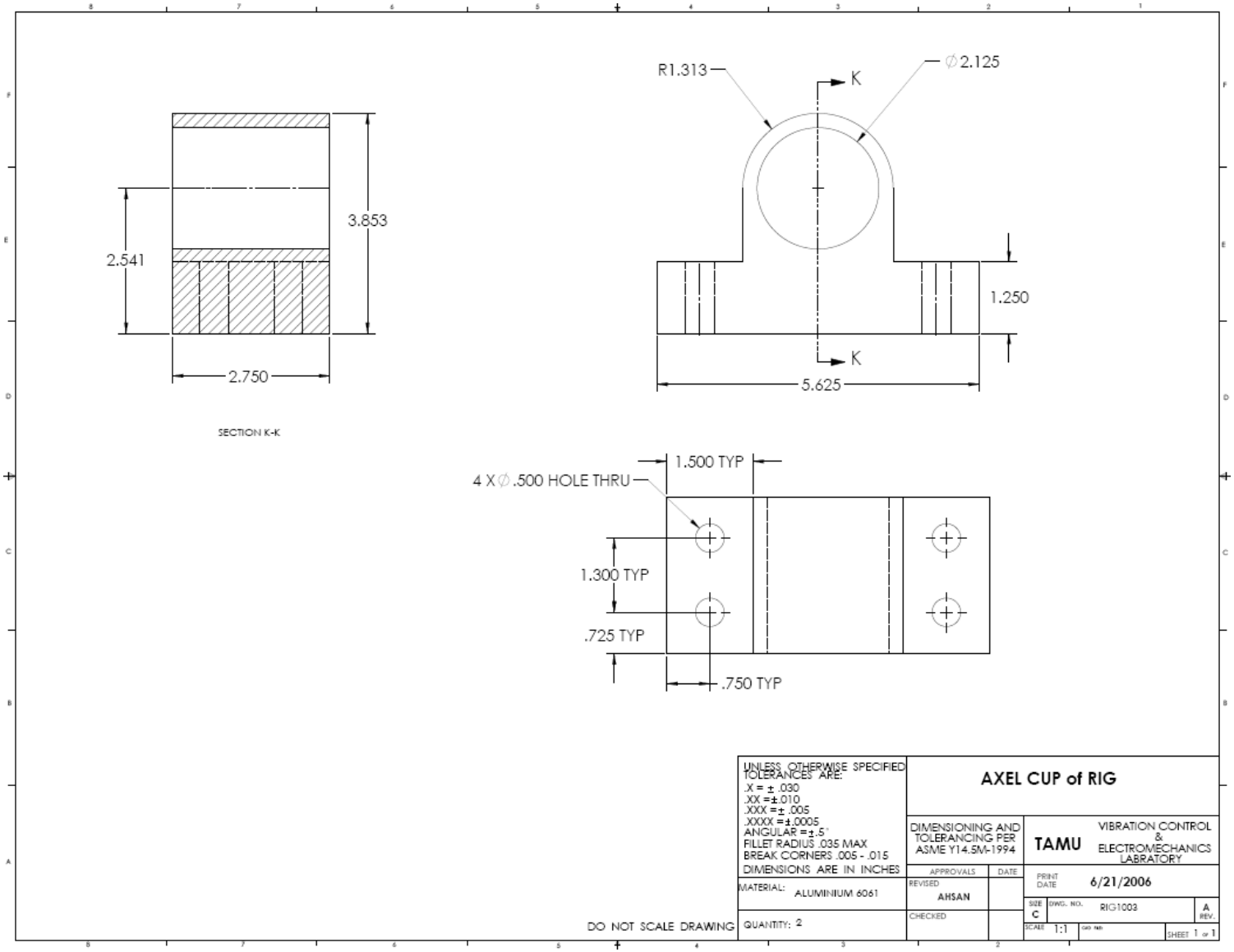
R1.313
K
∅2.125
3.853
2.541
1.250
K
2.750
5.625
SECTION K-K
1.500 TYP
4 X ∅.500 HOLE THRU
1.300 TYP
.725 TYP
.750 TYP
UNLESS OTHERWISE SPECIFIED TOLERANCES ARE:
.X = ± .030
.XX =±.010
.XXX =± .005
.XXXX =±.0005
ANGULAR =±.5°
FILLET RADIUS .035 MAX
BREAK CORNERS .005 - .015
DIMENSIONS ARE IN INCHES
MATERIAL: ALUMINIUM 6061
QUANTITY: 2
DO NOT SCALE DRAWING
AXEL CUP of RIG
DIMENSIONING AND TOLERANCING PER ASME Y14.5M-1994
APPROVALS
DATE
REVISED
AHSAN
CHECKED
TAMU
VIBRATION CONTROL & ELECTROMECHANICS LABRATORY
PRINT DATE
6/21/2006
SIZE C
DWG. NO.
RIG1003
A
REV.
SCALE 1:1
SHEET 1 of 1

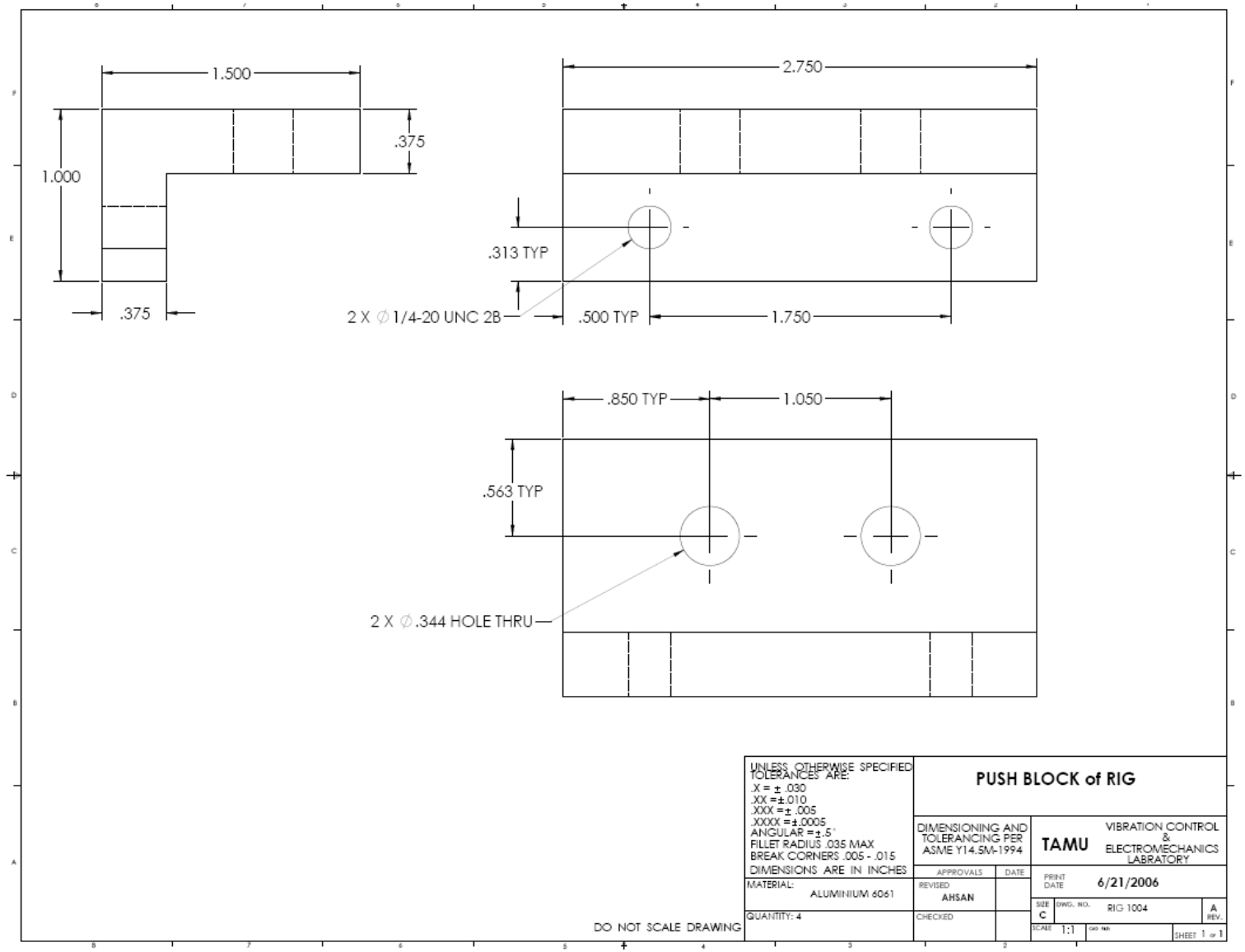
1.500
.375
1.000
.375
2.750
.313 TYP
2 X ∅1/4-20 UNC 2B
.500 TYP
1.750
.850 TYP
1.050
.563 TYP
2 X ∅.344 HOLE THRU
UNLESS OTHERWISE SPECIFIED TOLERANCES ARE:
.X = ± .030
.XX =±.010
.XXX =± .005
.XXXX =±.0005
ANGULAR =±.5°
FILLET RADIUS .035 MAX
BREAK CORNERS .005 - .015
DIMENSIONS ARE IN INCHES
MATERIAL: ALUMINIUM 6061
QUANTITY: 4
DO NOT SCALE DRAWING
PUSH BLOCK of RIG
DIMENSIONING AND TOLERANCING PER ASME Y14.5M-1994
APPROVALS
DATE
REVISED
AHSAN
CHECKED
TAMU
VIBRATION CONTROL & ELECTROMECHANICS LABRATORY
PRINT DATE 6/21/2006
SIZE C
DWG. NO. RIG 1004
A
REV.
SCALE 1:1
SHEET 1 of 1

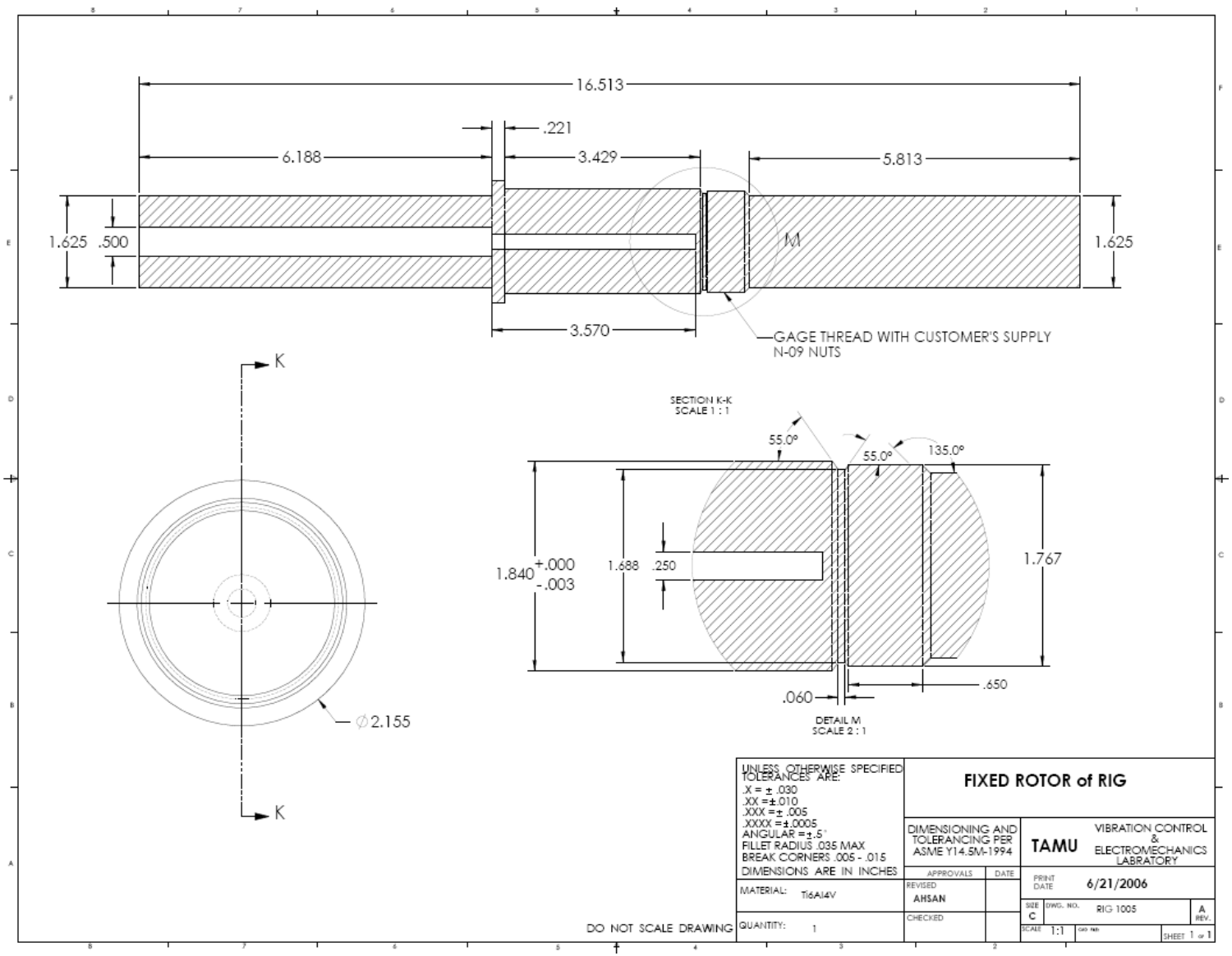
16.513
.221
6.188
3.429
5.813
1.625
.500
1.625
3.570
M
GAGE THREAD WITH CUSTOMER'S SUPPLY
N-09 NUTS
K
K
Ø2.155
SECTION K-K
SCALE 1 : 1
55.0°
55.0°
135.0°
1.840 +.000 -.003
1.688
.250
1.767
.650
.060
DETAIL M
SCALE 2 : 1
UNLESS OTHERWISE SPECIFIED TOLERANCES ARE:
.X = ± .030
.XX =±.010
.XXX =± .005
.XXXX =±.0005
ANGULAR =±.5°
FILLET RADIUS .035 MAX
BREAK CORNERS .005 - .015
DIMENSIONS ARE IN INCHES
DO NOT SCALE DRAWING
MATERIAL: Ti6Al4V
QUANTITY: 1
FIXED ROTOR of RIG
DIMENSIONING AND TOLERANCING PER ASME Y14.5M-1994
APPROVALS
DATE
REVISED
AHSAN
CHECKED
TAMU
VIBRATION CONTROL & ELECTROMECHANICS LABRATORY
PRINT DATE 6/21/2006
SIZE C
DWG. NO. RIG 1005
REV. A
SCALE 1:1
SHEET 1 of 1

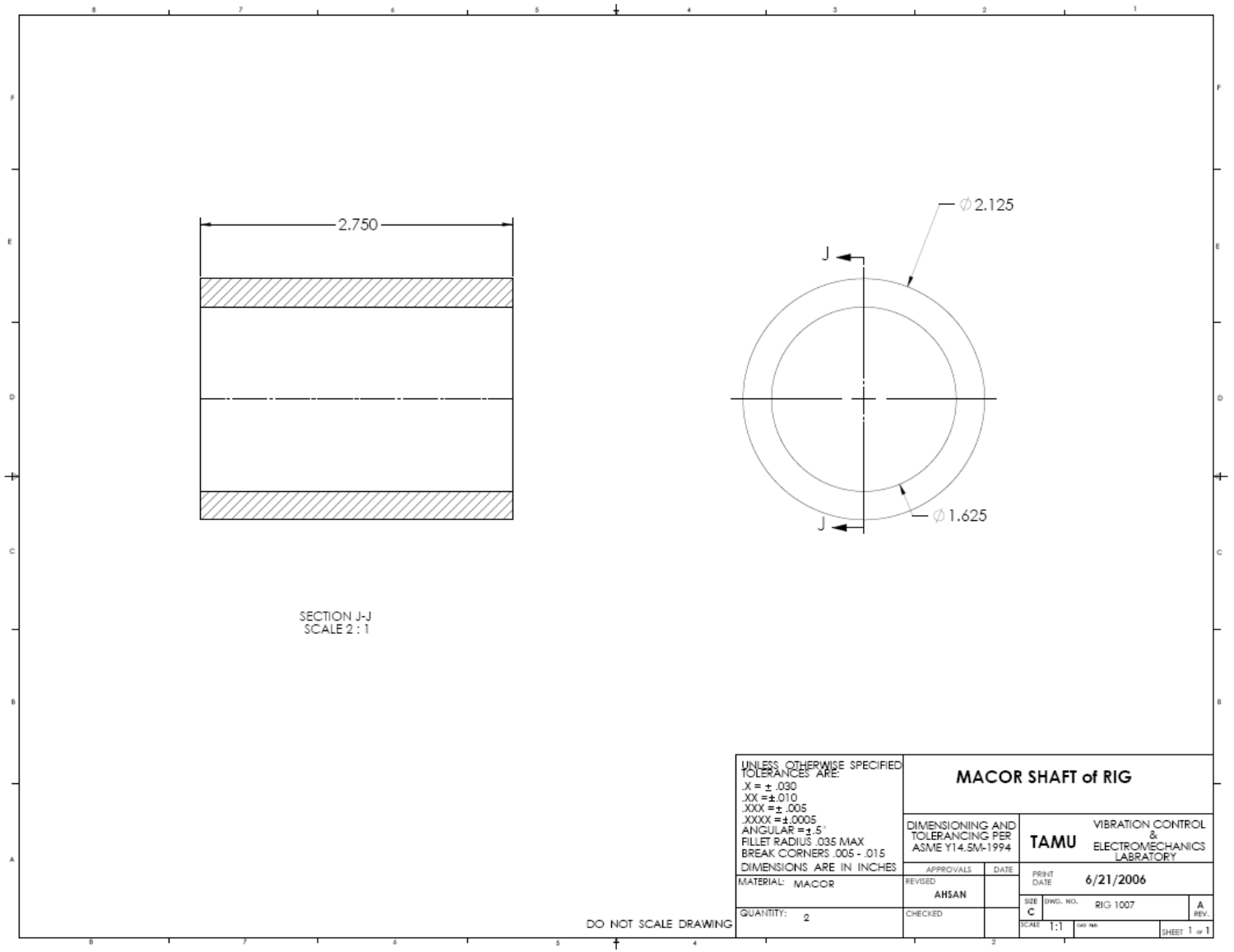
2.750
∅2.125
J
J
∅1.625
SECTION J-J
SCALE 2 : 1
UNLESS OTHERWISE SPECIFIED TOLERANCES ARE:
.X = ± .030
.XX = ± .010
.XXX = ± .005
.XXXX = ± .0005
ANGULAR = ± .5°
FILLET RADIUS .035 MAX
BREAK CORNERS .005 - .015
DIMENSIONS ARE IN INCHES
MATERIAL: MACOR
QUANTITY: 2
DO NOT SCALE DRAWING
MACOR SHAFT of RIG
DIMENSIONING AND TOLERANCING PER ASME Y14.5M-1994
APPROVALS
DATE
REVISED
AHSAN
CHECKED
TAMU
VIBRATION CONTROL & ELECTROMECHANICS LABRATORY
PRINT DATE 6/21/2006
SIZE C
DWG. NO. RIG 1007
REV. A
SCALE 1:1
SHEET 1 of 1

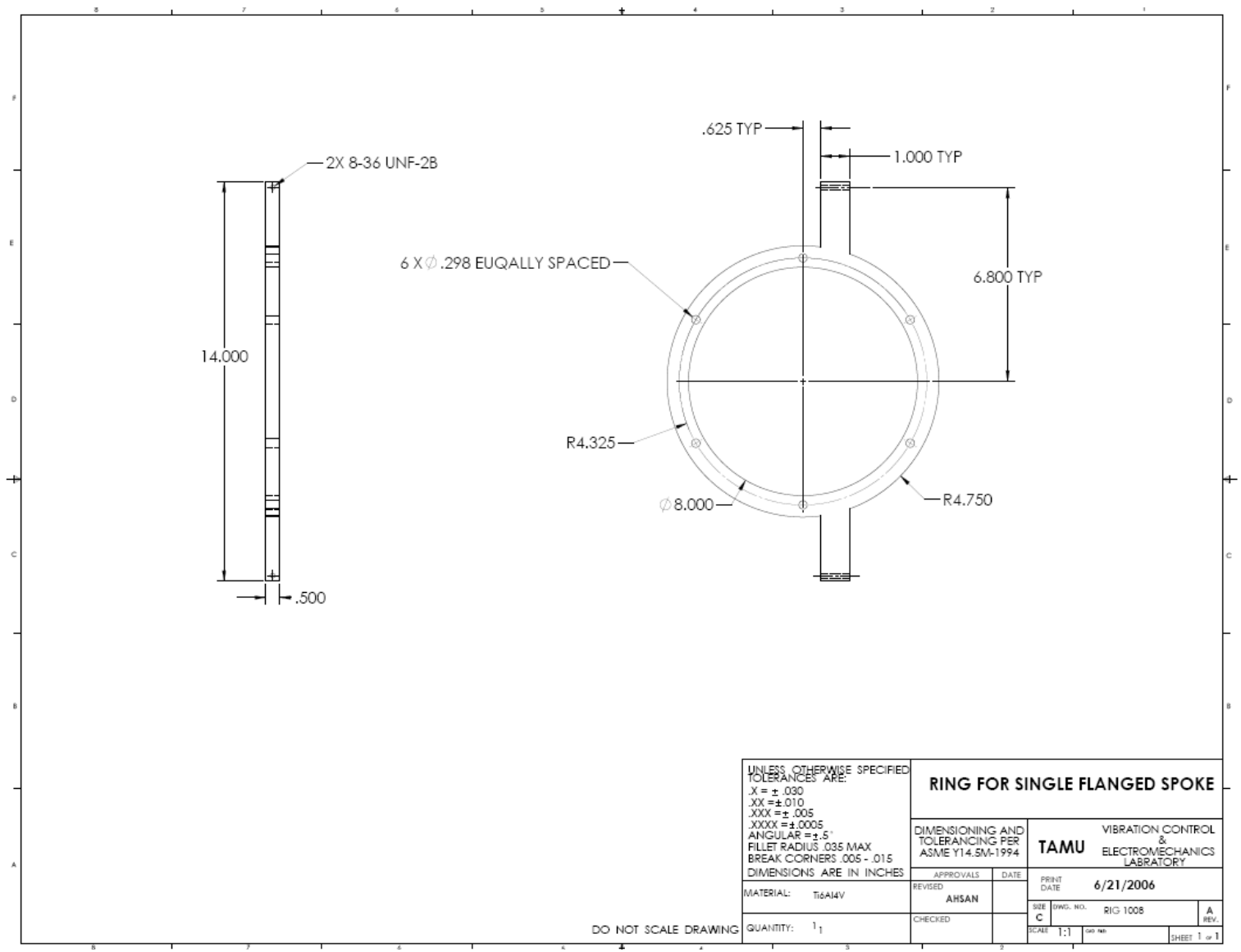
2X 8-36 UNF-2B
14.000
.500
.625 TYP
1.000 TYP
6.800 TYP
6 X ∅ .298 EUQALLY SPACED
R4.325
∅ 8.000
R4.750
UNLESS OTHERWISE SPECIFIED TOLERANCES ARE:
.X = ± .030
.XX =±.010
.XXX =± .005
.XXXX =±.0005
ANGULAR =±.5°
FILLET RADIUS .035 MAX
BREAK CORNERS .005 - .015
DIMENSIONS ARE IN INCHES
MATERIAL: Ti6Al4V
QUANTITY: 1
DO NOT SCALE DRAWING
RING FOR SINGLE FLANGED SPOKE
DIMENSIONING AND TOLERANCING PER ASME Y14.5M-1994
APPROVALS
DATE
REVISED
AHSAN
CHECKED
TAMU
VIBRATION CONTROL & ELECTROMECHANICS LABRATORY
PRINT DATE
6/21/2006
SIZE C
DWG. NO.
RIG 1008
REV. A
SCALE 1:1
SHEET 1 OF 1

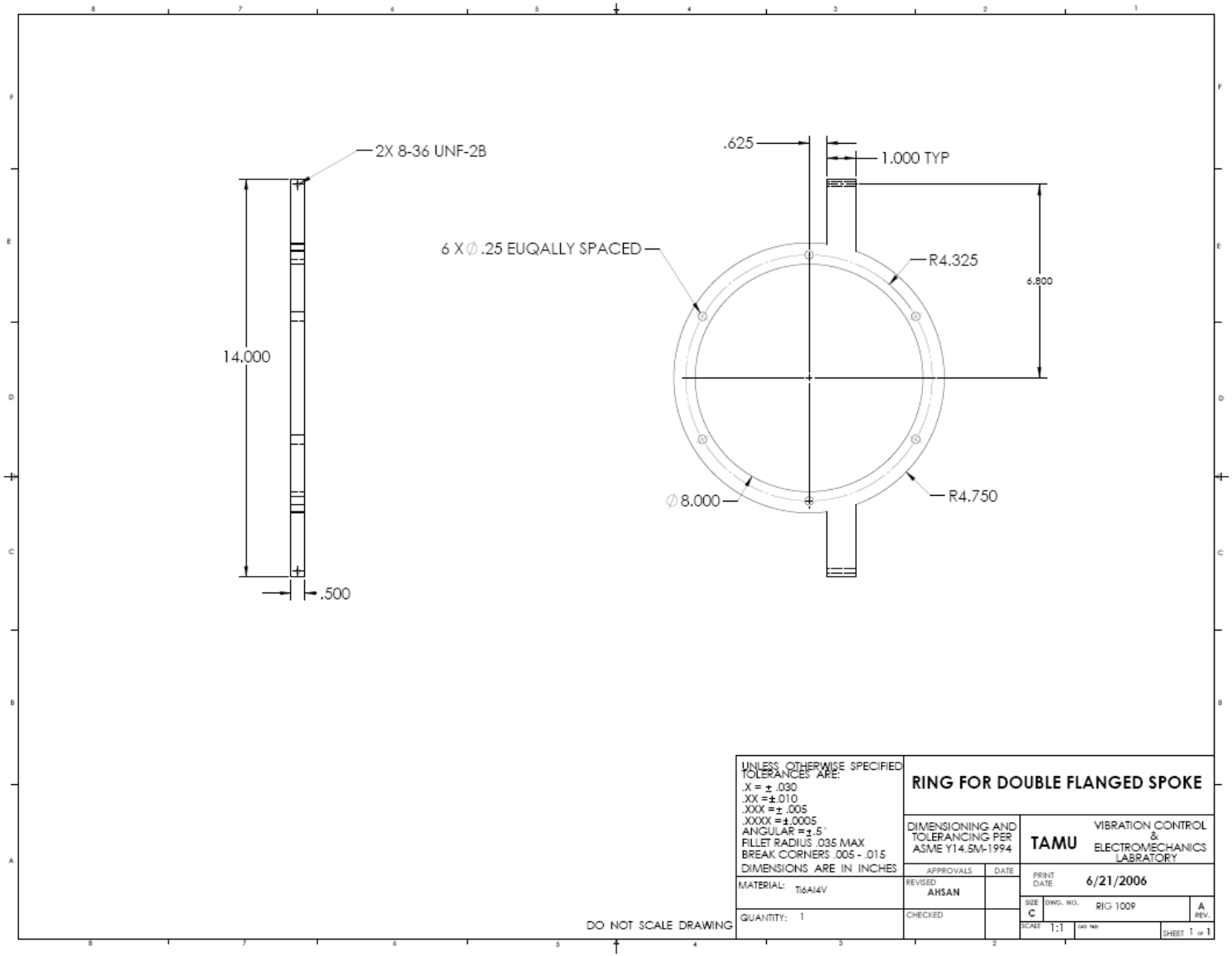
2X 8-36 UNF-2B
14.000
.500
.625
1.000 TYP
6 X ∅ .25 EUQALLY SPACED
R4.325
6.800
∅ 8.000
R4.750
UNLESS OTHERWISE SPECIFIED TOLERANCES ARE:
.X = ± .030
.XX = ± .010
.XXX = ± .005
.XXXX = ± .0005
ANGULAR = ± .5°
FILLET RADIUS .035 MAX
BREAK CORNERS .005 - .015
DIMENSIONS ARE IN INCHES
MATERIAL: Ti6Al4V
QUANTITY: 1
DO NOT SCALE DRAWING
RING FOR DOUBLE FLANGED SPOKE
DIMENSIONING AND TOLERANCING PER ASME Y14.5M-1994
APPROVALS
DATE
REVISED
AHSAN
CHECKED
TAMU
VIBRATION CONTROL & ELECTROMECHANICS LABRATORY
PRINT DATE 6/21/2006
SIZE C
DWG. NO. RIG 1009
REV. A
SCALE 1:1
SHEET 1 of 1

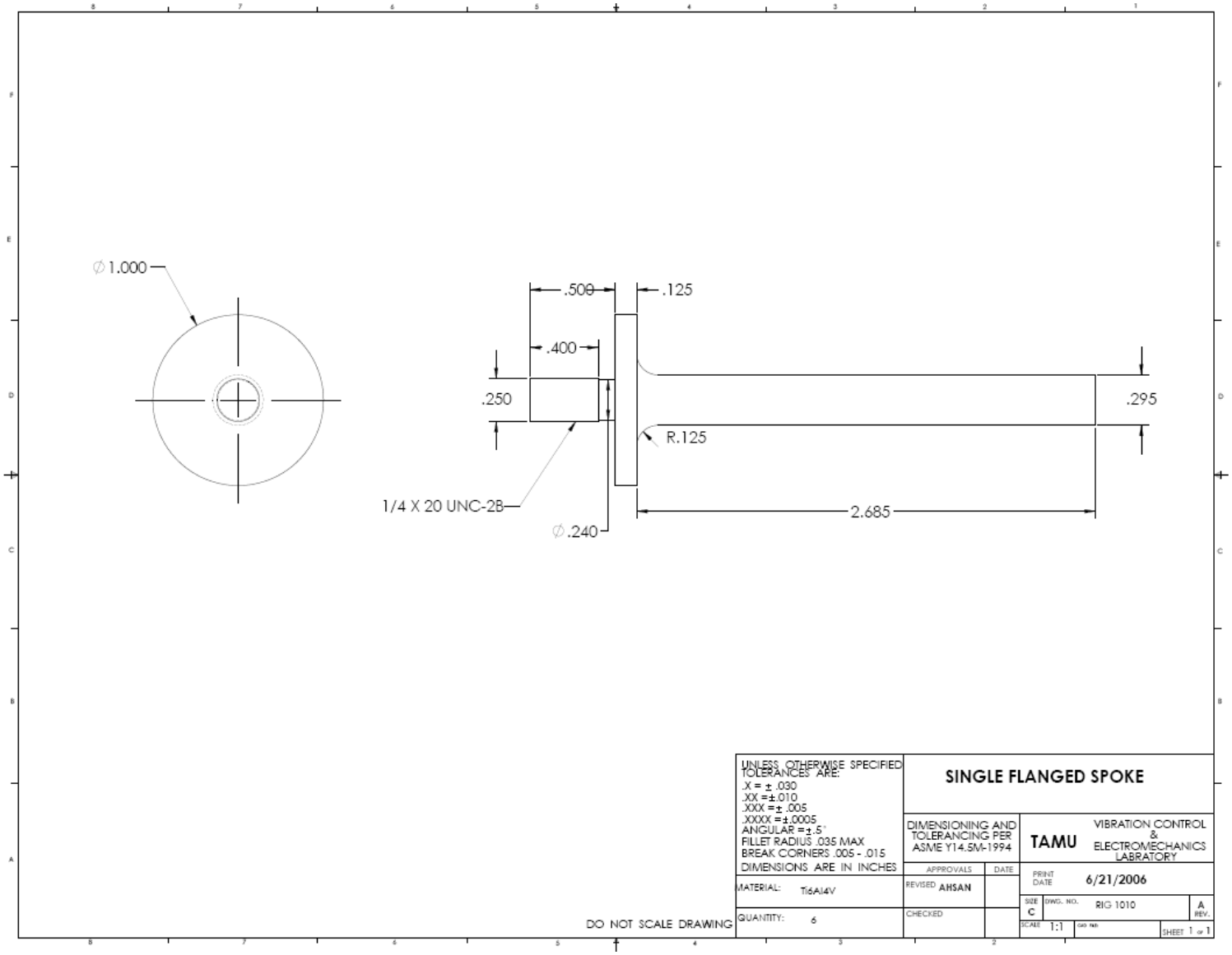
∅1.000
.500
.125
.400
.250
.295
R.125
1/4 X 20 UNC-2B
∅.240
2.685
UNLESS OTHERWISE SPECIFIED TOLERANCES ARE:
.X = ± .030
.XX =±.010
.XXX =± .005
.XXXX =±.0005
ANGULAR =±.5°
FILLET RADIUS .035 MAX
BREAK CORNERS .005 - .015
DIMENSIONS ARE IN INCHES
MATERIAL: Ti6Al4V
QUANTITY: 6
DO NOT SCALE DRAWING
SINGLE FLANGED SPOKE
DIMENSIONING AND TOLERANCING PER ASME Y14.5M-1994
APPROVALS
DATE
REVISED AHSAN
CHECKED
TAMU
VIBRATION CONTROL & ELECTROMECHANICS LABRATORY
PRINT DATE 6/21/2006
SIZE C
DWG. NO. RIG 1010
REV. A
SCALE 1:1
SHEET 1 of 1

APPENDIX D

FABRICATOIN DRAWINGS FOR HTRMB MOLD

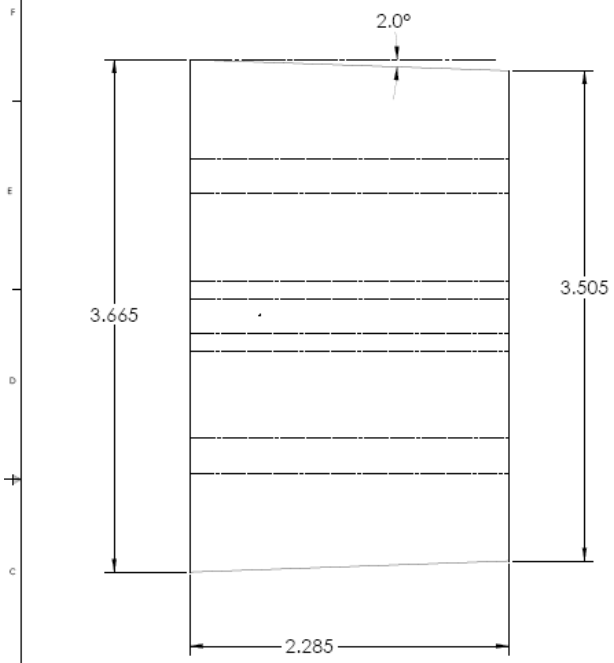

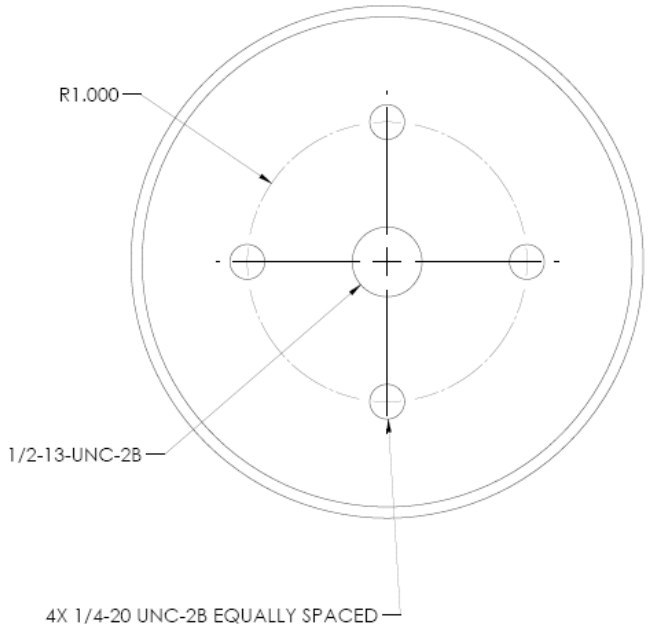

UNLESS OTHERWISE SPECIFIED TOLERANCES ARE:
.X = ± .030
.XX = ± .010
.XXX = ± .005
.XXXX = ± .0005
ANGULAR = ± .5°
FILLET RADIUS .035 MAX
BREAK CORNERS .005 - .015
DIMENSIONS ARE IN INCHES

MATERIAL: Al 6061

QUANTITY : 1

DO NOT SCALE DRAWING

BOTTOM SHAFT for MOLD

DIMENSIONING AND TOLERANCING PER ASME Y14.5M-1994

APPROVALS | DATE

REVISED **AHSAN**

CHECKED

TAMU VIBRATION CONTROL & ELECTROMECHANICS LABRATORY

PRINT DATE **6/21/2006**

SIZE C | DWG. NO. **MOLD 1001** | A REV.

SCALE 1:1 | SHEET 1 OF 1

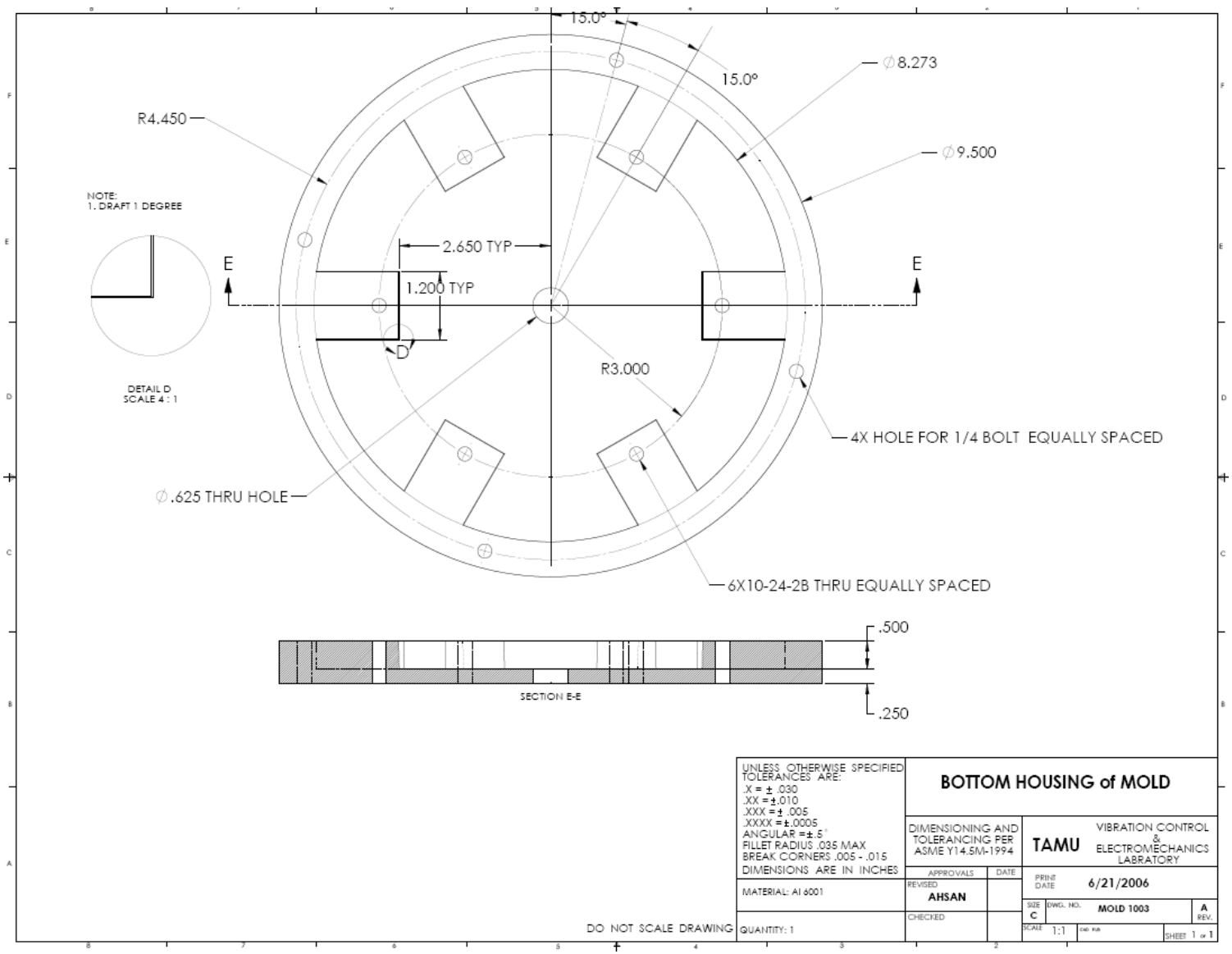
15.0°
15.0°
∅8.273
∅9.500
R4.450
NOTE:
1. DRAFT 1 DEGREE
2.650 TYP
1.200 TYP
E
E
D
DETAIL D
SCALE 4 : 1
R3.000
4X HOLE FOR 1/4 BOLT EQUALLY SPACED
∅.625 THRU HOLE
6X10-24-2B THRU EQUALLY SPACED
.500
.250
SECTION E-E
UNLESS OTHERWISE SPECIFIED TOLERANCES ARE:
.X = ± .030
.XX = ±.010
.XXX = ± .005
.XXXX = ±.0005
ANGULAR = ±.5°
FILLET RADIUS .035 MAX
BREAK CORNERS .005 - .015
DIMENSIONS ARE IN INCHES
MATERIAL: AI 6001
DO NOT SCALE DRAWING
QUANTITY: 1
BOTTOM HOUSING of MOLD
DIMENSIONING AND TOLERANCING PER ASME Y14.5M-1994
APPROVALS
DATE
REVISED
AHSAN
CHECKED
TAMU
VIBRATION CONTROL & ELECTROMECHANICS LABRATORY
PRINT DATE
6/21/2006
SIZE C
DWG. NO.
MOLD 1003
A
REV.
SCALE 1:1
SHEET 1 of 1

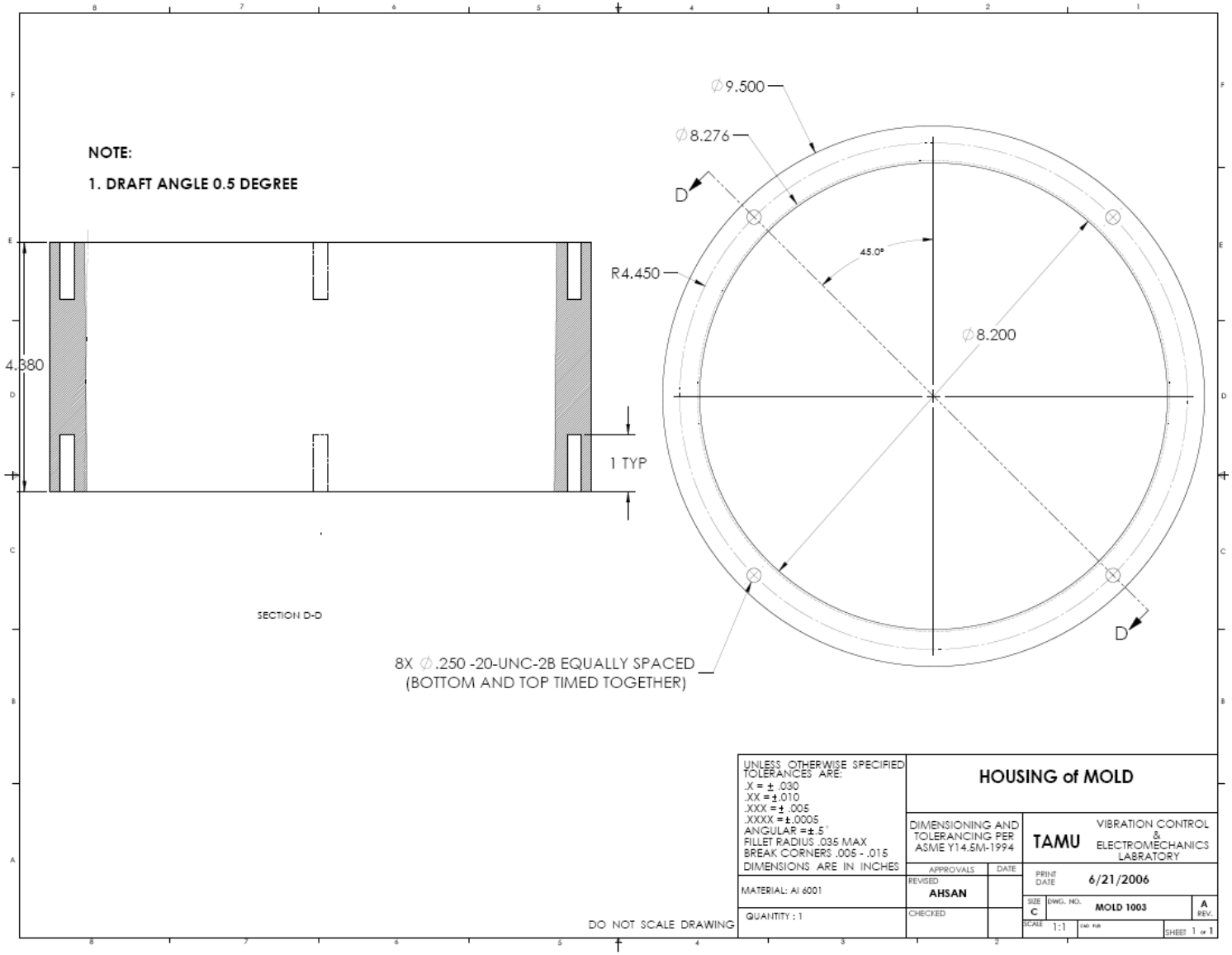
NOTE:
1. DRAFT ANGLE 0.5 DEGREE
∅9.500
∅8.276
D
45.0°
R4.450
∅8.200
4.380
1 TYP
SECTION D-D
D
8X ∅.250 -20-UNC-2B EQUALLY SPACED
(BOTTOM AND TOP TIMED TOGETHER)
UNLESS OTHERWISE SPECIFIED TOLERANCES ARE:
.X = ± .030
.XX = ±.010
.XXX = ± .005
.XXXX = ±.0005
ANGULAR = ± .5°
FILLET RADIUS .035 MAX
BREAK CORNERS .005 - .015
DIMENSIONS ARE IN INCHES
MATERIAL: Al 6001
QUANTITY : 1
DO NOT SCALE DRAWING
HOUSING of MOLD
DIMENSIONING AND TOLERANCING PER ASME Y14.5M-1994
APPROVALS
DATE
REVISED
AHSAN
CHECKED
TAMU
VIBRATION CONTROL & ELECTROMECHANICS LABRATORY
PRINT DATE 6/21/2006
SIZE C
DWG. NO. MOLD 1003
REV. A
SCALE 1:1
SHEET 1 OF 1

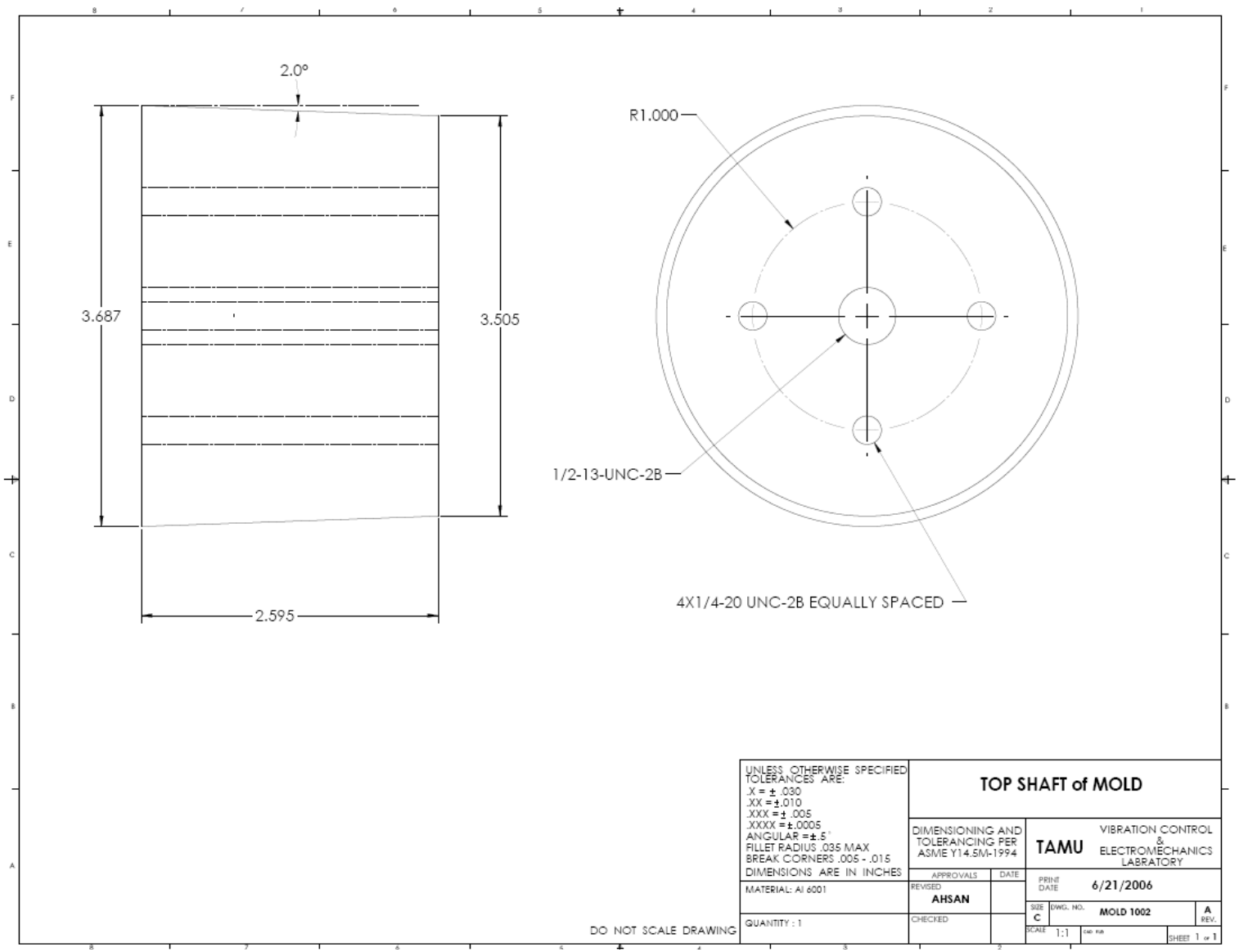
2.0°
3.687
3.505
2.595
R1.000
1/2-13-UNC-2B
4X1/4-20 UNC-2B EQUALLY SPACED
UNLESS OTHERWISE SPECIFIED TOLERANCES ARE:
.X = ± .030
.XX = ± .010
.XXX = ± .005
.XXXX = ± .0005
ANGULAR = ± .5°
FILLET RADIUS .035 MAX
BREAK CORNERS .005 - .015
DIMENSIONS ARE IN INCHES
MATERIAL: Al 6001
QUANTITY : 1
DO NOT SCALE DRAWING
TOP SHAFT of MOLD
DIMENSIONING AND TOLERANCING PER ASME Y14.5M-1994
APPROVALS
DATE
REVISED
AHSAN
CHECKED
TAMU
VIBRATION CONTROL & ELECTROMECHANICS LABRATORY
PRINT DATE
6/21/2006
SIZE C
DWG. NO.
MOLD 1002
REV. A
SCALE 1:1
SHEET 1 OF 1

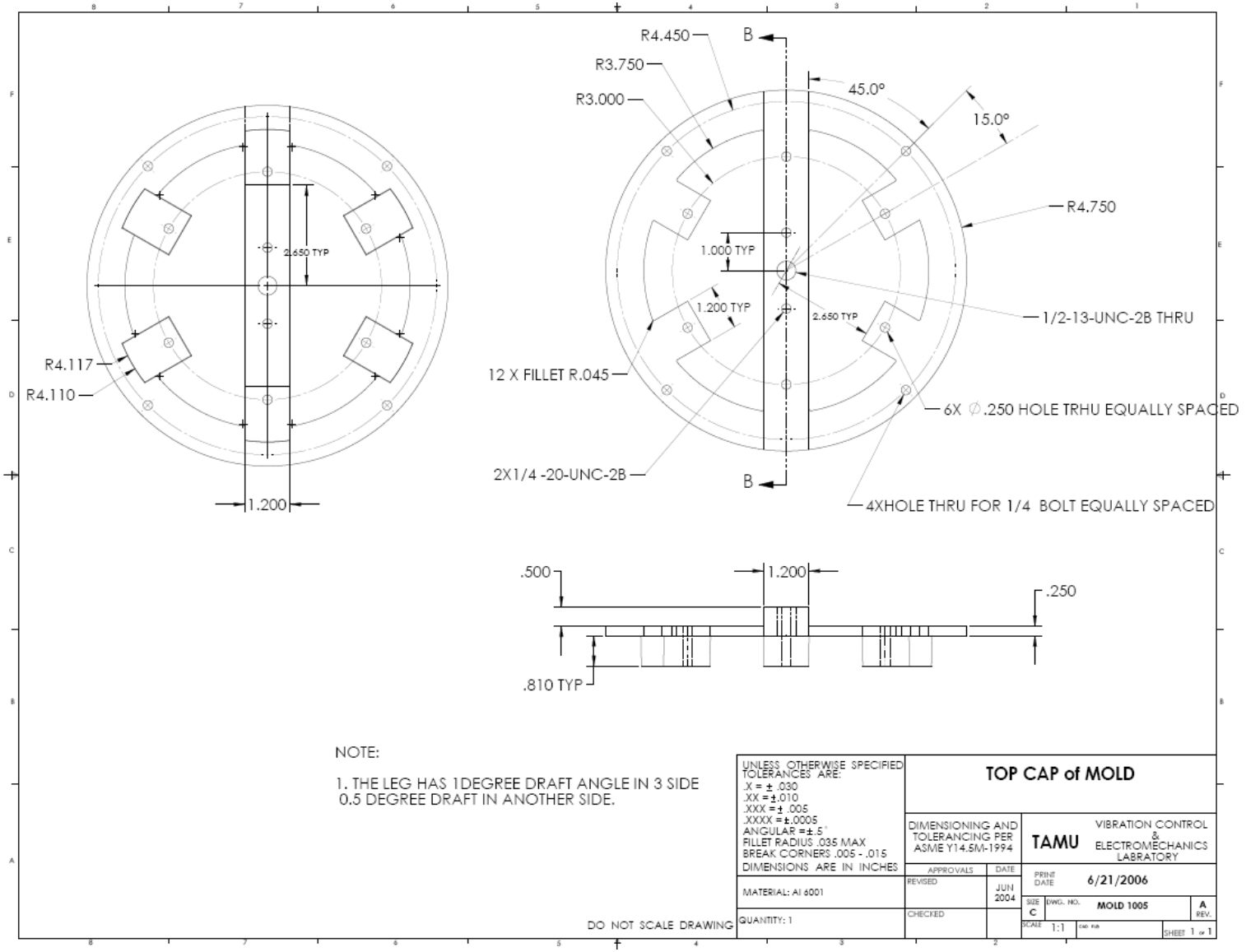
R4.450
B
R3.750
R3.000
45.0°
15.0°
R4.750
1.000 TYP
1.200 TYP
2.650 TYP
1/2-13-UNC-2B THRU
12 X FILLET R.045
6X ∅.250 HOLE TRHU EQUALLY SPACED
2X1/4 -20-UNC-2B
B
4XHOLE THRU FOR 1/4 BOLT EQUALLY SPACED
2.650 TYP
R4.117
R4.110
1.200
.500
1.200
.250
.810 TYP
NOTE:
1. THE LEG HAS 1DEGREE DRAFT ANGLE IN 3 SIDE
0.5 DEGREE DRAFT IN ANOTHER SIDE.
UNLESS OTHERWISE SPECIFIED TOLERANCES ARE:
.X = ± .030
.XX = ±.010
.XXX = ± .005
.XXXX = ±.0005
ANGULAR = ± .5°
FILLET RADIUS .035 MAX
BREAK CORNERS .005 - .015
DIMENSIONS ARE IN INCHES
MATERIAL: Al 6001
QUANTITY: 1
DO NOT SCALE DRAWING
TOP CAP of MOLD
DIMENSIONING AND TOLERANCING PER ASME Y14.5M-1994
APPROVALS
DATE
REVISED
JUN 2004
CHECKED
TAMU
VIBRATION CONTROL & ELECTROMECHANICS LABRATORY
PRINT DATE 6/21/2006
SIZE C
DWG. NO. MOLD 1005
REV. A
SCALE 1:1
SHEET 1 OF 1

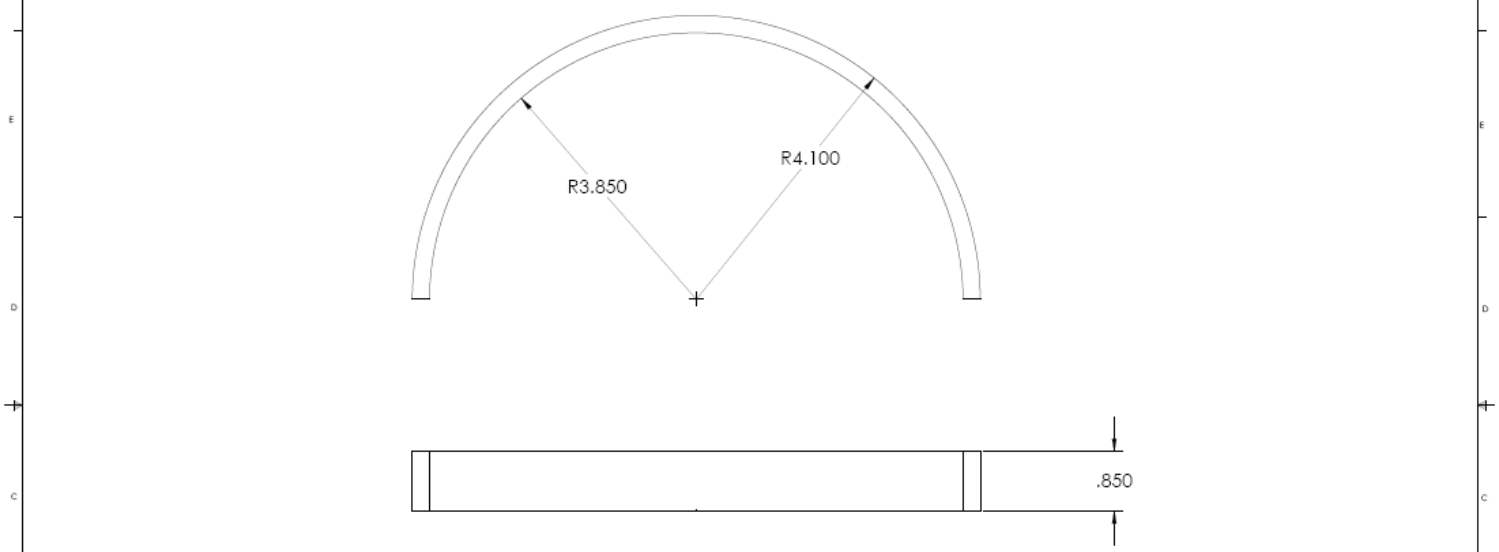

UNLESS OTHERWISE SPECIFIED TOLERANCES ARE:
.X = ± .030
.XX = ±.010
.XXX = ± .005
.XXXX = ±.0005
ANGULAR = ± .5°
FILLET RADIUS .035 MAX
BREAK CORNERS .005 - .015
DIMENSIONS ARE IN INCHES

MATERIAL: Al 6001

Quantity: 2

DO NOT SCALE DRAWING

SEPARATION RING of MOLD

DIMENSIONING AND TOLERANCING PER ASME Y14.5M-1994

APPROVALS | DATE

REVISED **AHSAN**

TAMU VIBRATION CONTROL & ELECTROMECHANICS LABRATORY

PRINT DATE 6/21/2006

SIZE C | DWG. NO. MOLD 1006 | A REV.

SCALE 1:1 | CAD FILE | SHEET 1 OF 1

VITA

Mohammad Ahsan Hossain was born on 31st October, 1979, in Dhaka Bangladesh. He completed his Bachelor of Science in Mechanical Engineering from Bangladesh University of Engineering and Technology in 2003. He continued his education at Texas A&M University, College Station and was awarded a Master of Science in Mechanical Engineering in August, 2006.

He may be reached at:

92 Najimuddin road,
Dhaka, Bangladesh
Email: itsahsan@gmail.com